# KASTAMONU UNIVERSITY JOURNAL OF ENGINEERING AND SCIENCES

e-ISSN 2667-8209

VOL: 08 ISSUE: 02

# KASTAMONU UNIVERSITY JOURNAL OF ENGINEERING AND SCIENCES

e-ISSN 2667-8209

**Kastamonu University Journal of Engineering and Science**

Kastamonu University Journal of Engineering and Science publish as blind peer review and two times in a year.

**Kastamonu University**
**Journal of Engineering and Science**

Vol: 8 Issue: 2 December 2022 E-ISSN:2667-8209

**Kastamonu University**
**Journal of Engineering and Science**

Vol: 8 Issue: 2 December 2022 E-ISSN:2667-8209



Kastamonu University Faculty of Engineering and Architecture 37150 Kastamonu / TÜRKİYE
Tel: +(90)366 2802901 Fax: +(90)366 2802900

Web: https://dergipark.org.tr/tr/pub/kastamonujes
e-mail: kujes@kastamonu.edu.tr

**This journal is published two times in a year.**
**June and December**
Kastamonu University Journal of Engineering and Science
Indexed and Abstracted in: Dergipark

**Kastamonu University**
**Journal of Engineering and Science**

Vol: 8 Issue: 2 December 2022 E-ISSN:2667-8209

**CONTENTS**

doi: 10.55385/kastamonujes.1123018 KUJES 8(2):90-97, 2022

Kastamonu University
Journal of Engineering and Sciences
e-ISSN 2667-8209
http://dergipark.gov.tr/kastamonujes

# Synthesis of Cu-Cr-$B_4C$-CNF hybrid composites

**Osama Ali Ehbil Kriewah[a], Serkan Islak[b,*]**

[a] Department of Materials Science and Engineering, Institute of Science, Kastamonu University, Kastamonu, Türkiye
[b] Department of Mechanical Engineering, Faculty of Engineering and Architecture, Kastamonu University, Kastamonu, Türkiye

***Corresponding Author:** serkan@kastamonu.edu.tr

Received: **May 30**, 2022 ◆ Accepted: **September 26**, 2022 ◆ Published Online: **December 26**, 2022

**Abstract:** In this study, the microstructural properties of Cu-Cr-$B_4C$-CNF hybrid composites produced by powder metallurgy were investigated. While microstructural properties were examined by optical, SEM-EDS and XRD analyzes, hardness test was performed to determine the mechanical properties. The microstructure results, especially the EDS-MAP analysis, showed that the reinforcement elements were relatively homogeneously dispersed in the copper matrix. Since carbon nanofiber has nano size, it was detected in SEM photographs with larger magnification. Cu, $CrB_2$, $Cr_2B_3$ and C phases were detected in the microstructure. The hardness of the composite increased with the addition of reinforcement and reached a maximum value (72.5 HB) of 1% of CNF, and after this CNF ratio, a very small decrease in the hardness value occurred. Compared to the undoped copper sample, the hardness value of the Cu-8$B_4C$-6Cr-1CNF hybrid composite increased by approximately 54%.

**Keywords:** Hybrid composite, Copper, CNF, $B_4C$, Synthesis.

**Öz:** Bu çalışmada toz metalürjisi ile üretilen Cu-Cr-$B_4C$-CNF hibrit kompozitlerin mikroyapı özellikleri araştırılmıştır. Mikroyapı özellikleri optik, SEM-EDS ve XRD analizleri ile incelenirken, mekanik özelliklerin tespiti için sertlik testi yapılmıştır. Mikroyapı sonuçları, özellikle EDS-MAP analizi takviye elemanlarının bakır matrisi içerisinde nispeten homojen dağıldığını göstermiştir. Karbon nanofiber nano boyuta sahip olduğu için daha büyük büyütmeli SEM fotoğraflarında tespit edilmiştir. Mikroyapıda Cu, $CrB_2$, $Cr_2B_3$ ve C fazları tespit edilmiştir. Kompozitin sertlikleri takviye ilavesiyle artış göstermiş ve CNF'nin % 1 oranında maksimum değere (72.5 HB) ulaşmış, bu CNF oranından sonra sertlik değerinde çok az miktarda azalma meydana gelmiştir. Katkısız bakır numuneye göre Cu-8$B_4C$-6Cr-1CNF hibrit kompozitin sertlik değerinde yaklaşık %54 artış meydana gelmiştir.

**Anahtar Kelimeler:** Hibrit kompozit, Bakır, CNF, $B_4C$, Sentez

## 1. Introduction

Pure copper is widely utilized in various electrical applications due to its high electrical and thermal conductivities [1]. Copper also has a range of other useful properties, such as high corrosion resistance, low cost, and ease of manufacture. Owing to its distinctive properties, copper is described as a significant engineering material and will continue to be relevant to future technological advances [2,3]. Copper and its alloys are widely used for various applications, such as automobile radiators, heat exchangers, home heating systems, and solar panels [4].

Even though copper has many excellent properties, its ductility makes it vulnerable to mechanical stresses [5]. Therefore, there are a great number of studies on copper alloys and copper matrix composite materials. Precipitation hardening improves the strength of copper alloys by adding different alloying elements into copper. Azimi and Akbari [6] used a mechanical alloying method to produce Cu-Zr alloys for use in the welding industry. While samples mechanically alloyed for 48 hours reached their maximum hardness, hardness declined after that period. Islamgaliev et al. [7] examined the effect of nanostructure formation by high-pressure torsion on strength and electrical conductivity in Cu-Cr alloy. Dynamic precipitation was observed to improve strength and electrical conductivity. However, these precipitates decompose in high-temperature applications, resulting in a decline in strength [8]. Copper matrix composite materials have gained significance in order to overcome this problem. Reinforcements such as carbide [9], oxide [10], nitride [11], carbon nanotubes [12], graphene [13], and diamond [14] have been added into copper in the literature. On a macro-scale, metal matrix composite materials are made up of a metal or alloy matrix and mostly particulate reinforcement material; on a micro-scale, hybrid composites are made up of more than one reinforcing element with distinct properties added to the matrix [15].

In this study, a powder metallurgy (PM) method was used to produce hybrid composites by adding Cr, $B_4C$, and CNF into copper. The microstructure properties of the hybrid composites so produced were then thoroughly examined.

## 2. Material and Method

### Material

In this study, Cu was used as the matrix (-325 mesh grain size and 99.99% purity) and $B_4C$ (-325 mesh grain size and 99.99% purity), Cr (-325 mesh grain size and 99.99% purity), and CNF (DxL 100 nm×20–200 µm size, 98% purity) were used as reinforcements. Cu, Cr, and $B_4C$ powders were obtained from Nanography and CNF from Sigma-Aldrich. Figure 1 shows scanning electron microscopy (SEM) images of the powders used in the present study. The Cu powder had a wormlike morphology, while Cr and $B_4C$ were sharp edged and CNF was fibrous. Different rates of Cr, $B_4C$, and CNF were added to Cu. Table 1 shows the powder mixture ratios.

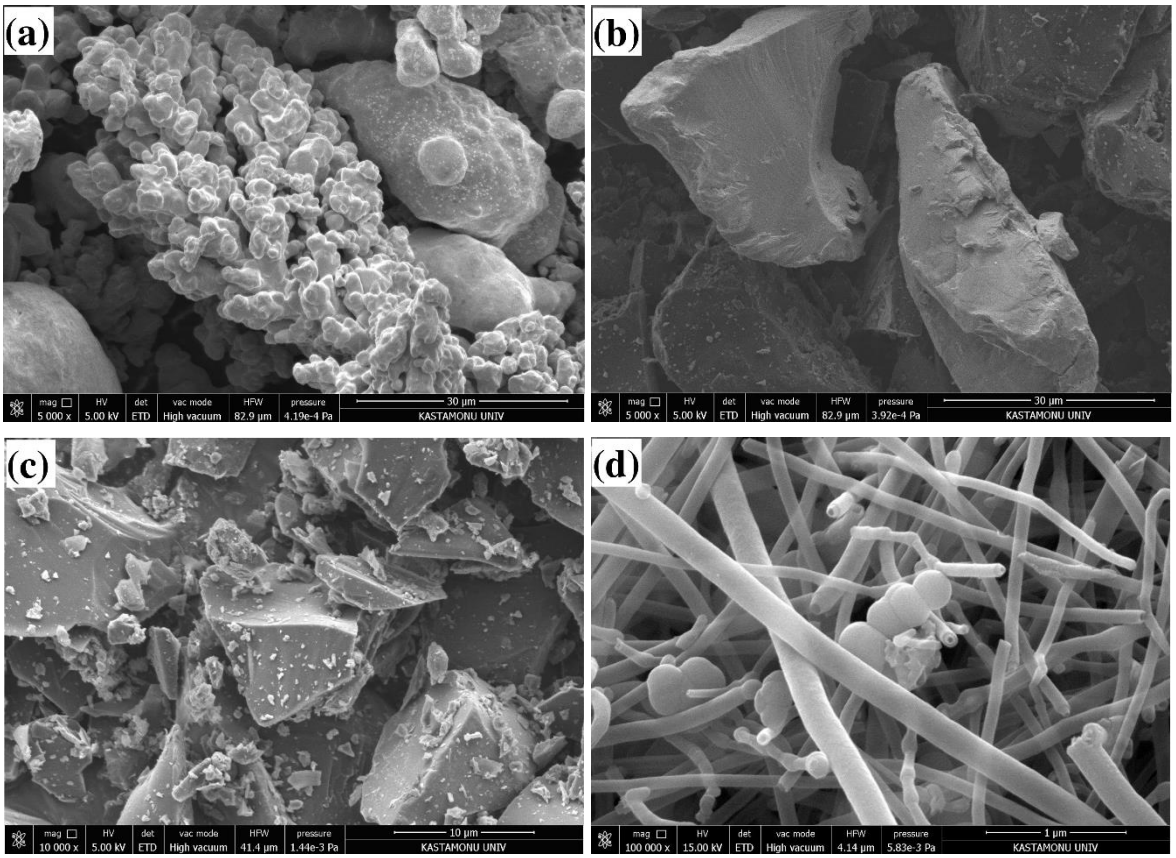


**Figure 1.** SEM images of the powders: (a) Cu, (b) Cr, (c) $B_4C$, and (d) CNF

**Table 1.** Powder mixture ratios (% by volume)

| No | Cu | $B_4C$ | Cr | CNF |
|---|---|---|---|---|
| **1** | 100 | 0 | 0 | 0 |
| **2** | 92 | 8 | 0 | 0 |
| **3** | 90 | 8 | 2 | 0 |
| **4** | 88 | 8 | 4 | 0 |
| **5** | 86 | 8 | 6 | 0 |
| **6** | 85 | 8 | 6 | 1 |
| **7** | 84 | 8 | 6 | 2 |
| **8** | 83 | 8 | 6 | 3 |

The powders were mixed at the appropriate mixture ratios for 2 hours at 400 rpm using a Retsch PM 100 model mechanical alloying device. 10mm diameter 100Cr6 balls were utilized in the mixture process, with the powder-ball ratio set at 1:5. In order to prevent cold welding and burning of the powders, 2% zinc stearate was added to the powder mixtures before mixing. Mechanically alloyed powder mixtures were pressed in a Specac GS15011 model hydraulic press under 400 MPa pressure, producing samples with a diameter of 20 mm and a height of 10 mm. The green pellet samples were sintered in a Protherm high-temperature tube furnace at 900 ºC for two hours at a heating/cooling rate of 10 ºC/min under an argon atmosphere.

For microstructure analysis, the samples were sanded using 320-2400 mesh sandpaper and polished using a 1-micron diamond solution. The polished samples were etched in a solution containing 100 mL distilled water + 25 mL hydrochloric

acid + 8 g iron (III) chloride. X-ray diffraction (XRD) analysis was performed using the Rigaku Ultra IV XRD. The Carl Zeiss Ultra PLus Gemini FE-SEM was used for SEM and energy dispersive spectrometry (EDS) analyses. Optical microscope examinations of the samples were performed using a Nikon brand inverted metallurgical microscope. Sintered densities were measured using an AND GR-200 balance with a density measuring kit at $10^{-4}$ precision in accordance with the Archimedes' principle established in the ASTM B 962-17 standard [16]. The hardness of the samples was measured with a Qness Q250 M hardness device under 62.5 kgf load and using 2.5 mm balls as Brinell according to TS EN ISO 6506-1 standard [17]. The work flow chart of the experimental work stages is shown in Figure 2.

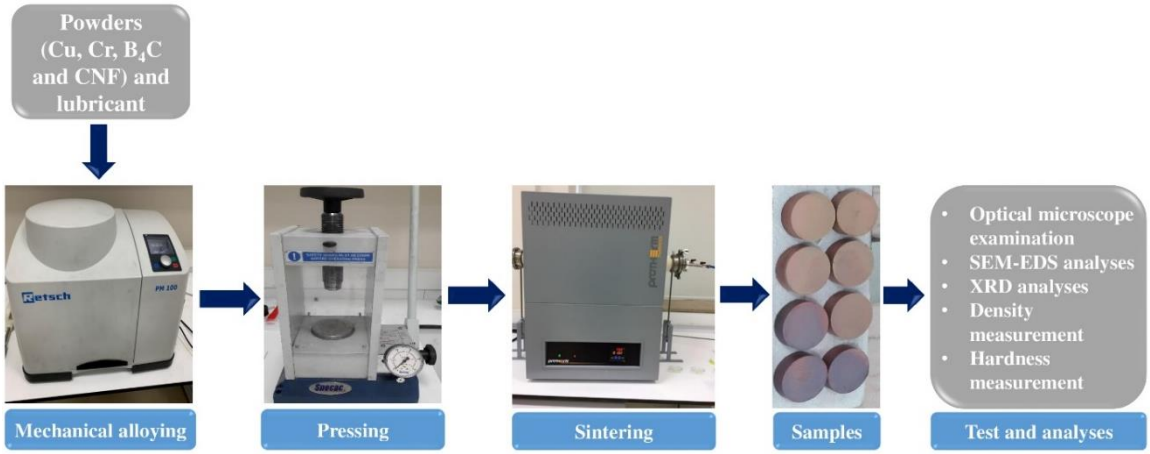


**Figure 2.** Work flow chart of experimental work stages

## 3. Result and Discussion

Figure 3 shows optical images of hybrid composites with different reinforcing types and quantities produced by PM. The matrix and reinforcing elements were located in microstructures of different colours. The Cu matrix was reddish, $B_4C$ was dark grey, and Cr was light grey. The optical images show that the $B_4C$ grains were homogeneously dispersed in the Cu matrix; Cr, on the other hand, was relatively homogeneously dispersed, and with increased Cr rates, it was observed to be dispersed in the form of agglomerations in some parts of the samples. SEM examination was performed at high magnification for Sample 6 in order to detect CNFs. Figure 4 shows SEM images of Sample 6. Although CNFs were originally longer, mechanical alloying caused them to be embedded in the copper matrix in a shortened form.

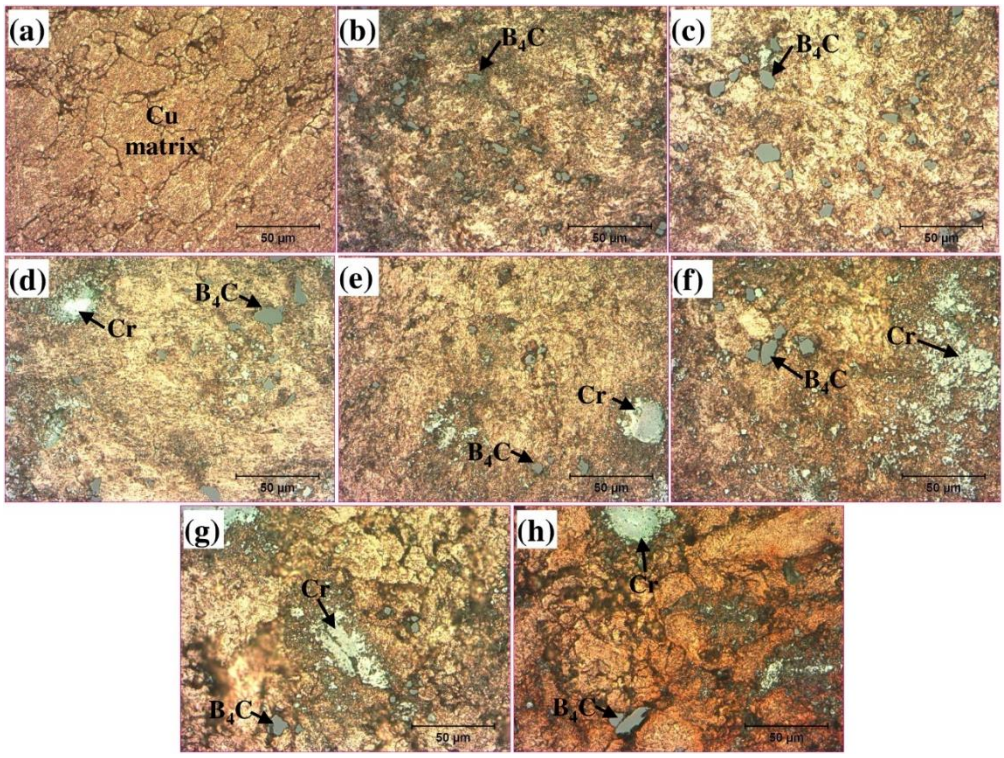


**Figure 3.** Optical images: (a) Pure Cu, (b) Cu-8$B_4C$, (c) Cu-8$B_4C$-2Cr, (d) Cu-8$B_4C$-4Cr, (e) Cu-8$B_4C$-6Cr, (f) Cu-8$B_4C$-6Cr-1CNF, (g) Cu-8$B_4C$-6Cr-2CNF, and (f) Cu-8$B_4C$-6Cr-3CNF

Figure 5 depicts a MAP-EDS analysis of the samples to provide information on the distribution of reinforcements in the Cu matrix. The pattern of distribution here broadly corresponds to the optical images. The mechanical and physical properties of the sample are improved by the homogenous distribution of the reinforcing elements in the matrix [18,19]. No crack formation was observed in the microstructure. However, pores formed in all samples.

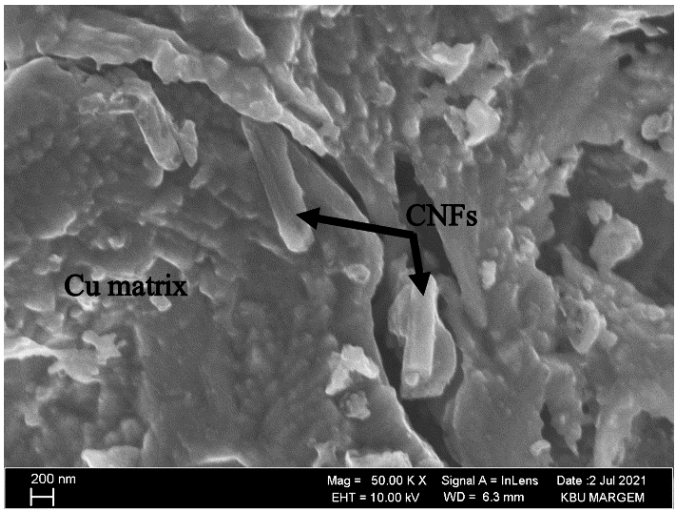


**Figure 4.** SEM images of Sample 6 (Cu-8$B_4C$-6Cr-1CNF)

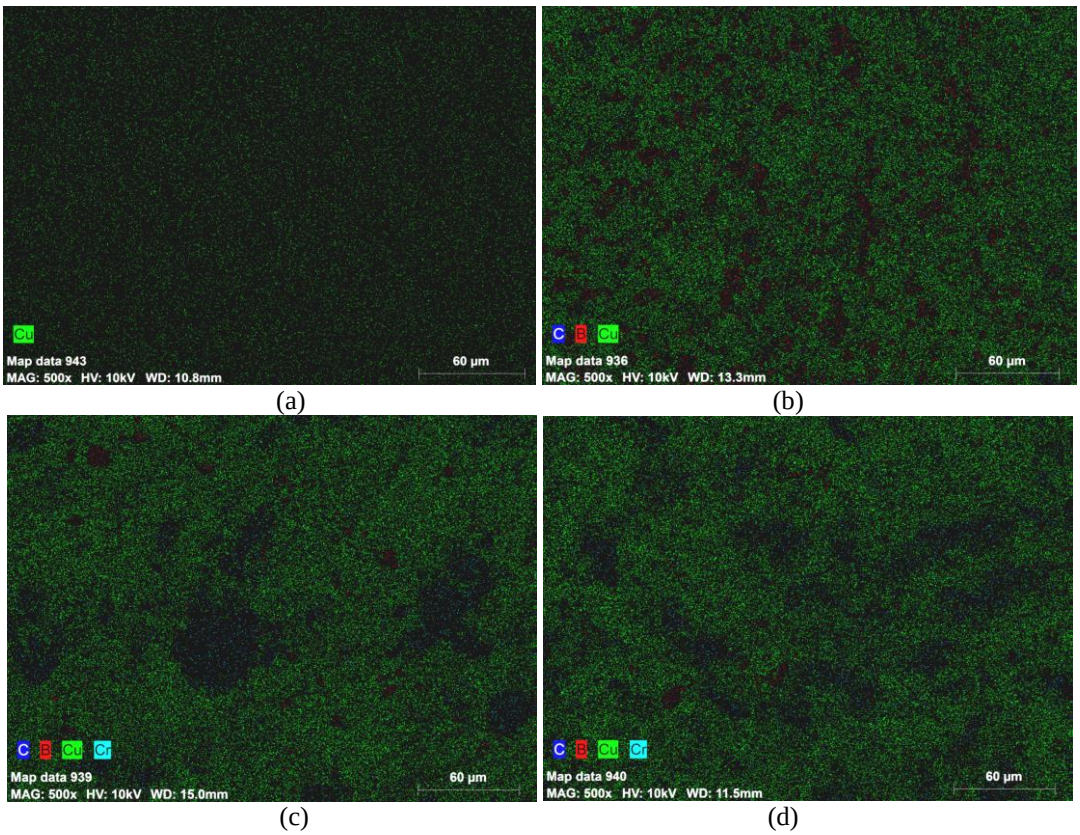


**Figure 5.** MAP-EDS analysis of: (a) Pure Cu, (b) Cu-8$B_4C$, (c) Cu-8$B_4C$-6Cr, and (d) Cu-8$B_4C$-6Cr-1CNF

Figure 6 shows the EDS analysis of Cu-8$B_4C$-6Cr-1CNF sample. Area 1 represents the Cu matrix. Small amounts of B, C and Cr also existed. Area 2 represents the $B_4C$ grain. Small amounts of Cr and Cu contaminate particles of $B_4C$. Area 3 represents Cr in general, while small amounts of B, C, and Cu were identified in EDS analysis. The coexistence of B, C, Cr, and Cu in all three EDS analysis areas might be caused by mechanical bonding during the mechanical alloying. According to the EDS results, no oxide formation was detected in the microstructure. This result may suggest that no oxidation took place during the sintering process. Jha et al. [20] argued in their study on the friction and wear behaviours of Cu–4 wt.% Ni–TiC composites that there was no oxidation during sintering.

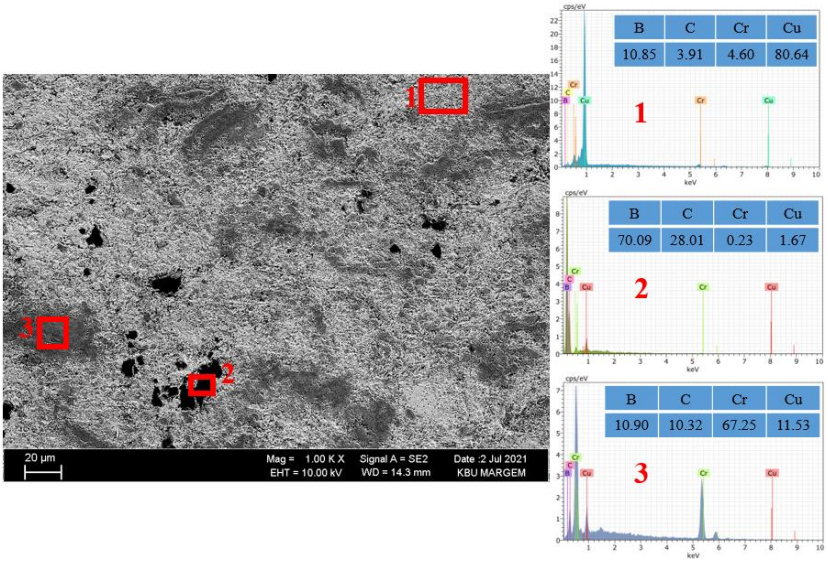


**Figure 6.** The EDS analysis of the Cu-8$B_4C$-6Cr-1CNF sample

Figure 7 shows the graphs generated following the XRD analysis performed to determine the phase of the samples. The pure Cu sample had the phase Cu (PDF card Cu 00-001-1241) with crystal planes (111), (200), (220), and (311). At 2-theta angles of 43.47°, 50.37°, 74.00°, and 89.93°, respectively, the Cu phase formed. $CrB_2$ (PDF card $CrB_2$ 03-065-1883) and $Cr_2B_3$ (PDF card $Cr_2B_3$ 00-37-1447) phases formed in addition to the Cu phase when the Cu matrix was reinforced with Cr, $B_4C$, and CNF. These phases had crystal planes (001) and (131), respectively. Also, the $CrB_2$ phase formed at a 2-theta angle of 29.10°, whereas the $Cr_2B_3$ phase formed at a 2-theta angle of 45.42°. In their study, Sun et al. [21] detected the $Cr_2B_3$ phase. Wang et al. [22] reported that they obtained the $CrB_2$ phase in their study on the sintering of $B_4C$ and $Cr_2O_3$.

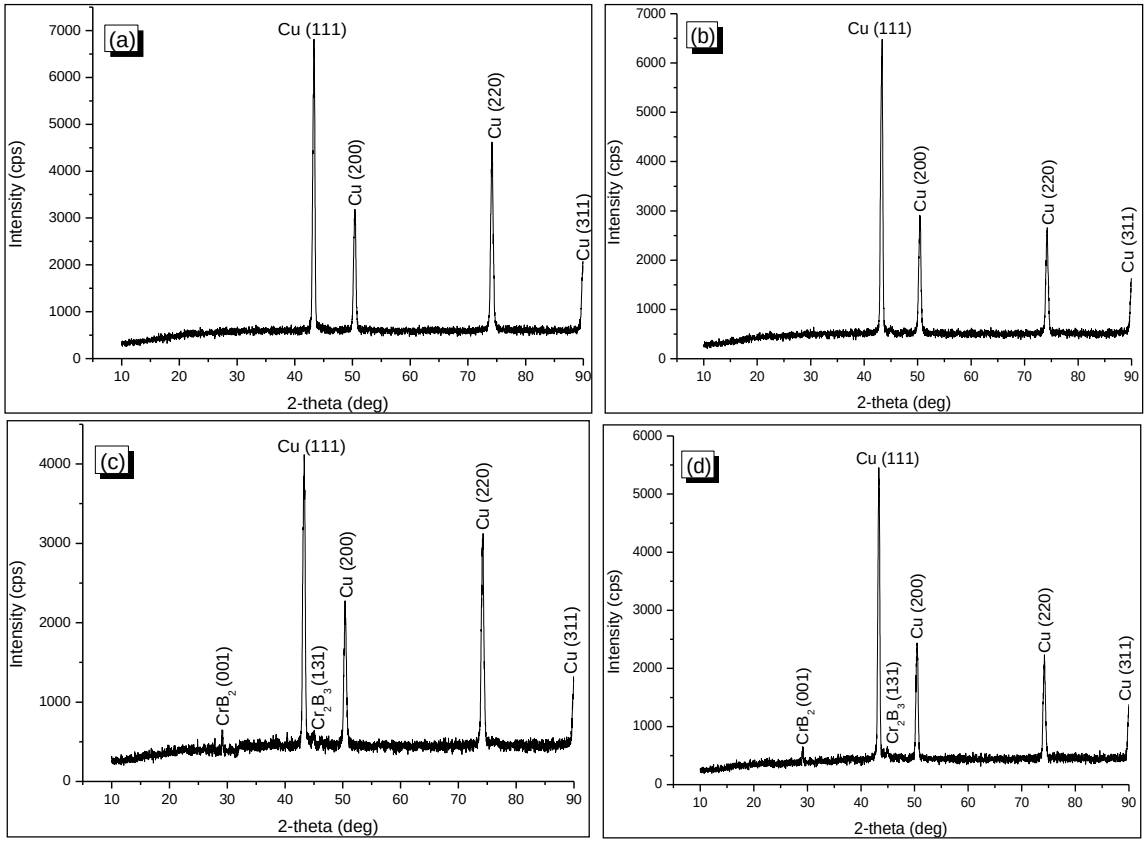


**Figure 7.** XRD graphs of samples of: (a) Pure Cu, (b) Cu-8$B_4C$, (c) Cu-8$B_4C$-6Cr, and (d) Cu-8$B_4C$-6Cr-1CNF

The graph in Figure 8 shows the experimental and relative densities of hybrid composites. In general, both the experimental and relative densities declined, depending on the increasing rate and type of reinforcing elements. The

decline in experimental densities is due to the fact that the natural densities of chromium (7.19 g/cm$^3$), boron carbide (2.52 g/cm$^3$), and carbon nanofiber (1.9 g/cm$^3$) reinforcing elements are less than the density of copper (8.96 g/cm$^3$). The decline in relative densities stopped at Sample 3, peaked at Sample 6, and then resumed its decline. CNFs displayed the impact of filling the pores in Sample 6; on the other hand, in Samples 7 and 8, there was a decline in relative densities, partially due to aggregation of CNFs. The overall decline in relative densities can also be associated with the fact that the increased reinforcement rate had a negative impact on compressibility. Yet another reason is that the substantial difference in melting temperatures between the matrix and the reinforcing elements was a factor that prevented the particles' movements during sintering [23,24].

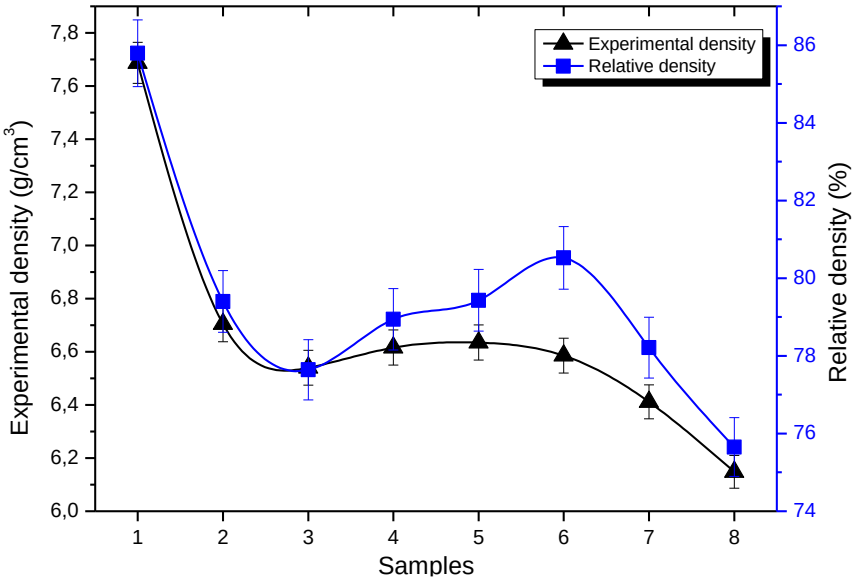


**Figure 8.** Experimental and relative densities of the samples

Figure 9 shows the hardness values of the samples. Hardness increased towards Sample 6 (maximum of 72.5 HB) among the Samples 1-6; on the other hand, the hardness of Samples 7 and 8 declined. The decline can be associated with the heterogeneous distribution of CNFs in Samples 7 and 8. In comparison to the pure Cu sample (Sample 1), there was an increase of approximately 54%. Here, $B_4C$, CNF, $CrB_2$, and $Cr_2B_3$ phases increased hardness by blocking movement of dislocations. In their study, Lim et al. reported that CNFs increased hardness by blocking movement of dislocations [25]. Islak et al. reported that the hardness of the samples produced by adding CNF to the bronze increased depending on the increasing amount of CNF [26].

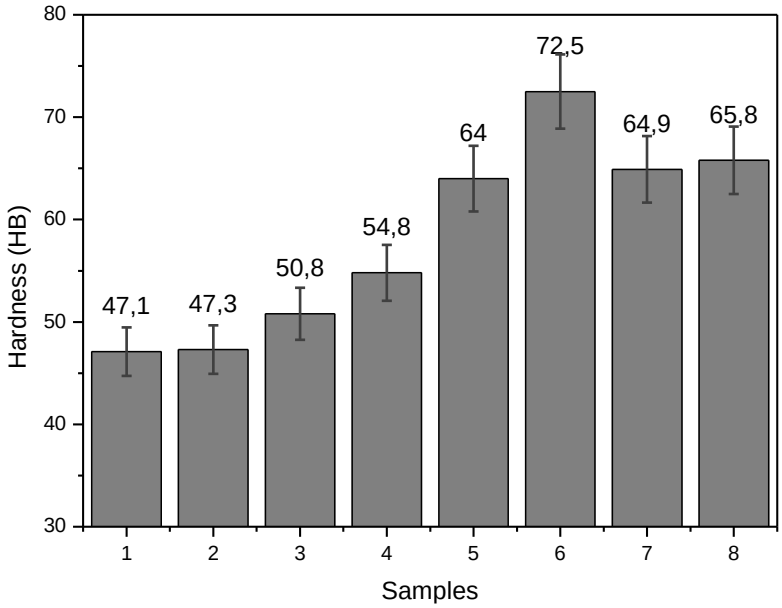


**Figure 9.** Hardness of the samples

## 4. Conclusions

The microstructure properties of Cu-Cr-$B_4C$-CNF hybrid composites produced by PM were thoroughly examined, and the following results were achieved:

1. PM was used to successfully produce Cu-Cr-$B_4C$-CNF hybrid composites. No cracks or discontinuities were noted in the samples.

2. Optical microscope images demonstrated that Cr and $B_4C$ were partially homogeneously dispersed in the Cu matrix. CNFs could not be viewed with an optical microscope. Therefore, SEM images were captured at high magnifications, and clearly showed CNFs. Intermetallic phases, such as $CrB_2$ and $Cr_2B_3$, formed between the element B forming as a result of the degradation of $B_4C$ and the Cr added to the matrix.

3. While the relative and experimental densities of the samples decreased with increasing reinforcement, there was an increase in hardness values up to Sample 6 and subsequently a partial decrease. Sample 6 had the maximum hardness observed in any sample (72.5 HB).

## Competing Interest / Conflict of Interest

The authors declare that they have no competing interests.

## Author Contribution

We declare that all Authors equally contribute.

## 6. References

[1] Islak, S., Çalıgülü, U., Hraam, H. R., Özorak, C., & Koç, V. (2019). Electrical conductivity, microstructure and wear properties of Cu-Mo coatings. Research on Engineering Structures and Materials, 5(2), 137-146.

[2] ASM Handbook: Properties and Selection: Nonferrous Alloys and Special-Purpose Materials, Vol.2, 10th ed., 1990.

[3] Deshpande, P. K., & Lin, R. Y. (2006). Wear resistance of WC particle reinforced copper matrix composites and the effect of porosity. Materials Science and Engineering: A, 418(1-2), 137-145.

[4] Buytoz, S., Dagdelen, F., Islak, S., Kok, M., Kir, D., & Ercan, E. (2014). Effect of the TiC content on microstructure and thermal properties of Cu–TiC composites prepared by powder metallurgy. Journal of Thermal Analysis and Calorimetry, 117(3), 1277-1283.

[5] Chen, H., Jia, C. C., & Li, S. J. (2013). Effect of sintering parameters on the microstructure and thermal conductivity of diamond/Cu composites prepared by high pressure and high temperature infiltration. International Journal of Minerals, Metallurgy, and Materials, 20(2), 180-186.

[6] Azimi, M., & Akbari, G. H. (2011). Development of nano-structure Cu–Zr alloys by the mechanical alloying process. Journal of Alloys and Compounds, 509(1), 27-32.

[7] Islamgaliev, R. K., Nesterov, K. M., Bourgon, J., Champion, Y., & Valiev, R. Z. (2014). Nanostructured Cu-Cr alloy with high strength and electrical conductivity. Journal of Applied Physics, 115(19), 194301.

[8] Correia, J. B., Davies, H. A., & Sellars, C. M. (1997). Strengthening in rapidly solidified age hardened Cu-Cr and Cu-Cr-Zr alloys. Acta Materialia, 45(1), 177-190.

[9] Islak, S., Kır, D., & Buytoz, S. (2014). Effect of sintering temperature on electrical and microstructure properties of hot pressed Cu-TiC composites. Science of Sintering, 46(1), 15-21.

[10] Rajkovic, V., Bozic, D., & Jovanovic, M. T. (2010). Effects of copper and $Al_2O_3$ particles on characteristics of Cu–$Al_2O_3$ composites. Materials & Design, 31(4), 1962-1970.

[11] Yin, J., Yao, D., Xia, Y., Zuo, K., & Zeng, Y. (2014). The effect of modified interfaces on the mechanical property of β-silicon nitride whiskers reinforced Cu matrix composites. Journal of alloys and compounds, 615, 983-988.

[12] Sule, R., Olubambi, P. A., Sigalas, I., Asante, J. K. O., & Garrett, J. C. (2014). Effect of SPS consolidation parameters on submicron Cu and Cu–CNT composites for thermal management. Powder Technology, 258, 198-205.

[13] Peng, W., & Sun, K. (2020). Effects of Cu/graphene interface on the mechanical properties of multilayer Cu/graphene composites. Mechanics of Materials, 141, 103270.

[14] Schubert, T., Zieliński, W., Michalski, A., Weißgärber, T., & Kieback, B. (2008). Interfacial characterization of Cu/diamond composites prepared by powder metallurgy for heat sink applications. Scripta Materialia, 58(4), 263-266.

[15] Torralba, J. D., Da Costa, C. E., & Velasco, F. (2003). P/M aluminum matrix composites: an overview. Journal of Materials Processing Technology, 133(1-2), 203-206.

[16] ASTM B962-17, Standard test methods for density of compacted or sintered powder metallurgy (PM) products using Archimedes' principle, ASTM International, 2017.
[17] TS EN ISO 6506-1:2014. "Metallic materials - Brinell hardness test - Part 1: Test method", TSE, Ankara, Türkiye.
[18] Akkaş, M., Islak, S., & Özorak, C. (2018). Corrosion and wear properties of Cu-TiC composites produced by hot pressing technique. Celal Bayar University Journal of Science, 14(4), 465-469.
[19] Lee, D. W., Ha, G. H., & Kim, B. K. (2001). Synthesis of Cu-$Al_2O_3$ nano composite powder. Scripta materialia, 44(8-9), 2137-2140.
[20] Jha, P., Gautam, R. K., & Tyagi, R. (2017). Friction and wear behavior of Cu–4 wt.% Ni–TiC composites under dry sliding conditions. Friction, 5(4), 437-446.
[21] Sun, Y. Z., Li, J. B., Wellburn, D., & Liu, C. S. (2016). Fabrication of wear-resistant layers with lamellar eutectic structure by laser surface alloying using the in situ reaction between Cr and $B_4C$. International Journal of Minerals, Metallurgy, and Materials, 23(11), 1294-1301.
[22] Wang, S., Xing, P., Gao, S., Yang, W., Zhuang, Y., & Feng, Z. (2018). Effect of in-situ formed $CrB_2$ on pressureless sintering of B4C. Ceramics International, 44(16), 20367-20374.
[23] Rahimian, M., Ehsani, N., Parvin, N., & reza Baharvandi, H. (2009). The effect of particle size, sintering temperature and sintering time on the properties of Al–$Al_2O_3$ composites, made by powder metallurgy. Journal of Materials Processing Technology, 209(14), 5387-5393.
[24] Islak, S., & Çelik, H. (2015). Effect of sintering temperature and boron carbide content on the wear behavior of hot pressed diamond cutting segments. Science of Sintering, 47(2), 131-143.
[25] Lim, J. Y., Oh, S. I., Kim, Y. C., Jee, K. K., Sung, Y. M., & Han, J. H. (2012). Effects of CNF dispersion on mechanical properties of CNF reinforced A7xxx nanocomposites. Materials Science and Engineering: A, 556, 337-342.
[26] Islak, S., Özorak, C., Abouacha, N. M. E., Çalıgülü, U., Koç, V., & Küçük, Ö. (2021). The effects of the CNF ratio on the microstructure, corrosion, and mechanical properties of CNF-reinforced diamond cutting tool. Diamond and Related Materials, 119, 108585.

doi:10.55385/kastamonujes.1151603 KUJES 8(2):98-106, 2022

Kastamonu University
Journal of Engineering and Sciences
e-ISSN 2667-8209
http://dergipark.gov.tr/kastamonujes

# Radiometric Measurements in of Japanese barberry (*Berberis thunbergii* DC.), Boxwood (*Buxus sempervirens* L.) and Gold tassel (*Euonymus japonica* Thunb.) Under Cadmium and Zinc Stress

**Nezahat Turfan**[a *], **Erkan Genç**[b]

[a] Department of Biology, Science Faculty, Kastamonu University, Kastamonu, Türkiye
[b] Central Second School, Kastamonu, Türkiye
***Corresponding Author:** nturfan@kastamonu.edu.tr

Received: **July 31, 2022** ◆ Accepted: **November 28, 2022** ◆ Published Online: **December 26, 2022**

**Abstract:** In this study, the effects of Cd and Zn applications on the activity concentration and transfer factors in the Japanaesebarberry, Boxwood, and Gold tassel leaves were investigated using gamma-ray spectrometry. The mean concentrations (in Bq kg-1) of radionuclides in the studied soil samples were found to be 289.40±32.47 for 238U, 241.76±27.47 for 232Th, 783.63±83.46 for 40K, and 31.44±5.63 for R 137Cs while the respective values in the studied species were 168.6±20.1- 288.8±34.5, 145.9±19.1-250.3±32.4, 434.6±52.2-828.4±99.4, and 16.1±1.8-28.3±3.3. The activity concentrations were found to be at the lowest in the control group and 400 µM Zn for all three species, and at the highest level at 25 µM Cd in general in the species. The order of radionuclides by the highest activity concentrations was 40K>238Uz232Th>137C, whereas the order of species was Gold tassel>Boxwood>Japanaese barberry. TF (232U, 232Th, 40K, and 137Cs) values were found to be between 0.583 and 0.998, between 0.604 and 1.036, between 0.555 and 1.057, and between 0.513 and 0.899. And also, while the order of species by the activity concentration was Gold tassel>Boxwood>Japanaese barberry the order of species by the TF values was Boxwood>Gold tassel>Japanaese barberry. In conclusion, plants' radionuclide activity concentrations were found to be at the highest level in 25 µM Cd group and at the lowest level in the control group. Considering all the data, it can be stated that a low dose of Cd was effective on the radioactivity concentrations and Gold tassel could be used as the indicator plant in radiation pollution.

**Keywords:** Cadmium, Zinc, Radioavtivity, Transfer factor

**Öz:** Bu çalışmada, kadın tuzluğu, şimşir ve altuni taflan bitkilerinde Cd ve Zn uygulamalarının radyoaktivite konsantrasyon değişiklikleri ve topraktan yaprağa taşınma faktörü üzerindeki etkileri gama ışını spektrometresi kullanılarak araştırılmıştır. İncelenen toprak örneklerinde radyonuklitlerin ortalama konsantrasyonları (Bq kg-1) 238U için 289.40±32.47, 232Th için 241.76±27.47, 40K için 783.63±83.46 ve R 137Cs için 31.44±5.63 olarak bulunurken, bitki türlerinde bu değerler sırası ile 168.6±20.1- 288.8±34.5, 145.9±19.1-250.3±32.4, 434.6±52.2-828.4±99.4, ve 16.1±1.8-28.3±3.3 (Bq kg-1) olarak bulunmuştur. Türlerde aktivite konsantrasyonları her üç bitki türünde kontrol grubu bitkilerde ve 400 µM Zn dozlarında en düşük ve 25 µM Cd dozunda ise genel olarak en yüksektir. Rayonuklitlerin en yüksek aktivite konsantrasyolarına göre sıralaması 40K>238Uz232Th>137C ve türlerin sıralaması ise Altuni taflan>Şimşir>Kadın tuzluğu olmuştur. Türlerde TF (232U, 232Th, 40K ve 137s) değerleri sırası ile 0.583-0.998, 0.604-1.036, 0.555-1.057 ve 0.513-0.899 arasında bulunmuştur. TF değerlerine göre radyonuklitlerin sıralaması 40K>232Th>238U>137Cs ve türlerin sıralaması ise Şimşir>Altuni taflan>Kadın tuzluğu şeklindedir. Sonuç olarak bitkilerde radyonuklit aktivite konsantrasyonları 25 µM Cd dozunda en yüksek, kontrol grubu bitkilerde ise en düşüktür. Tüm veriler göz önünde bulundurulduğunda düşük dozda Cd'ın radyoaktivite konsantrasyonlarında etkili olduğu ve Altuni taflanın radyasyon kirliliğinde indikatör bitki olarak kullanılabileceği söylenebilir.

**Anahtar Kelimeler:** Kadmiyum, Çinko, Radyoaktivite, Transfer faktörü

## 1. Introduction

As in other organisms, plants are inevitably subjected to radiation effect because the radioactive elements having a very long lifetime have created a natural radiation surface in the ecosystem throughout the history of the world [1]. However, the rapid development of industry, rapid growth of population, industrial and domestic wastes caused by unplanned urbanization, and mining and nuclear energy wastes do cause and have caused radiation pollution in air, water, and soil. Moreover, fossil fuels, nitrogenous fertilizer industry, and synthetic fertilizer technology might cause the release of natural radionuclides into the environment [1, 2]. Natural radiation sources consist of natural radionuclides naturally existing in nature such as 238U, 232Th, and 40K and the 238U and 232Th degradation series products (226Ra and 222Rn), while the artificial radionuclides such as 90Sr, 137Cs, and 131I are released to the environment through nuclear accidents and nuclear weapon trials [3, 4]. Natural and artificial radionuclides bind to the inorganic matter in soil and sediments through

air and water and accumulate in herbal tissues via the roots. Moreover, radionuclides accumulating in aerosols from the atmosphere might penetrate the plant tissues via leaves and barks [3, 5]. Intake of radionuclides from soil to the plant is defined as transfer factor (TF) and it varies depending on soil characteristics such as pH, clay mineral, Ca, K, and organic matter content [6, 7], leaf characteristics of plants, developmental status of organs, and plant species [8], and climatic parameters such as wind speed, precipitation, and humidity [6-9]. Radionuclides' activity concentrations in plant tissues might vary depending on plant genotype and developmental status of organs, as well as the concentration of radionuclides and their chemical behaviors [10]. In literature, it was emphasized that plants took large amount of 40K and 226Ra, low amount of 238U2u, and very low amount of 232Th from the soil [7, 11]. In plants, it was reported that the intake of 40K and 137Cs occurJapanaesethrough the same mechanism as fundamental element K that 40K and K+ were analogous and 238U and 226Ra were analogous to Ca, and that concentrations of 40K and 232U in plant tissues might be higher than those of other radionuclides. Besides that, it is also asserted that application of phosphatic fertilizers increased the 238U activity concentration in soil and plant tissues [12]. Until now, in studies on the effects of heavy metal stress in plants, the changes in the amount of necessary molecules in plant growth and development such as photosynthetic pigments, nitrogenous compounds, carbonaceous compounds, secondary metabolites [13], enzymatic and non-enzymatic defense systems [14, 15] and nutrients have been investigated [16, 17]. And also, radioactivity measurements were performed on organs of many plant species such as leaf, stem, and flower [11, 15, 18], various food sources [19, 20], mushrooms [21], soils [2, 22] and water samples [23] from different regions, in Turkey. However, there is no study carried out on the effects of heavy metal stress on the radionuclide activity concentrations in plant leaves. In the present study, it was aimed to investigate the capacity of Cd and Zn treatments to accumulate 238U, 232Th, 40K, and 137Cs radionuclides in Japanaesebarberry, Boxwood, and Gold tassel plant species widely grown in parks, gardens, and roadsides in the city center of Kastamonu.

## 2. Material and Method

In the present study, 2-year-old Japanaesebarberry (*Berberis thunbergii* DC. var. *atropurpurea* Chenault), Boxwood (*Buxus sempervirens* L. var. *rotundifolia* Baill.), and Golden Tassel (*Euonymus japonicus* Thunb. var. *aureomarginatus* Rehder) plants obtained from Kastamonu Municipality's Department of Parks and Gardens were used. Plants were removed out of the plastic tubes, in which they were grown (S1), and planted into 5L pots containing turf and garden soil (Soil 2; 2:1) and irrigated for 4 weeks by using tap water. Then, the plants were grouped as control, cadmium (Cd: 25 µM and 50 µM-$CdSO_4H_2O$), and zinc (Zn: 200 µM and 400 µM-$ZnCl_2$) and they were subjected to metal stress applications by using soil (300 ml) depending on the water retention capacity of soil. The concentrations determined for Cd and Zn were dissolved in Hoagland-Arnon's nutrient solution. While the plants in the control group were given only the nutrient solution, the metal stress application was performed using with the nutrient solution. Metal stress application on plants was performed for 8 weeks (twice a week).

### Characteristics of soil samples used in the experiment

pH value of soil samples (S1, S2) was found to range between 6.88 and 6.96 and that of irrigation water was found to be 8.60. Of the soil samples used, K, P, S, Mg, and Ca contents (mg $kg^{-1}$) were found to vary between 27540- 29681, between 5195-3228, between 3074-2712, between 12950-17580, and between 111700- 27880, respectively (Table 1). Fe, Mn, Cu, Zn, Ni, and Cd contents were found to range between 34960- 38490, between 460.5- 709.2, between 36.8- 37, between 71- 80.7, between 58.8 - 74.80, and between 0.41-3.45 (Table 1).

**Table 1.** Characteristics of soil mixture used in the experiments

| | pH | K | P | S | Mg | Ca | Fe | Mn | Cu | Zn | Ni | Cd |
|---|---|---|---|---|---|---|---|---|---|---|---|---|
| S1 | 6.88 | 27540±30 | 5195±2.8 | 3074±3 | 12950±60 | 111700±100 | 34960±30 | 460.5±2.0 | 36.8±0.7 | 71±0.7 | 58.8±20.6 | 3.45±0.3 |
| S2 | 6.96 | 29681±6.5 | 3228 ±2.4 | 2712 ± | 17580 ± | 27880± 32 | 38490 ±30 | 709.2 ±1.8 | 37 ±0.6 | 80.7±1.4 | 74.80± 1.1 | 0.41 ±0.1 |
| W | 8.60 | 2894±4.7 | 11.96±0.3 | - | 15951±60 | 14782.86±60 | 7.82±0.4 | 0.322± | 20.24±0.4 | 14.70±0.8 | 10.23± | 1.63±0.1 |

### Preparation of leaf and soil samples for the radioactivity measurements

Leaf samples harvested from the plants were dried in an environment without direct sunlight exposure. The samples were kept in a drying oven at 85°C for 24 hours and then pulverized using a blender. The soil samples used in the experiment were dried at room temperature and then pulverized using the laboratory blender. In order to ensure the homogeneity of samples, they were passed through a sieve with 80 Mesh and left for drying in a drying oven at 85°C temperature for 48 hours.

**pH measurements in soil samples**

pH values of samples were determined using the method of Gülçur [24]. The samples were kept in 1/2.5 pure water for 24 hours and the pH was measured using a digital pH-meter.

**Elemental analysis of soil and leaf samples**

Some of the dried soil and leaf samples were used in the elemental analysis in Kastamonu University's Central Research Laboratory by using SPECTRO brand XEPOS model XRF device. Some of samples were put into polyethylene containers with 6 cm diameter and 5 cm height and the lids were closed tightly. In order for samples to reach radioactive balance, they were kept for 1 month [11].

**Method for the activity concentrations of radionuclides**

Gamma-ray spectrometry was performed with FoodGuard-1 3 x 3-inch NaI (Tl) model radiation detector (ORTEC, Oak Ridge, USA) in the Central Research Laboratory of Kastamonu University. The ground leaves were placed into plastic boxes having a diameter of 8 cm and a height of 8 cm and designed to fit the geometry of the detector. Then, the boxes were tightly closed and kept for 1 month. Thus, the formation of radioactive equilibrium between $^{238}$U and $^{232}$Th and their decay products was allowed and the samples were prepared for counting. The detector was calibrated before the analysis. To analyze the spectra collected in computer memory, the channel corresponding to the input energy must be known. Thus, the types of radioactive nuclei present in the sample can be found. To accomplish the energy calibration, a standard source(s) consisting of nuclei with previous energies is needed. Standard point sources including the peaks of $^{109}$Cd, $^{57}$Co, $^{133}$Ba, $^{22}$Na, $^{137}$Cs, $^{54}$Mn, and $^{60}$Co, with energies ranging between 80 and 1400 keV were used for the calibration. After the calibration, each sample was counted in the gamma spectrometer for 50000 sec. Activities of radionuclides obtained at end of the measurements were determined using the following equation:

$$\textbf{Activity} = \frac{\textbf{Net area}}{\textbf{Counting time} \times \textbf{Sample amount} \times \textbf{Abundance} \times \textbf{Yield}} \quad (1)$$

The net areas under the peaks were calculated by subtracting the background from the total area. The radioactivity concentrations of $^{238}$U, $^{232}$Th, $^{40}$K, and $^{137}$Cs in the samples were determined by making use of the gamma peaks of natural radionuclides, which were the degradation products of these radionuclides. After determining the activity concentrations of $^{238}$U, $^{232}$Th, and $^{40}$K, the activity concentration of $^{137}$Cs isotope in the samples was also determined. The activity concentrations of radionuclides ($^{238}$U, $^{232}$Th, $^{40}$K, and $^{137}$Cs) were expressed as Bq kg$^{-1}$ dry weight.

**Calculation of Transfer Factor**

The rate of radionuclides, which are present in the soil, to transfer from the plant tissues is named transfer factor (TF). Using the equation given below, TF values were calculated with the mean radionuclide activity concentrations found in the leaves of Red barberry, Boxwood, and Gold tassel plants and the soil samples used in growing the plants [11, 25].

$$\text{TF=Activity concentration of plant (Bq kg}^{-1}\text{)/Activity concentration of soil (Bq kg}^{-1}\text{)} \quad (2)$$

**3. Result and Discussion**

Plants illustrate an important link in the transport and distribution of radionuclides and other pollutants in the environment and are often consideJapanaeseas biomonitors of atmospheric pollution [3, 6,7, 15]. Naturally occurring and fallout radionuclides were investigated in samples of Japanaese barberry, Boxwood, and Golden tassel plants.

**Changes in 238U, 232Th, 40K, and 137Cs activity in soil samples**

The elemental contents of soil samples used in growing the plants are presented in Table 1. The mean values found in the soil samples were 289.40±32.47 for 238U activity concentration, 241.76±27.47 for 232Th activity concentration, 783.63±83.46 for 40K activity concentration, and da 31.44±5.63 for 137Cs activity concentration (Table 2). The 238U, 232Th, 40K, and 137Cs activity concentrations of the tap water used in the experiment were 1.48±0.1, 1.17±0.1, 2.65±0.3, and 0.42±0.04, respectively (Table 2). Study results were found to overlap with the activity concentrations reported by Kaya et al. [22] for the soil samples collected from different regions of Gümüşhane province. Researchers found the 232Th, 40K, and 137Cs activity concentrations in the soil samples to range between 9.7±1.15 and 32.52±2.65, between 236.83±7.53 and 889.65±17.63, and between 7.63±1.26 and 39.44±8.57. In another study, Adesiji & Ademola [25] found the 238U, 232Th, and 40K activity concentrations of soil samples they used in growing corn plant to be in the range of 242.13 ± 429.10-2763.90 ± 2345.77, 15294.77 ± 6924.46-26211.90 ± 7178.22, and 374.01 ± 590.51-5008.18 ± 2427.165 Bqkg-1, respectively, and those values are much higher than the results achieved in the present study. 40K activity

concentration was similar to the value reported by Bilgici Cengiz et al. [2-20] (245.6±34.6 Bqkg-1 and 814.2±35.7 Bqkg-1) but 232Th (22.2±6.8-44.6±7.5 Bqkg-1) activity concentration was much lower than the value found in the present study.

**Table 2.** Radioactivity concentration changes in the soil samples used in the experiment

| | $^{238}$U | $^{232}$Th | $^{40}$K | $^{137}$Cs |
|---|---|---|---|---|
| Soil 1 | 236.35±26.20 | 196.87±16.60 | 678.64±68.52 | 22.44±2.70 |
| Soil 2 | 322.45±38.73 | 286.64±38.33 | 876.62±98.40 | 38.44±8.56 |
| Mean | 289.40±32.47 | 241.76±27.47 | 783.63±83.46 | 31.44±5.63 |
| Water | 1.48±0.1 | 1.17±0.1 | 2.65±0.3 | 0.42±0.04 |

137Cs activity concentration found in the present study was confirmed by the results achieved by Lamarque et al. [26] (0-5 cm: 61-280 Bqkg$^{-1}$; 10-15 cm: 14-224 Bq kg$^{-1}$). But Absar et al. [27] reported the 232Th, 40K, and 137Cs activity concentrations in soil to be in the ranges of 50 ±19-65± 21, 245 ±30-635 ±35, and 137Cs 3±1-9±1, respectively. In the present study, 232Th and 137Cs values were lower than those values but 40K was found to be in a similar range.

**Radionuclide activity concentration changes in plant samples**

The activity concentrations for 238U, 232Th, 40K, and 137Cs radionuclides found in leaves of Japanaese barberry, Boxwood, and Gold tassel plants subjected to Cd and Zn application are presented in Table 3. Given the results, although the activity concentrations of those radionuclides varied by the species and concentration, radioactivity concentrations were found to be higher than in control for all three plants (Table 3).

**238U activity concentration changes and TF values in plants subjected to Cd and Zn**

238U, a natural radionuclide, exists in nature generally in form of uranium minerals with elements such as Ca, Mg, and P. Since it has low solubility in soil solution, its intake by the plants is also at a low level. However, since its chemical behavior is similar to that of Ca, it was reported to have positive effects on metabolic reactions, in which Ca is effective [6, 12, 26]. In the present study, 238U activity concentrations found in leaves of Red barberry, Boxwood, and Gold tassel were found to be 168.6±20.1-223.7±26.4 1 Bq kg$^{-1}$, 171.0±20.6-265.9±31.7 1 Bq kg$^{-1}$, and 176.5±21.2-288.8±34.5 Bq kg$^{-1}$ (Table 3). In comparison to the control group, the highest level of 238U activity concentration was found at 25 µM Cd dose in all three species. The lowest activity concentration was found in the control group plants. The second-highest activity concentration was achieved at 50 µM Cd dose for Red barberry and Gold tassel leaves and 200 µM Cd dose for Boxwood leaves (Table 3). Among the plant species, the highest 238U activity concentrations were found in Gold tassel leaves and with Cd doses (288.8±34.5; 270.1±32.1 Bq kg$^{-1}$), whereas the lowest activity concentration was found in the control group samples of Red barberry leaves (168.6±20.1 Bq kg$^{-1}$). 238U accumulation capacities of plants were found to be Gold tassel>Boxwood>Red barberry. In these plants, TF (238U) value was reported to be 0.583-0.773 for Red barberry, 0.591-0.919 for Boxwood, and 0.610-0.998 for Gold tassel. In comparison to the control group, the highest TF value was achieved at 25 µM Cd dose for all three plants. TF values reached the maximum levels in Red barberry and Gold tassel leaves with Cd doses and in Boxwood leaves with 25 µM Cd and 200 µM Zn doses (Table 3).

**Table 3.** Effects of Cd (25 µM and 50 µM) and Zn (200 µM and 400 µM) applications on 238U and 232Th activity concentrations and TF changes in Red barberry, Boxwood, and Gold leaves (Bq kg$^{-1}$)

| Plant | Group | 238U | 232Th | 238U | 232Th |
|---|---|---|---|---|---|
| Japanaese barberry | Control | 168.6±20.1 | 148.0±19.1 | 0.583 | 0.612 |
| | 25 µM Cd | 223.7±26.4 | 232.5±30.1 | 0.773 | 0.962 |
| | 50 µM Cd | 214.5±25.3 | 173.4±22.4 | 0.742 | 0.718 |
| | 200 µM Zn | 198.2±23.4 | 218.1±28.1 | 0.685 | 0.903 |
| | 400 µM Zn | 184.7±22.1 | 168.5±21.7 | 0.638 | 0.697 |
| Boxwood | Control | 171.0±20.6 | 151.9±19.6 | 0.591 | 0.628 |
| | 25 µM Cd | 265.9±31.7 | 244.2±31.4 | 0.919 | 1.010 |
| | 50 µM Cd | 217.8±26.2 | 179.4±23.3 | 0.753 | 0.742 |
| | 200 µM Zn | 245.4±29.4 | 211.9±27.4 | 0.848 | 0.877 |
| | 400 µM Zn | 200.9±24.3 | 167.7±21.6 | 0.695 | 0.694 |
| Gold tassel | Control | 176.5±21.2 | 145.9±19.1 | 0.610 | 0.604 |
| | 25 µM Cd | 288.8±34.5 | 250.3±32.4 | 0.998 | 1.036 |
| | 50 µM Cd | 270.1±32.1 | 211.7±27.3 | 0.933 | 0.876 |
| | 200 µM Zn | 259.1±31.5 | 222.0±28.6 | 0.896 | 0.919 |
| | 400 µM Zn | 201.4±24.7 | 161.6±21.0 | 0.696 | 0.669 |

The 238U activity concentration found in the present study was higher in comparison to the results reported in the literature. Examining several tree species and epiphyte plants, Manigandan et al. [4] reported the mean 238U activity concentration to range between 9.6 ± 0.4 and 11.4 ± 0.4 and TF value to range between 0.249 and 0.313. However, Tshivhase et al. [28] reported the 238U activity concentration to be 31.36±9.40, 0.02±0.01, and 0.16 ±0.14 Bq $kg^{-1}$ and TF value to be 0.19±0.06, 0.307±0.89, and 0.11±0.01 Bq $kg^{-1}$, respectively. In the present study, the finding that 238U activity concentration in experimental groups was higher than in the control group was related to the P concentration in soil and low Cd and Zn doses stimulating the 238U absorption of species. In literature, it was reported that the mean P concentration in soil was 500-800 mg $kg^{-1}$, that P values in soils in Turkey ranged between 146.2 and 3125 mg $kg^{-1}$, and that the P concentration required for plant was 0.3-3 kg $ha^{-1}$ [29, 30].

**232Th activity concentration changes in plants treated with Cd and Zn**

232Th activity concentration was found to be within the ranges of 148.0±19.1-232.5±30.1 Bq $kg^{-1}$ in Japanaese barberry leaves, 151.9±19.6-244.2±31.4 Bq $kg^{-1}$ in Boxwood leaves, and 145.9±19.1-250.3±32.4 Bq $kg^{-1}$ in Gold tassel leaves. In the control group plants, the highest activity concentration was achieved in Boxwood leaves and in Gold tassel. 232Th activity concentrations that were the highest in comparison to the control group were observed at 25 µM Cd and 200 µM Zn doses for all three species. Among the plant species, the highest 232h activity concentration was found in Gold tassel leaves (250.3 ± 32.4 Bq $kg^{-1}$) and the lowest one in Gold tassel control group (145.9 ± 19.1 Bq $kg^{-1}$). In the samples, TF(232Th) values were in the ranges of 0.612-0.962 for Japanaese barberry leaves, 0.628-1.010 for Boxwood leaves, and 0.604-1.036 for Gold tassel leaves. TF values were generally at the highest levels in low Cd and Zn doses (Table 3). 232Th activity concentration changes achieved in the present study overlapped with the results reported by Adesiji & Ademola [25]. Examining two different corn leaves which they grew in two different soil samples, researchers reported the 232Th activity concentration to vary between 238.05 ± 64.64 and 826.37 ±1182.03 Bq $kg^{-1}$, activity concentration in soil samples to range between 1776.08 ± 4164.89 and 26211.90 ± 7178.22 Bq $kg^{-1}$, and TF value to range between 0.02 ± 1.27 and 0.08 ± 3.70. However, Chakraborty et al. [31] examining grass and Bilgici Cengiz & Çağlar [32] analyzing 45 wheat flour samples reported 232Th activity concentration values that were much lower than in the present study. Similarly, Absar et al. [27] reported the 232Th activity concentration of tea plant leaves to be 2.4 ±0.5-5.8 ±0.9 Bq $kg^{-1}$ and that of soil to be 50±13-63±5 Bq $kg^{-1}$, whereas TF (232Th) was found to be 0.05±0.04. Bilgici Cengic & Çağlar [20] analyzed various herbs widely used in the Eastern Anatolian region and reported the 232Th activity concentration to be 55.99±4.32 Bq $kg^{-1}$ and TF value to be 0.88.

**40K activity concentration changes in plants treated with Cd and Zn**

40K activity concentration was found to be 434.6±52.2-536.2±64.3 Bq $kg^{-1}$ in Japanaesebarberry leaves, 529.8±63.6-828.4±99.4 Bq $kg^{-1}$ in Boxwood leaves, and 534.9±64.2-821.4±98.6 Bq $kg^{-1}$ in Gold tassel leaves. In comparison to the control group, the highest activity concentration was found to be 828.4±99.4 in Boxwood leaves treated with 25 µM Cd, followed by Gold tassel leaves treated with 200 µM Zn (821.4 ± 98.6 Bq $kg^{-1}$). The lowest activity concentration was found in the control group Japanaese barberry leaves, followed by Japanaese barberry leaves treated with 400 µM Zn (Table 4). Similar to 232Th activity concentration, 40K activity concentration reached the highest levels with low Cd and Zn doses. Among the plants, the highest activity concentration was found in 40K and the order of plants was found to be Boxwood > Gold tassel >Japanaese barberry (Table 3). TF(40K) values were found to range between 0.555 and 0.685 in Japanaese barberry leaves, between 0.676 and 1.057 in Boxwood leaves, and between 0.683 and 1.048 in Gold tassel leaves. TF (4K) was found to be high in low Cd and Zn treatments in comparison to the control group and other treatments and the highest value was found in Boxwood leaves. Besides that, the order of species by the TF (40) values was Gold tassel>Boxwood>Japanaese barberry (Table 3). The 40K activity concentrations found in plants are in corroboration with the literature. $^{40}K$ is a naturally rich radionuclide in plants. The fact that we found high concentrations of 40K in the leaves of sample plants is not surprising given that plants obtain their nutrients and water through root uptake from the soil, in which there are high 40K concentrations. The amount of potassium in plants is high because of its essential role in most physiological processes needed to maintain plant growth and development. Potassium has an important role in photosynthesis, translocation of starches and sugars, plant-water relations, protein synthesis, activation of plant enzymes, resistance to plant diseases [8, 29]. Similar results were reported in the studies examining the herbaceous and woody plants [7, 15, 27]. Manigandan et al. [3] reported the 40K activity concentration in some plant species grown in rain forests of India to vary between 160.4 ± 12.3 and 206.4 ± 13.4 Bq $kg^{-1}$ and TF value to vary between 0.802 and 0.954. Similar to the present study, Shayeb et al. [33] determined the 40K activity concentration in date samples to be 181 ± 17 Bq $kg^{-1}$, the activity concentration in soil samples to be 329 ± 87 Bq $kg^{-1}$, and TF value to be 0.51 ± 2.0. In another study examining the medicinal plants used in traditional medicine in Thailand, the mean 40K activity concentration was found to be 610±260 Bq $kg^{-1}$ and TF value to be 2.0±1.4 and it was determined that the activity concentration was at a higher level in leaves in comparison to flowers and stem Saenboonruang et al. [7]. In their study carried out on forests in Southwestern Serbia region, Hadrović et al. [34] reported the 40K activity concentration of evergreen species to be 102 ± 25 Bq $kg^{-1}$, that of non-evergreen species to be 140 ± 26 Bq $kg^{-1}$, and that of samples from the soil, where the plants were grown, to be 62±5-970±60 Bq $kg^{-1}$. TF (40K) was found to be 0.022-0.22 in non-evergreen species and 0.007-0.19 in coniferous species. Much higher level of 40K activity concentrations in soil and plant tissues in comparison to other

radionuclides was related to the chemical behaviors of 40K and essential element K+. Researchers reported that the intakes of $K^+$ and 40K occurJapanaesethrough similar mechanisms and their roles in metabolic reactions were also the same [8, 29, 35].

**137Cs activity concentration changes in plants treated with Cd and Zn**

The 137Cs activity concentration changes found in the plant samples were in the ranges 16.1±1.8-26.2±3.1 Bq $kg^{-1}$ in Japanaesebarberry leaves, 17.7±2.3-26.3±3.2 Bq $kg^{-1}$ in Boxwood leaves, and 17.3±2.1-28.3±3.3 Bq $kg^{-1}$ in Gold tassel leaves (Table 4). The highest activity concentration was found at 200 μM Zn dose in Golden Tassel (28.3±3.3 Bq $kg^{-1}$) leaves, followed by 25 μM Cd dose in Japanaese barberry (26.3 ± 3.2 Bq $kg^{-1}$) and Gold tassel leaves (26.3±3.2 Bq $kg^{-1}$). 137Cs activity concentration was found to be higher in Boxwood and Gold tassel leaves at 25 μM Cd and 200 μM Zn doses, whereas it was high in Japanaese barberry leaves at Cd (25-50 μM) doses. The lowest activity concentration in plants was found in 137Cs radionuclide and the order of plants by this parameter was found to be Gold tassel>Boxwood>Japanaese barberry (Table 4).

TF (137Cs) values were found to be between 0.550 and 0.899 in Japanaese barberry, 0.563 and 0.836 in Boxwood, and 0.513 and 0.835 in Gold tassel leaves. TF (137Cs) was found to be high at low Cd and Zn doses in the first two species and at Cd doses in Gold tassel leaves. The order of species by TF value was Japanaese barberry>Boxwood>Gold tassel (Table 4). 137Cs activity concentration data were in corroboration with the literature. In previous studies, the lowest activity concentration in soil and plant organs was reported to belong to 137Cs [36]. Lamarque et al. [26] monitoJapanaesethe seasonal activity concentration changes of 137Cs in *Fagus sylvatica* and *Picea abies* grown in forests, which were polluted because of the Chernobyl disaster, in Franche-Comté region in Northeastern France. Researchers determined that 137Cs activity concentration in soil samples ranged between 61 and 280 Bq $kg^{-1}$ (0-5 cm) and between 14 and 224 Bq $kg^{-1}$ (10-15 cm), that TF values in leaves varied seasonally, and that TF (137Cs) was 0.0074 for *F. sylvatica* and 0.0179 for *P. Abies*. Researchers also reported that there was no direct relationship between cesium activity in soil and cesium activity in plant organs and that it might be because the intake of 137Cs might have occurJapanaesethrough roots from the soil and through leaves from aerosols in the air. 137Cs activity concentrations in soil and grass in Bangladesh were reported to be 0.17 ± 0.02 Bq $kg^{-1}$ and 2.41 ± 0.18 Bq $kg^{-1}$, respectively, whereas TF value was found to be 0.061 [31]. Shayeb et al. [34] compaJapanaesethe 137Cs activity concentrations in date and soil samples collected from different regions of Saudi Arabia and they reported the activity in soil to be 10.2 ± 2.1 Bq $kg^{-1}$ and the activity in date samples to be below the limit of detector. In a study carried out using tea leaves, 137Cs activity concentration was found to be <0.4 Bq $kg^{-1}$ in the leaves and 3±1-10±1 Bq $kg^{-1}$ in the soils, whereas TF (137Cs) was found to be belwo the limit of detector [4]. Hadrović e al. [34] examining the 137Cs activity concentration in forests of Southwestern Serbia reported the 137Cs activity concentration to be 4.9 ± 7.1 Bq $kg^{-1}$ in some non-evergreen species and 5.9 ± 4.8 Bq $kg^{-1}$ in evergreen samples.

**Table 4.** Effects of Cd (25 μM and 50 μM) and Zn (200 μM and 400 μM) treatments on 40K and 137Cs activity concentration and TF changes in Red barberry, Boxwood, and Gold leaves (Bq $kg^{-1}$)

| Plant | Group | 40K | 137Cs | 40K | 137Cs |
|---|---|---|---|---|---|
| Red barberry | Control | 434.6±52.2 | 16.1±1.8 | 0.555 | 0.550 |
| | 25 μM Cd | 536.2±64.3 | 26.2±3.1 | 0.685 | 0.836 |
| | 50 μM Cd | 492.9±59.1 | 19.1±2.3 | 0.629 | 0.835 |
| | 200 μM Zn | 520.3±62.4 | 18.7±2.4 | 0.664 | 0.899 |
| | 400 μM Zn | 454.6±54.6 | 18.1±2.2 | 0.580 | 0.630 |
| Boxwod | Control | 529.8±63.6 | 17.7±2.3 | 0.676 | 0.563 |
| | 25 μM Cd | 828.4±99.4 | 26.3±3.2 | 1.057 | 0.836 |
| | 50 μM Cd | 643.9±77.3 | 20.2±2.4 | 0.822 | 0.641 |
| | 200 μM Zn | 745.1±89.4 | 23.7±2.6 | 0.951 | 0.753 |
| | 400 μM Zn | 581.7±69.8 | 19.6±2.5 | 0.743 | 0.624 |
| Gold tassel | Control | 534.9±64.2 | 17.3±2.1 | 0.683 | 0.513 |
| | 25 μM Cd | 804.8±96.6 | 26.3±3.2 | 1.027 | 0.835 |
| | 50 μM Cd | 792.6±95.1 | 26.2±3.2 | 1.012 | 0.608 |
| | 200 μM Zn | 821.4±98.6 | 28.3±3.3 | 1.048 | 0.595 |
| | 400 μM Zn | 584.3±70.1 | 19.8±2.5 | 0.746 | 0.575 |

TF (137Cs) was found to be 5.2 in non-evergreen trees and in the range between 0.021 and 0.18 in coniferous species and activity concentration and TF values were found to be at the highest in leaves. Researchers reported that 137Cs intake of plants occur Japanaese through the same mechanism as $K^+$ intake and it accumulated more in leaves as with the K. Moreover, it was claimed that the plants with larger leaf surface area genes need $K^+$ element more because of higher transpiration, stomal conductivity, and photosynthetic activity and, thus, more 40K and 137Cs might accumulate in the

plants having larger leaf surface area [8, 36]. Depending on the activity concentrations of radionuclides and the changes in TF, the order of plants by the (1) activity concentration was Gold tassel>Boxwood>Japanaese barberry and the order by TF values was Boxwood>Gold tassel>Japanaese barberry and that (2) 25 µM Cd and 200 µM Zn doses yielded the highest radionuclide activity concentration and TF values. It suggests that, regarding the order of species by TF and activity concentrations, leaf characteristics were also important as well as the factor genotype. The larger leaves of Gold tassel in comparison to other two species might increase the competition for radionuclide absorption from both soil and air. Boxwood leaves have also larger surface areas when compaJapanaeseto Japanaesebarberry leaves. High 40K and 238U activity concentrations in both species confirm this conclusion. The plants having more aboveground volume have higher transpiration, hydrolytic resistance, and stoma activity and these plants necessitate more $K^+$ and $Ca^+$ elements. K+ plays important roles in stoma movements, as well as controlling the events of osmosis and turgor [29], while Ca has a specific importance in strengthening the cell wall [37, 38]. In literature, it was reported that 40K was analogous to essential element $K^+$ and 238U was analogous to $Ca^+$ [ 26, 36, 38]. The higher activity concentrations and TF values at lower doses were related to the possibility that low doses of (Cd-Zn) metals might stimulate the radionuclide absorption. It was stated that Cd was a very mobile element and, thus, rate of its transfer from soil to plant and its speed of transfer within the plant were high [37, 38, 39].

## 4. Conclusions

In the present study, in which the effects of Cd and Zn treatments on 238U, 232Th, 40K, and 137Cs activity concentrations and TF values of Japanaese barberry, Boxwood, and Gold tassel plants were examined, it was revealed that activity concentrations varied depending on plant species, metal species, and concentration. In all three species, the radionuclide activity concentrations were found to be at the lowest levels in the control group and 400 µM Zn groups, whereas the 25 µM Cd dose generally yielded the highest level. 238U and 232Th activity concentrations in Gold tassel (25 µM Cd), 40K activity concentration Boxwood (25 µM Cd), and 137Cs activity concentration in Gold tassel (400µM Zn) were found to be the highest ones in comparison to the control and other groups. Among the control group plants, the lowest activity concentrations were found in Japanaese barberry (23U, 40K, 137Cs) and Gold tassel (232Th) leaves, whereas the order of radionuclides by the highest activity concentrations was 40K>238Uz>232Th>137C and that of species by the highest radionuclide activity concentration was Gold tassel>Boxwood>Japanaese barberry. Similar to the activity concentration results, TF values of species were found to be at lower levels in control group plants. The lowest TF values were found in Japanaese barberry leaves for TF (238U) and TF (40K) and in Gold tassel leaves for TF (232Th) and TF (137C). The highest TF (238), TF (232Th), and TF (40K) were obtained at 25 µM Cd dose and the highest TF (137Cs) was achieved at 200 µM Zn dose. The order of radionuclides by the highest TF values 40K>232Th>238U>137Cs and that of species was Boxwood>Gold tassel>Japanaese barberry. Given the results obtained, it can be stated that low doses of Cd and Zn might increase the radioactivity concentrations and that Gold tassel and Boxwood plants could be used as an indicator regarding the radiation pollution.

## Competing Interest / Conflict of Interest

The authors declare that they have no competing interests.

## Author Contribution

We declare that all Authors equally contribute.

## Availability of data and material:

The datasets obtained from this study are available from the corresponding author on reasonable request.

**Competing interests:** The authors declare no competing interests.

**Funding:** There is no financial support and commercial support.

## 5. References

[1] Isinkaralar, K. (2022). Some atmospheric trace metals deposition in selected trees as a possible biomonitor. Romanian Biotechnological, 27(1), 3227-3236.

[2] Bilgici Cengiz, G., & Çağlar, İ. (2019). Determination of natural radioactivity concentrations of some fertilizers used in Eastern Anatolia of Turkey. Caucasian Journal of Science, 6(2), 147-155.

[3] Manigandan, P.K., & Chandar Shekar, B. (2014). Uptake of some radionuclides by woody plants growing in the rainforest of Western Ghats in India. Journal of Environment Rdioactivity, 130,63-67.

[4] Manigandan, P.K., & Chandar Shekar, B. (2015). Leaves of Woody Plants As Bio-İndicators Of Radionuclides In Forest Ecosystems. Journal of Radioanalytical and Nuclear Chemistry, 303, 911-917.

[5] Kılıç, Ö., Belivermiş, M., Topcuoğlu, S., Çotuk, Y., Coşkun, M., Çayır, A., & Küçer, R. (2008). Radioactivity concentrations and dose assessment in surface soil samples from East and South of Marmara region Turkey. Radiation Protection Dosimetry, 128 (3), 324-330.

[6] Kumar, A., Sınghal, R.K., Preetha, J., Rupali, K., Naravanan, U., Suresh, S., Mıshra, M.K., & Ranade, A.K. (2008). Impact of tropical ecosystem on the migrational behaviour of K-40, Cs-137, Th-232 U-238 in perennial plants. Water, Air, and Soil Pollution 192(1-4), 293-302.

[7] Saenboonruang, K., Phonchanthuek, E., & Prasandee, K. (2018). Soil-to-Plant Transfer Factors of Natural Radionuclides (226Ra and 40K) in Selected Thai Medicinal Plants. Journal of Environmental Radioactivity, 184-185, 1-5.

[8] Bréda, N. (2008). Leaf Area Index. Encycl. Ecol. 2148-2154.

[9] Doi, T., Masumoto, K., Toyoda, A., Tanaka, A., Shibata, Y., Hirose K. (2013). Anthropogenic radionuclides in the atmosphere observed at Tsukuba: Characteristics of the radionuclides derived from Fukushima. Journal of Environmental Raioactivitiy, 122,55-62.

[10] Chandrashekara, K., & Somashekarappa, H. (2015). Soil to plant transfer factors of radionuclides in *Ficus racemosa* (L.): A medicinal plant. International Research Journal of Biological Sciences, 4(9), 43-47.

[11] Özden, S., & Aközcan, S. (2020). Determınatıon of radıonuclıde transfer in sunflower on agrıcultural lands in Kırklareli. Kırklareli University Journal of Engineering and Science, 6(2),153-16.

[12] Bramki, A., Ramdhane, M., Benrachi, F. (2018). Natural radioelement concentrations in fertilizers and the soil of the Mila Region of Algeria. Journal of Radiation Research and Applied Sciences, (11),49-55.

[13] Chen, S., Wang, Q., Lu, H, Li, J., Yang, D., Liu, J., Yan, C. (2019). Phenolic Metabolism and Related Heavy Metal Tolerance Mechanism in *Kandelia obovata* under Cd and Zn Stress. Ecotoxicology And Environmental Safety, 169,134-143.

[14] Kandziora-Ciupa, M., Ciepał, R., Nadgo´rska-Socha, A., & Barczyk, G. (2016). Accumulation of heavy metals and antioxidant responses in *Pinus sylvestris* L. Needles in Polluted and non-Polluted Sites. Ecotoxicology, 25,70-981.

[15] Turfan, N., Kunaz, A., & Sarıyıldız, T. (2021). Effect of air pollution on element profile and radioactive compounds in six tree species. Tree and Forest *2*(2),82-92.

[16] Saleh, E.A.A., & Işınkaralar, Ö. (2022). Analysis of trace elements accumulation in some landscape plants as an indicator of pollution in an urban environment: Case of Ankara. Kastamonu University Journal of Engineering and Sciences, 8(1)1-5.

[17] Karakeçi, H., Kaya, Ö.F., Çelik, T.H. (2021). An Investigation on heavy metal pb, zn, cu, ni and cd accumulation in leaves of *Robinia Pseudoacacia* L. "Umbraculifera" arising from motor vehicles. Kastamonu University Journal of Engineering and Sciences 7(2)114-126.

[18] Kılıç, Ö. (2012). Bıomonıtorıng of 137Cs, 40K, 232Th, and 238U usıng oak bark in Belgrade Forest, Istanbul, Turkey. Nuclear Technolog and Radiation Orotection, 27(2),137-143.

[19] Kurnaz A., &Turfan N (2017). The effect of different storage conditions on the radiometric and element content of the Taşköprü garlic (*Allium sativum*). Turkish Journal of Agricultue-Food Science and Technology, *5*(4), 373-379.

[20] Bilgici Cengiz, G., & Çağlar, İ. (2022). Transfer Factors of Natural Radionuclides from Soil to Medicinal Plants Used by Local People in Eastern Anatolia, Turkey. International Journal of Environment and Geoinformatics, 9(2), 039-044.

[21] Pekşen, A., Kurnaz, A., Turfan, N., & Kibar, B. (2021). Determination of radioactivity levels in different mushroom species from Turkey. Yuzuncu Yil University Journal of Agricultural Science, 31(1), 30-41.

[22] Kaya, S., Karabıdak, S.M., & Çevik, U. (2015). Determination of natural (226ra, 232ta and 40k) and artificial (137cs) radioactivity concentrations in soil and moss samples collected from around Gümüşhane. Gümüşhane Unversity Journal of Science and Technology, 5 (1), 24-33.

[23] Kurnaz, A., Turhan, Ş., & Alzaridi, F.M.N.S. (2021). Radiological and physicochemical properties of drinking waters consumed in the Western Black Sea Region of Turkey. Journal of Radioanalytical Nuclear Chemistry, 328, 805-814.

[24] Gülçur, F. (1974). Physical and chemical analysis methods of soil. Istanbul University Faculty of Forestry Publications No: 201, Istanbul.

[25] Adesiji, N.E., & Ademola, J.A. (2019). Soil-to-maize Transfer Factor of Natural Radionuclides in a Tropical Ecosystem of Nigeria. Nigeria Journal of Pure & Applied Physics, 9(1),6-10.

[26] Lamarque, S., Lucot, E., & Badot, P.M. (2005). Soil-plant transfer of radiocaesium in weakly contaminated forest ecosystems. Radioprotection, 1(40),407-412.

[27] Absar, N., Abedin, J., Rahman, M.M., Miah, M.M.H., Siddique, N., Kamal, M., Chowdhury, M.I., Sulieman, A., Faruque, M.R.I., Khandaker, M.U., Bradley, D.A., & Alsubaie, A. (2021). Radionuclides transfer from soil to tea leaves and estimation of committed effective dose to the Bangladesh Populace. Life, 11, 282.

[28] Tshivhase, V.M., Njinga, R.L., Mathuthu, M., & Dlamini, T.C. (2015). Transfer rates of 238U and 232Th for *E. globulus, A. mear*nsii, *H. filipendula* and hazardous effects of the usage of medicinal plants from around gold mine dump environs. International Journal of Environmental Research and Public Health 12(12), 15782-15793.

[29] Marschner, H., & Marschner, P. (2012). Marschner's mineral nutrition of higher plants, 3rd ed. (San Diego, Elsevier Academic Press), 1-651.

[30] Mordoğan, N., Ceylan, Ş., Delibacak, S., Çakıcı, H., Günen, E., Pekcan, T., & Çolak, B. (2012). Effect of organic fertilization to nutrients content in soils cultivated olives. Journal of Adnan Menderes University Agricultural Faculty, 10(3),7-13.

[31] Chakraborty, S.R., Azim, R., Rahman, A.R., & Sarker, R. (2013). Radioactivity concentrations in soil and transfer factors of radionuclides from soil to grass and plants in the Chittagong City of Bangladesh. Journal of Physical Science, 24 (1), 95.

[32] Bilgici Cengiz, G., & Çaglar, İ. (2021). Determınatıon of the natural radıoactıvıty dıstrıbutıon and consumptıon effectıve dose rate ff cereal crops in Ardahan Provınce, Turkey. Journal of Scientific Reports-A, 47, 174-183.

[33] Shayeb MA, Alharbi T, Baloch MA, Rahman Alsamhan OA (2017). Transfer Factors for Natural Radioactivity into Date Palm Pits. Journal of Environmenta Radioactivity, 167,75-79.

[34] Hadrovıć, S.H., Čelıkovıć I.T., Krneta Nıkolıć, J.D., Rajačıć M.M., & Todorovıć, D.J. (2021). Radıonuclıdes' content in forest ecosystem located in southwestern part of Serbıa. Nuclear Technology and Radiation Protection, 36(2),192-196.

[35] Kant, S., Kant, P., & Kafkafi, U. (2005). Potassium uptake by higher plants: from field application to membrane transport. Acta Agronomica Hungarica, 53, 443-459.

[36] Wilkins, K.A., Matthus, E., Swarbreck, S. M., & Davies, J.M. (2016). Calcium Mediated Abiotic Stress Signaling in Roots. Frontie in Olant Sciences, 7,1296.

[37] Thury, Y., & Van Hess, M. (2008). Evolution of pH, organic matter and (226) Radium/calcium partitioning in U-mining debris following revegetation with pine trees. Science of the Total Environment, 393,111-117.

[38] Salt, D.E., & Wagner, R.J. (1993). Cadmium transport across the tonoplast of vesicles from oat roots evidence for a $Cd2^{+}/H^{+}$ antiport activity. Journal of Biological Chemistry, 268, 12297-12307.

[39] Kabata-Pendias, &A., Pendias, H. (2001). Trace elements in soils and plants. 3rd Edition, CRC Press, Boca Raton, 403 p.

doi:10.55385/kastamonujes.159789 KUJES 8(2):107-115, 2022

Kastamonu University
Journal of Engineering and Sciences
e-ISSN 2667-8209
http://dergipark.gov.tr/kastamonujes

# Synthesis, Spectroscopic Investigations, Thermal Analysis and DFT Calculations of Some Pentacarbonyl(Mercaptopyrimidine) Metal(0) Complexes of Group VI B Elements

**Özlem Ünlü[a], İzzet Amour Morkan[b*]**

[a] Department of Chemistry, Faculty of Arts and Science, Düzce University, Düzce, Türkiye
[b] Department of Chemistry, Faculty of Arts and Science, Bolu Abant İzzet Baysal University, Bolu, Türkiye
***Corresponding Author:** morkan_i@ibu.edu.tr

Received: **August 09, 2022** ◆ Accepted: **December 08, 2022** ◆ Published Online: **December 26, 2022**

**Abstract:** Pentacarbonyl-*N*-mercaptopyrimidinemetal(0) complexes of VIB metals (M: Cr, Mo, W) were formed when hexacarbonylmetal(0) complexes are treated photochemically with 4,6-dimethyl-2-mercaptopyrimidine at 10 ºC. The reported organometallic complexes were purified and isolated under an inert atmosphere. All $M(CO)_5L$ complexes were characterized in solution by FTIR-, $^1$H- and $^{13}$C-NMR spectroscopies. The FTIR spectroscopy results showed three absorption bands in the carbonyl region which indicates that the pentacarbonyl metal unit of the complexes has a local $C_{4v}$ symmetry. The $^1$H- and $^{13}$C-NMR spectroscopies showed that the mercaptopyrimidine ligand bonded to the metal complex through the mercaptopyrimidine-nitrogen atom symmetrically. The $^{13}$C-NMR spectroscopy results also showed a 1:4 ratio of two peaks in the CO-region, the ratio of the peaks proved the $C_{4v}$ symmetry of these complexes. The thermal behavior of these organometallic complexes is investigated by using DTA/TGA methods. The results of thermal analyses showed that the complexes decomposed at three different temperatures. The density functional theory (DFT) calculations were computed in B3PW91 formalism by Gaussian03W Software. The comparison of the experimental data with the theoretical values showed that the results obtained are compatible with each other. Thus, the accuracy of the experimentally given structural proposal of the obtained organometallic complex compounds was also confirmed through theoretical calculations.

**Keywords:** Mercaptopyrimidine, Photochemical synthesis, Metal carbonyls, Thermal analysis, DFT

**Öz:** VIB metallerinin (M: Cr, Mo, W) pentakarbonil-N-merkaptopirimidinmetal(0) kompleksleri, hekzakarbonilmetal(0) kompleksleri 10 ºC'de 4,6-dimetil-2-merkaptopirimidin ligandı ile fotokimyasal olarak sentezlendi. Bildirilen organometalik kompleksler, inert atmosfer altında saflaştırılırılarak izole edilir. Tüm $M(CO)_5L$ kompleksleri çözelti içinde FTIR-, $^1$H- ve $^{13}$C-NMR spektroskopileri ile karakterize edildi. FTIR spektroskopi sonuçları, karbonil bölgesinde, komplekslerin pentakarbonil metal biriminin yerel bir $C_{4v}$ simetrisine sahip olduğunu gösteren üç absorpsiyon bandı gösterdi. $^1$H- ve $^{13}$C-NMR spektroskopileri merkaptopirimidin ligandının, merkaptopirimidin-azot atomu yoluyla metal kompleksine simetrik olarak bağlandığını gösterdi. $^{13}$C-NMR spektroskopi sonuçları ayrıca CO-bölgesinde 1:4'lük bir oran gösterdi, bu oran komplekslerin $C_{4v}$ simetrisini kanıtladı. Bu organometalik komplekslerin termal davranışı DTA/TGA yöntemleri kullanılarak araştırılmıştır. Termal analizlerin sonuçları, komplekslerin üç farklı sıcaklıkta bozunduğunu göstermiştir. Yoğunluk fonksiyonel teorisi (DFT) hesaplamaları Gaussian03W Software ile B3PW91 formalizmi kullanılarak yapıldı. Deneysel çalışmaların verileri teorik değerlerle karşılaştırıldığında elde edilen sonuçların birbiri ile uyumlu olduğu görülmüştür. Böylece elde edilen organometalik kompleks bileşikleri için deneysel olarak verilen yapısal önermenin doğruluğu teorik olarak da desteklenmiştir.

**Anahtar Kelimeler:** Merkaptopirimidin, Fotokimyasal sentez, Metal karboniller, Termal analiz, DFT

## 1. Introduction

As one of the most common π ligands, carbon monoxide plays an essential role in organometallic chemistry due to its ability to coordinate strongly with metals in the zero oxidation state [1-3]. Transition metal carbonyl complexes also have both of industrial and catalytic value and significant structural interest [4, 5] In particular, hexacarbonylmetal(0) complexes of VIB transition metals (Cr, Mo, W) are practical starting materials for many organometallic complex synthesis [6]–[9] since they are air-stable, highly hydrophobic, ready to sublime under vacuum, soluble in polar solvents and very slightly soluble in nonpolar solvents [10]. The photochemical substitution reaction of M(CO)6 complexes is a widely used method to obtain new coordination complexes by releasing carbon monoxide by acceleration of light in photolysis resulting with M(CO)5L type complexes [7]–[9]. The vibrational spectra is very informative and guide the estimation of certain group frequencies in metal carbonyl studies since CO stretching bands in infrared spectra are sharp, environmentally sensitive, and tend to be intense[1]. Metal carbonyl complexes where one or more carbonyl ligand bonded to a single metal center show intense FTIR-bands between 2200 and 1800 $cm^{-1}$ due to the polarization of CO on binding metal atom [11], [12]. The coordination chemistry of heterocyclic ligands is a field of growing interest in

coordination chemistry since they have multiple sites, allowing the use of various coordination modes [13]–[16]. Pentacarbonyl(pyridine)metal(0) complexes (M: Cr, Mo, W) have been known for a long time [13]. Since VIB transition metal carbonyls photochemically active, the complexes of these have found to be used in photocatalytic hydrogenation activity [17], CO delivery agent in biochemical and pharmaceutical sources [4,18]. Pyridine has many properties similar to pyrimidine [19], [20] they both act primarily as a σ-donor ligand with weak π-acceptor capacity, the M-N bond in these low-valence metal complexes is not very strong [8]. As one of the main component of nucleic acids, pyrimidines are essential in many biological systems. The coordination chemistry of transition metal complexes containing mercaptopyrimidine ligand are especially interesting. They contain thiolate-S and aromatic-N functional groups that form a variety of complexes with different kind of metals. Additionally, these ligands have the ability to chelate and bind transition metals, providing access to both mononuclear and oligonuclear products [21]–[23]. The ligand 4,6-dimethyl-2-mercaptopyrimidine is an ligand that can coordinate through the S and the pyrimidine ring of N atom [24], [25].

In this study, it was aimed that synthesize and characterize of the pentacarbonyl(primidinethiol)metal(0) complexes of Group VI elements for the first time for this purpose 4,6-dimethyl-2-mercaptopyrimidine (4,6- dimethyl-2-mercaptopyrimidine) ligand was used as mercaptopyrimidine ligand. A useful synthetic technique for producing novel coordination compounds has been the photochemical substitution of ligands, by accelerating with light, most frequently carbonyl groups [6], [8, 9]. For this reason, substituted mercaptopyrimidine ligand photochemically reacted with hexacarbonylmetal(0), M: Cr, Mo, W and resulting complexes were purified by recrystallization. The next part of this work was the structural identification of the synthesized complexes using FTIR-, $^{1}$H- and $^{13}$C-NMR spectroscopies. Then, by using TGA/DTA methods thermal behavior of the complexes was investigated. Finally, DFT calculations of these organometallic complexes was computed in B3PW91 formalism by Gaussian03W Software.

## 2. Material and Method

All manipulations, reactions and purification processes were carried out under inert nitrogen atmosphere. Deuterated and analytical grade solvents were purchased from Sigma-Aldrich. Analytical grade solvents were refluxed over metallic sodium for 3-4 days under an inert atmosphere before used. Hexacarbonylchromium(0), hexacarbonylmolibdenum(0), hexacarbonyltungsten(0) and 4,6-dimethyl-2-mercaptopyrimidine were purchased from the Merck GmbH, Darmstadt, Germany, and used without further purification. High pressure mercury lamp (Hg-Tauchlampe TQ 150, Quarzlampen GmbH, Hereaus, Germany, solidex glass, λ>280 nm) was used for photochemical substitution reactions in an immersed apparatus that cooled by circulating water. Photochemical reactions were followed by taking FTIR-spectra from solutions on a Schmadzu FTIR- 8400S spectroscopy. The UV/Vis spectra were recorded from solutions in CH2Cl2 using JASCO V-530 UV/VIS spectrophotometer. The 1H- and $^{13}$C-NMR spectra of these complexes were recorded from their dichloroform and d-dimethylsulfoxide solutions using Brucker-Spectroscopin DPX 400 MHz spectrometer. TMS used as an internal reference in all chemical shift values for $^{1}$H-, and $^{13}$C-NMR. The thermal analyses of the complexes were measured by using SII EXSTAR 6000 TG/DTA6300.

The proposed organometalic complexes have been synthesized using the following reactions where L: 4,6-dimethyl-2-mercaptopyrimidine; M: Cr, Mo, W.

$$M(CO)_6 + THF \xrightarrow{h\upsilon/(-CO)} M(CO)_5(THF) \xrightarrow{h\upsilon/+L} M(CO)_5L + THF$$

0,5 gram $M(CO)_6$ [M: Cr (2,27mmol), Mo (1,89mmol), W (1,42mmol)] was dissolved in THF and illuminated (150 W mercury lamp, λ>280 nm) for 60 minutes at room temperature under oxygen free nitrogen gas. At the of reaction time a stoichiometric amount of 4,6-dimethyl-2-mercaptopyrimidine (0,318g, 0,266g, 0,148g respectively) was added to the reaction vessel and the illumination was kept until the reaction completed (135min. for Cr, 240min. for Mo, 120min. for W). The reaction process was followed by FTIR-spectra taken in every 20 minutes. At the end of the reaction, the color of solutions was yellow for $Cr(CO)_5$(dmmp), red for $W(CO)_5$(dmmp), and dark red for $Mo(CO)_5$(dmmp). Solutions filtered to evacuated schlenk tubes under nitrogen atmosphere. Excess solvents were removed by evaporating under high vacuum. The pure coordination compounds were then isolated by recrystallization from 1:5 mixture $CH_2Cl_2$ : n-hexane solution producing the solids which were then dissolved in n-hexane to remove out any $M(CO)_6$ remain unreacted. The pure solids were then stored under nitrogen atmosphere at low temperature for analysis.

### Spectroscopic Data

Pentacarbonyl(4,6-dimethyl-2-mercaptopyrimidine)chromium(0) (1)

*$Cr(CO)_5$(dmmp)*; FTIR- (in dichloromethane) ν(CO) ($cm^{-1}$)= 2061.9 (m), 1930.8 (s), 1886.4 (m), $^{1}$H-NMR (in d-chloroform) of free ligand δ (ppm)=12.15 (S-H, $H_{(20)}$), 2.33 ($CH_3$($H_{(22,24)}$-$H_{(26,27)}$), 6.93 ($H_{(18)}$) ref. TMS. $^{1}$H-NMR (in d-chloroform) δ (ppm)=13.1 (S-H, $H_{(20)}$), 1.40 ($CH_3$($H_{(22,24)}$-$H_{(26,27)}$), 6.70 ($H_{(18)}$) ref. TMS. $^{13}$C-NMR (in d-dimethylsulfoxide) of free ligand δ (ppm)= 180 ($C_{(13)}$), 165.1($C_{(14)}$), 111.7 ($C_{(16)}$), 165.1 ($C_{(17)}$), 24.7 ($C_{(21)}$), 24.7 ($C_{(25)}$) ref. TMS. $^{13}$C-NMR (in d-dimethylsulfoxide) δ (ppm)= 179.6 ($C_{(13)}$), 168.3($C_{(14)}$), 112.8($C_{(16)}$), 168.3 ($C_{(17)}$), 29.43 ($C_{(21)}$), 28.32 ($C_{(25)}$), 214.9 (Trans-CO), 209.3 (cis-CO) ref. TMS. UV-Vis (in dichloromethane) 243 nm, 2.09557 Abs.

Pentacarbonyl(4,6-dimethyl-2-mercaptopyrimidine)molybdenum(0) (2)

*$Mo(CO)_5$(dmmp)*; FTIR- (in dichloromethane) ν(CO) ($cm^{-1}$)= 2061.9 (m), 1932.7(s), 1888.3(m), $^1$H-NMR (in d-chloroform) of free ligand δ (ppm)=12.15 (S-H, $H_{(20)}$), 2.33 ($CH_3$($H_{(22,24)}$-$H_{(26,27)}$), 6.93 ($H_{(18)}$) ref. TMS. $^1$H-NMR (in d-chloroform) δ (ppm)=13.5 (S-H, $H_{(20)}$), 1.38 ($CH_3$($H_{(22,24)}$-$H_{(26,27)}$), 6.70 ($H_{(18)}$) ref. TMS. $^{13}$C-NMR (in d-dimethylsulfoxide) of free ligand δ (ppm)= 180 ($C_{(13)}$), 165.1($C_{(14)}$), 111.7 ($C_{(16)}$), 165.1 ($C_{(17)}$), 24.7 ($C_{(21)}$), 24.7 ($C_{(25)}$) ref. TMS. $^{13}$C-NMR (in d-dimethylsulfoxide) δ (ppm)= 181.05 ($C_{(13)}$), 166.03($C_{(14)}$), 109.7($C_{(16)}$), 166.03 ($C_{(17)}$), 30.39 ($C_{(21)}$), 30.39 ($C_{(25)}$), 206.8 (Trans-CO), 200.9 (cis-CO) ref. TMS. UV-Vis (in dichloromethane) 234 nm, 0.8893 Abs., 287nm,1.3061 Abs., 349nm, 0.3203 Abs. and 507nm, 0.1456 Abs.

Pentacarbonyl(4,6-dimethyl-2-mercaptopyrimidine)tungsten(0) (3)

*$W(CO)_5$(dmmp)*; FTIR- (in dichloromethane) ν(CO) ($cm^{-1}$)= 2067.7 (m), 1926.6(s), 1891.9(m), $^1$H-NMR (in d-chloroform) of free ligand δ (ppm)=12.15 (S-H, $H_{(20)}$), 2.33 ($CH_3$($H_{(22,24)}$-$H_{(26,27)}$), 6.93 ($H_{(18)}$) ref. TMS. $^1$H-NMR (in d-chloroform) δ (ppm)=12.85 (S-H, $H_{(20)}$), 1.42 ($CH_3$($H_{(22,24)}$-$H_{(26,27)}$), 6.75 ($H_{(18)}$) ref. TMS. $^{13}$C-NMR (in d-dimethylsulfoxide) of free ligand δ (ppm)= 180 ($C_{(13)}$), 165.1($C_{(14)}$), 111.7 ($C_{(16)}$), 165.1 ($C_{(17)}$), 24.7 ($C_{(21)}$), 24.7 ($C_{(25)}$) ref. TMS. $^{13}$C-NMR (in d-dimethylsulfoxide) δ (ppm)= 180.8 ($C_{(13)}$), 165.6($C_{(14)}$), 111.71($C_{(16)}$), 166.0 ($C_{(17)}$), 30.32 ($C_{(21)}$), 30.32 ($C_{(25)}$), 198.2 (Trans-CO), 190.6 (cis-CO) ref. TMS. UV-Vis (in dichloromethane) 243nm, 2.04778 Abs., 294nm, 0.5262 Abs. and 352nm, 0.3904 Abs

## 3. Result and Discussion

Photolysis of hexacarbonylmetal(0) complexes of VIB transition metals in the presence of an excess amount of tetrahydrofuran (THF) leads to the formation of pentacarbonyl(THF)metal(0), $M(CO)_5$(THF) intermediate compound. UV-irradiation with 4,6-dimethyl-2-mercaptopyrimidine of the intermediate pentacarbonyl complex leads to the formation of pentacarbonyl(4,6-dimethyl-2-mercaptopyrimidine)metal(0); M: Cr, Mo, W complexes. The photochemical substitution reactions were followed by IR spectra. It was seen that the absorption band at 1980 $cm^{-1}$ which is specific to $M(CO)_6$ υ(CO) band decreases while three new distinct bands occurred with proceeding of the photochemical reaction.

The FTIR spectra of $M(CO)_5L$ (L:4,6-dimethyl-2-mercaptopyrimidine) in dichloromethane exhibits three prominent absorption bands (one in strong, the others in medium intensities) in the CO stretching vibrational region (1800–2300 $cm^{-1}$). The three-band ν(CO) pattern of these complexes indicates that the C4v local symmetry of $M(CO)_5$ skeleton, which is generally observed for $M(CO)_5L$ complexes with a pattern $2A_1$+E [5]. The A1 and E modes are both IR-active modes where E must be lower in frequency than one of A1- modes as explained by Orgel [26].

The $^1$H-NMR spectrum of free 4,6-dimethyl-2-mercaptopyrimidine ligand shows three singlets with different intensities at 2.33, 6.93 and 12.15 ppm. Upon coordination to the metal atom the signal due to the SH group show no significant shift from that of free ligands. The appearance of only one singlet for the SH group proton which show no shift from that of the free ligand could rule out any metalsulfure coordination. The appearance of only one singlet for the $CH_3$ groups with no significant chemical shift in an indication of the metal-nitrogen coordination through the nitrogen lone pair of the pyrimidine ring. From these 1H-NMR and previous IR-data discussed, the can conclude the appearance of metal-pyrimidine coordination through the nitrogen atom lone pair of the pyrimidine ring rather than the expected metal-thiol coordination.

The 13C-NMR spectra of the complexes M(CO)5(4,6-dimethyl-2- mercaptopyrimidine); M: Cr, W were recorded from their d-chloroform solutions, M: Mo recorded from its d-dimethylsulfoxide solution. The $^{13}$C-NMR spectra show four signals in the region of 20-180 ppm for the pyrimidine ring and its substituents. The carbonyl groups give two signals 37 with relative intensities 1:4 in the region of 190-230 ppm. The $^{13}$C-{1H}-NMR spectrum of the free 4,6-dimethyl-2-mercaptopyrimidine ligand (dmmp) show four signals with relative intensities at 179.9, 169, 118.7 and 23.8 ppm. Upon coordination to the metal atom, the signal belongs to C(13) show no significant shift comparing with that of free ligand. From the 13C-NMR data of the complexes one can said that (i) The appearance of only one singlet for all the carbons of the pyrimidine ring an indication for the symmetric metal-ligand coordination through on of the ring nitrogen atoms, (ii) All the 13C-signals of all carbons of the pyrimidine ring and substituents show no significant shift from these of free ligands indicates weak metal-nitrogen coordination, (iii) The appearance of two signals of relative intensities 1:4 in the CO region indicates the formation of pentacarbonylmetal, $M(CO)_5$.

The thermal analysis of the complexes M(CO)5L (M: Cr, W ; L: 4,6-dimethyl-2-mercaptopyrimidine) was measured by using TG/DTA method. $Cr(CO)_5$(dmmp) complex dissociates at four different temperatures, in order of 105.9 $^oC$ , 214.9 $^oC$ , 452.7 $^oC$ and 890.2 $^oC$. It can be postulated that the complex Cr(CO)5(4,6-dm-2-mp) was dissociated to $CrO_3$. $Mo(CO)_5$(dmmp) complex (2) dissociates at five different temperatures, in order of 59.7 $^oC$, 119.8 $^oC$, 169.7 $^oC$, 370.2 $^oC$ and 900.9 $^oC$ and the main dissociation of the complex is occurred at 160 $^oC$. Thermal dissociations of the complexes were given in Table 1 and Table 2.

**Table 1.** Thermal dissociation of $Cr(CO)_5$(dmmp) complex

| Decomposition Steps | Sample Amount *(mg)* | Lost Amount *%* | Lost Molecular Weight *(g/mol)* |
|---|---|---|---|
| 1st | 1,873 | 7% | 21,247 |
| 2nd | 1,468 | 19,33% | 64 |
| 3rd | 0,932 | 50,24% | 166,38 |
| 4th | 0,631 | 66,31% | 219,59 |

**Table 2.** Thermal dissociation of $Cr(CO)_5$(dmmp) complex

| Decomposition Steps | Sample Amount *(mg)* | Lost Amount *%* | Lost Molecular Weight *(g/mol)* |
|---|---|---|---|
| 1st | 4,613 | 2,60% | 9,78 |
| 2nd | 4,493 | 17,58% | 66,13 |
| 3rd | 3,802 | 41,45% | 155,9 |
| 4th | 2,387 | 48,25% | 181,52 |

## 4. Computational Details

The optimized molecular structure, bond distances and bond angles of the pentacarbonyl(4,6-dimethyl-2-mercaptopyrimidine)metal(0); M: Cr, Mo, W complexes have been computed by using DFT-B3PW91formalism. Optimized geometry of M(CO)5(dmmp) complex is given in Figure 2 with atom labels, grey atoms represent hydrogen, dark grey atoms represent carbon, blue atoms represent nitrogen, yellow atom represents sulphur, turquoise atom represents metal, and red atoms represent oxygen. Bond distances between atoms and bond angles between selected atoms were given in Table 3 and Table 4.

**Table 3.** DFT (B3PW91/SDD) Calculated bond distances between atoms

| Atoms | $Cr(CO)_5$(dmmp) | $Mo(CO)_5$(dmmp) | $W(CO)_5$(dmmp) |
|---|---|---|---|
| $M_{(1)}$ - $C_{(2)}$ | 1,8264 | 1,9691 | 1,9852 |
| $M_{(1)}$ - $C_{(4)}$ | 1,8892 | 2,045 | 2,0541 |
| $M_{(1)}$ - $C_{(6)}$ | 1,8649 | 2,0232 | 2,034 |
| $M_{(1)}$ - $C_{(8)}$ | 1,8893 | 2,0448 | 2,0539 |
| $M_{(1)}$ - $C_{(10)}$ | 1,8647 | 2,024 | 2,0351 |
| $M_{(1)}$ - $N_{(12)}$ | 2,2434 | 2,3667 | 2,3509 |
| $C_{(2)}$ - $O_{(3)}$ | 1,1832 | 1,1845 | 1,1857 |
| $C_{(4)}$ - $O_{(5)}$ | 1,1766 | 1,1775 | 1,1789 |
| $C_{(6)}$ - $O_{(7)}$ | 1,1811 | 1,1818 | 1,1834 |
| $C_{(8)}$ - $O_{(9)}$ | 1,1765 | 1,1772 | 1,1786 |
| $C_{(10)}$ - $O_{(11)}$ | 1,181 | 1,1817 | 1,1832 |
| $N_{(12)}$ - $C_{(13)}$ | 1,3746 | 1,3739 | 1,377 |
| $N_{(12)}$ - $C_{(14)}$ | 1,3842 | 1,3827 | 1,3847 |
| $C_{(13)}$ - $N_{(15)}$ | 1,3447 | 1,3437 | 1,3425 |
| $C_{(13)}$ - $S_{(19)}$ | 1,8034 | 1,8017 | 1,801 |
| $C_{(14)}$ - $C_{(16)}$ | 1,4054 | 1,4044 | 1,4038 |
| $C_{(14)}$ - $C_{(21)}$ | 1,5013 | 1,4993 | 1,499 |
| $N_{(15)}$ - $C_{(17)}$ | 1,3527 | 1,3538 | 1,3537 |
| $C_{(16)}$ - $C_{(17)}$ | 1,4008 | 1,4017 | 1,4015 |
| $C_{(16)}$ - $H_{(18)}$ | 1,0828 | 1,0829 | 1,0828 |
| $C_{(17)}$ - $C_{(25)}$ | 1,4994 | 1,4994 | 1,4991 |
| $S_{(19)}$ - $H_{(20)}$ | 1,3741 | 1,3747 | 1,3752 |
| $C_{(21)}$ - $H_{(22)}$ | 1,0922 | 1,0949 | 1,0949 |
| $C_{(21)}$ - $H_{(23)}$ | 1,0932 | 1,0932 | 1,0932 |
| $C_{(21)}$ - $H_{(24)}$ | 1,092 | 1,0911 | 1,0913 |
| $C_{(25)}$ - $H_{(26)}$ | 1,096 | 1,0961 | 1,0962 |
| $C_{(25)}$ - $H_{(27)}$ | 1,093 | 1,0931 | 1,093 |
| $C_{(25)}$ - $H_{(28)}$ | 1,0959 | 1,0959 | 1,0959 |

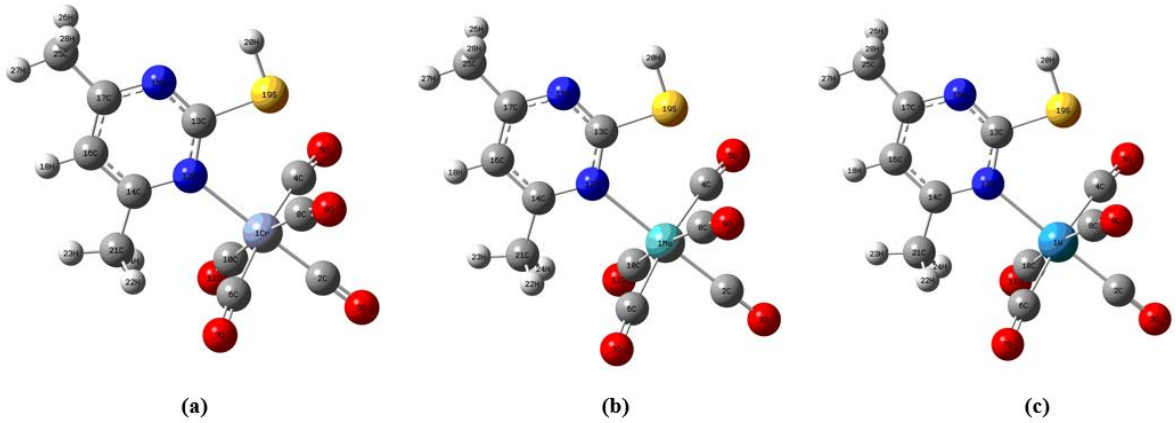

**(a)** **(b)** **(c)**

**Figure 1.** The optimized structure of $M(CO)_5$(dmmp) complexes,; a) Cr, b) Mo, c) W.

**Table 4.** DFT (B3PW91/SDD) Calculated bond angles between atoms

| Atoms | $Cr(CO)_5$(dmmp) | $Mo(CO)_5$(dmmp) | $W(CO)_5$(dmmp) |
|---|---|---|---|
| $C_{(2)}$-$M_{(1)}$-$C_{(4)}$ | 85,99 | 85,82 | 85,84 |
| $C_{(2)}$ - $M_{(1)}$ - $C_{(6)}$ | 86,6 | 86,21 | 86,2 |
| $C_{(2)}$ - $M_{(1)}$ - $C_{(8)}$ | 86,17 | 86,63 | 86,59 |
| $C_{(2)}$ - $M_{(1)}$ -$C_{(10)}$ | 86,8 | 87,05 | 86,99 |
| $C_{(4)}$ - $M_{(1)}$ - $C_{(8)}$ | 95,01 | 94,36 | 94,41 |
| $C_{(4)}$ - $M_{(1)}$ -$C_{(10)}$ | 86,29 | 86,19 | 86,23 |
| $C_{(4)}$ - $M_{(1)}$ -$C_{(12)}$ | 93,01 | 93,19 | 93,13 |
| $C_{(6)}$ - $M_{(1)}$ - $C_{(8)}$ | 86,33 | 86,92 | 86,96 |
| $C_{(6)}$ - $M_{(1)}$ -$C_{(10)}$ | 91,46 | 91,65 | 91,51 |
| $C_{(6)}$ - $M_{(1)}$ -$C_{(12)}$ | 94,42 | 94,8 | 94,86 |
| $C_{(8)}$ - $M_{(1)}$ -$C_{(12)}$ | 93,09 | 92,6 | 92,53 |
| $C_{(10)}$ -$M_{(1)}$-$C_{(12)}$ | 93,98 | 93,73 | 93,91 |
| $M_{(1)}$- $N_{(12)}$-$C_{(13)}$ | 121,07 | 121,19 | 121,31 |
| $M_{(1)}$- $N_{(12)}$-$C_{(14)}$ | 124,28 | 123,8 | 123,77 |
| $C_{(13)}$-$N_{(12)}$- $C_{(14)}$ | 114,65 | 114,97 | 114,9 |
| $N_{(12)}$-$C_{(13)}$ -$N_{(15)}$ | 126,52 | 126,35 | 126,26 |
| $N_{(12)}$ - $C_{(13)}$-$S_{(19)}$ | 119,86 | 119,3 | 119,39 |
| $N_{(15)}$ - $C_{(13)}$-$S_{(19)}$ | 113,62 | 114,36 | 114,36 |
| $N_{(12)}$- $C_{(14)}$-$C_{(16)}$ | 120,95 | 120,85 | 120,83 |
| $N_{(12)}$ -$C_{(14)}$-$C_{(21)}$ | 121,78 | 121,06 | 121,19 |
| $C_{(16)}$ -$C_{(14)}$-$C_{(21)}$ | 117,27 | 118,09 | 117,98 |
| $C_{(13)}$ -$N_{(15)}$-$C_{(17)}$ | 118,95 | 118,85 | 119,02 |
| $C_{(14)}$ -$C_{(16)}$-$C_{(17)}$ | 120,05 | 119,9 | 120,01 |
| $C_{(14)}$ -$C_{(16)}$-$H_{(18)}$ | 119,42 | 119,52 | 119,42 |
| $C_{(17)}$-$C_{(16)}$ -$H_{(18)}$ | 120,53 | 120,58 | 120,57 |
| $N_{(15)}$ -$C_{(17)}$-$C_{(16)}$ | 118,87 | 119,06 | 118,97 |
| $N_{(15)}$ -$C_{(17)}$-$C_{(25)}$ | 117,35 | 117,28 | 117,3 |
| $C_{(16)}$ -$C_{(17)}$-$C_{(25)}$ | 123,77 | 123,67 | 123,73 |
| $C_{(13)}$ -$S_{(19)}$-$H_{(20)}$ | 92,97 | 93,03 | 92,91 |
| $C_{(14)}$-$C_{(21)}$- $H_{(22)}$ | 111,78 | 110,75 | 110,86 |
| $C_{(14)}$-$C_{(21)}$- $H_{(23)}$ | 109,61 | 110,02 | 109,93 |
| $C_{(14)}$-$C_{(21)}$- $H_{(24)}$ | 112,02 | 112,13 | 112,17 |
| $H_{(22)}$-$C_{(21)}$- $H_{(23)}$ | 107,72 | 107,91 | 107,9 |
| $H_{(22)}$ -$C_{(21)}$-$H_{(24)}$ | 107,79 | 107,43 | 107,42 |
| $H_{(23)}$-$C_{(21)}$- $H_{(24)}$ | 107,73 | 108,45 | 108,41 |
| $C_{(17)}$-$C_{(25)}$- $H_{(26)}$ | 109,98 | 109,96 | 109,96 |
| $C_{(17)}$-$C_{(25)}$- $H_{(27)}$ | 111,85 | 111,85 | 111,86 |
| $C_{(17)}$-$C_{(25)}$- $H_{(28)}$ | 110,01 | 110,03 | 110,03 |
| $H_{(26)}$-$C_{(25)}$- $H_{(27)}$ | 108,94 | 108,92 | 108,92 |
| $H_{(26)}$-$C_{(25)}$- $H_{(28)}$ | 106,94 | 106,94 | 106,92 |
| $H_{(27)}$-$C_{(25)}$- $H_{(28)}$ | 108,99 | 109,01 | 109,02 |

The vibrational frequencies, the nuclear magnetic resonance chemical shift values and energies of the pentacarbonyl(4,6-dimethyl-2-mercaptopyrimidine)metal(0); M: Cr, Mo, W complexes have been computed by using DFT-B3PW91 with SDD. The comparison table of the FTIR spectra of the complexes and DFT calculated stretching bands of the complexes is given in Table 5. Calculated NMR chemical shifts of the complexes were given in Table 6.

**Table 5.** Experimental and DFT (B3PW91/SDD) Calculated vibrational streching frequencies of $M(CO)_5$(dmmp) complexes

| Vibration | $Cr(CO)_5$(dmmp) | | $Mo(CO)_5$(dmmp) | | $W(CO)_5$(dmmp) | |
|---|---|---|---|---|---|---|
| | Experimental ($cm^{-1}$) | Theoretical ($cm^{-1}$) | Experimental ($cm^{-1}$) | Theoretical ($cm^{-1}$) | Experimental ($cm^{-1}$) | Theoretical ($cm^{-1}$) |
| υ(CO) | 2061,9 | 2036,06 | 2061,97 | 2036,68 | 2034,12 | 2067,5 |
| υ(CO) | 1930,81 | 1925,7 | 1932,74 | 1917,33 | 1926,56 | 1913,3 |
| υ(CO) | 1886,44 | 1914,3 | 1888,37 | 1905,8 | 1891,88 | 1900,18 |
| υ(C=C)Aromatic | 1604,83 | 1633,76 | 1653,49 | 1634,07 | 1653,05 | 1635,43 |
| υ(C=C)Aromatic | 1535,39 | 1565,4 | 1558,91 | 1564,48 | 1558,5 | 1563,2 |
| υ(M-N) | 420,5 | 419,36 | 418,51 | 397,01 | 418,5 | 402,55 |
| υ(C-C) | 1429,3 | 1449,57 | 1437,21 | 1449,52 | 1431,23 | 1449,74 |
| υ(C-C) | 1425,44 | 1451,6 | 1429,46 | 1450,58 | 1454,38 | 1451,09 |
| υ($CH_3$) | 3064,99 | 3097,37 | 3080,37 | 3087,32 | 3078,44 | 3087,46 |
| υ($CH_3$) | 3053,42 | 3070,74 | 3074,61 | 3070,68 | 3068,5 | 3070,69 |
| υ(C-N) | 1290,42 | 1303,74 | 1290,71 | 1306,96 | 1292,5 | 1309,34 |
| υ(C=N) | 1411,94 | 1400,09 | 1244,48 | 1238,5 | 1242,2 | 1236,74 |
| υ(C-H) Bend | 794,7 | 795,01 | 889,23 | 794,98 | 794,81 | 794,35 |
| υ(C-H) Bend | 893,07 | 896,96 | 901,02 | 894,67 | 906,41 | 895,68 |
| υ(C-S) | 889,21 | 879,66 | 893,27 | 880,93 | 889,31 | 879,55 |

**Table 6.** Experimental and DFT-Calculated NMR chemical shifts (ppm) of $M(CO)_5$(dmmp) complexes, TMS reference.

| δ (ppm) | Free Ligand | $Cr(CO)_5$(dmmp) | | $Mo(CO)_5$(dmmp) | | $W(CO)_5$(dmmp) | |
|---|---|---|---|---|---|---|---|
| | | Experimental | DFT-B3PW91 | Experimental | DFT-B3PW91 | Experimental | DFT-B3PW91 |
| S-H, $H_{(20)}$ | 12.15 | 13.1 | 4.93 | 13.5 | 4.82 | 12.85 | 4.82 |
| $CH_3(H_{(22,24)}$-$H_{(26,27)}$ | 2.33 | 1.40 | 1.82 | 1.38 | 1.78 | 1.42 | 1.77 |
| $H_{(18)}$ | 6.93 | 6.70 | 6.33 | 6.70 | 6.33 | 6.75 | 6.28 |
| $C_{(13)}$ | 179.9 | 179.6 | 182.04 | 181.05 | 180.6 | 180.8 | 180.68 |
| $C_{(14)}$ | 169.0 | 168.3 | 165.7 | 166.03 | 164.18 | 165.6 | 164.1 |
| $C_{(16)}$ | 118.7 | 112.8 | 106.9 | 109.7 | 106.07 | 111.71 | 106.1 |
| $C_{(17)}$ | 169.0 | 168.3 | 157.13 | 166.03 | 157.53 | 166.0 | 157.07 |
| $C_{(21)}$ | 23.8 | 29.43 | 15.69 | 30.39 | 15.81 | 30.32 | 15.69 |
| $C_{(25)}$ | 23.8 | 28.32 | 21.7 | 30.39 | 21.93 | 30.32 | 15.8 |
| trans-CO | | 214.9 | 225.4 | 206.8 | 225.4 | 198.2 | 216.78 |
| cis-CO | | 209.3 | 218.9 | 200.9 | 215.3 | 190.6 | 208.38 |

The HOMO-LUMO transition energies of the complexes was calculated by Gaussian molecular visualization program by using DFT-B3PW91 method as shown in Figure 3. HOMO electrons mostly occupied on mercaptopyrimidine ligand part while LUMO electrons localized on pentacarbonyl metal moiety of the complex. Electronic transition calculations of pentacarbonyl(mercaptoyrimidine)metal(0) complexes were carried out by DFT-B3PW91/SDD formalism (Table 7). Thermodynamic energy term table is given in Table 8.

**Table 7.** DFT (B3PW91/SDD) Calculated electronic transitions of $M(CO)_5$(dmmp) complexes

| Exited States | $Cr(CO)_5$(dmmp) | | | $Mo(CO)_5$(dmmp) | | | $W(CO)_5$(dmmp) | | |
|---|---|---|---|---|---|---|---|---|---|
| | λ *(nm)* | E *(eV)* | f | λ *(nm)* | E *(eV)* | f | λ *(nm)* | E *(eV)* | f |
| H - 2 → L + 4 | 397,2 | 3,1214 | 0,0172 | 386,9 | 3,2048 | 0,0154 | 403,4 | 3,0738 | 0,0153 |
| H - 2 → L + 3 | 389,6 | 3,1822 | 0,0124 | 382,4 | 3,2424 | 0,0177 | 397,9 | 3,1158 | 0,016 |
| H → L | 384,7 | 3,2226 | 0,0006 | 399,6 | 3,1029 | 0,0011 | 421 | 2,9451 | 0,0004 |
| H - 2 → L + 1 | 372,6 | 3,3279 | 0,003 | 373,1 | 3,3233 | 0,0467 | 388,7 | 3,1894 | 0,0669 |

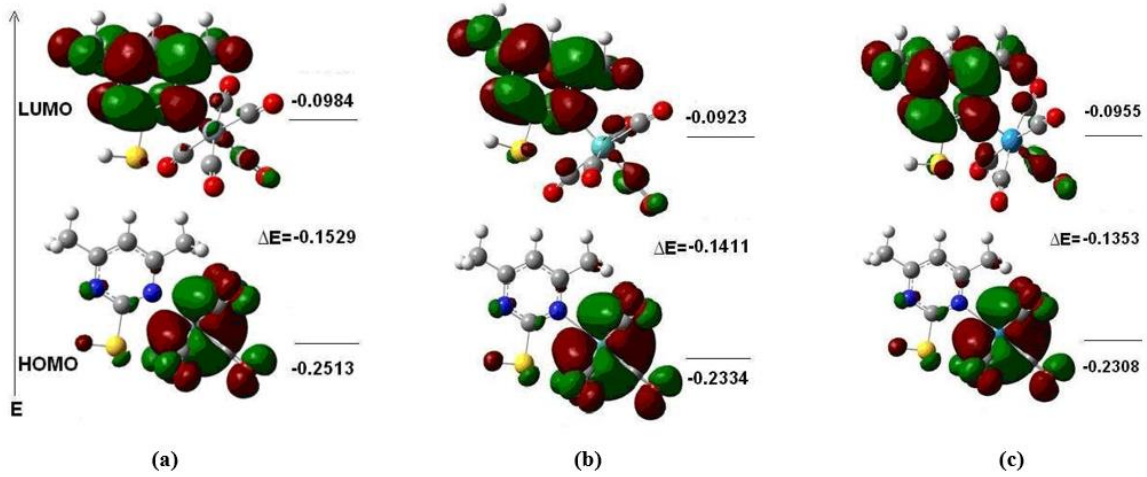


**Figure 2.** The electronic transition from HOMO to LUMO of the $M(CO)_5$(dmmp) complexes; (a) $Cr(CO)_5$(dmmp), (b) $Mo(CO)_5$(dmmp), (c) $W(CO)_5$(dmmp)

**Table 8.** DFT (B3PW91/SDD) Calculated thermodynamic properties of $M(CO)_5$(dmmp) complexes

| Thermodynamic Properties | Cr | Mo | W |
|---|---|---|---|
| Total Energy (a.u.) | -1394,203 | -1375,5869 | -1374,4947 |
| Zero-Point Energy (KCal/Mol) | 110,1081 | 109,0723 | 109,0984 |
| Rotational Constants (GHZ) | 0,4306 | 0,3995 | 0,397 |
| | 0,2339 | 0,213 | 0,2063 |
| | 0,2017 | 0,1861 | 0,1807 |
| Rotational Temperatures (K) | 0,0207 | 0,0192 | 0,0191 |
| | 0,0112 | 0,0102 | 0,0099 |
| | 0,0097 | 0,0089 | 0,0087 |
| Dipole Moment (Debye) | 9,0125 | 9,3578 | 9,7212 |
| RMS Gradient Norm (a.u.) | 1,86E-06 | 1,508E-05 | 6,74E-06 |
| Virial Ratio (a.u.) | 2,0361 | 2,0381 | 2,0375 |
| Entropy (Cal/Mol-Kelvin) | | | |
| Total | 161,66 | 162,36 | 162,524 |
| Translational | 43,295 | 43,681 | 44,293 |
| Rotational | 34,025 | 34,273 | 34,34 |
| Vibrational | 84,341 | 84,406 | 83,892 |
| Thermal Energy (KCal/Mol) | | | |
| Total | 123,809 | 123,102 | 123,087 |
| Translational | 0,889 | 0,889 | 0,889 |
| Rotational | 0,889 | 0,889 | 0,889 |
| Vibrational | 122,031 | 121,325 | 121,309 |

Reliable molecular structure prediction is one of the main goals of computational chemistry. According to the bond length and vibrational calculation data collected by DFT (B3PW91/SDD) of these synthesized organometallic complexes, the mercaptopyrimidine ligand is attached to the central atom through nitrogen atom, rather than the expected metal-thiol coordination. DFT calculations of $^{1}$H- and $^{13}$C- chemical shifts of the complexes and free ligand are compared to experimental results also shows bonding through pyrimidine nitrogen atom with $C_{4v}$ symmetry. Accurate thermochemical data for each metal-ligand bond strength is crucial for the rational design of catalytic processes. Calculated thermodynamic properties of pentacarbonyl(4,6-dimethyl-2-mercaptopyrimidine)metal(0); M: Cr, Mo, W complexes are important in terms of directing further catalytic studies.

## 5. Conclusions

The In this study, pentacarbonyl(4,6-dimethyl-2-mercaptopyrimidine)metal(0); M: Cr, Mo, W complexes were photochemically synthesized, and their structures have been characterized by the mean of IR-, UV-, $^{1}$H-NMR and $^{13}$C-NMR spectroscopies and their thermal behavior investigate by TG/DTA methods. The ligand 4,6-dimethyl-2-

mercaptopyrimidine is chosen because of its multifunctional groups and multibonding probability. There are three basic centers in the ligand that are available to bond lewis acid (metal center). The most basic center is that N atom due to the spectroscopic investigations so the central atom is bonded to ligand from N atom of mercaptopyrimidine. Despite the fact that the CO group is the strongest - acceptor ligand, the bond lengths have changed, making the M-C bond weaker and, of course, creating a synergistic energy in the M-CO bond. The $^{1}$H- and $^{13}$C-NMR spectroscopies showed that the mercaptopyrimidine ligand bonded to metal complex through the mercaptopyrimidine nitrogen atom symmetrically. Also, the $^{13}$C-NMR spectroscopy results showed 1:4 ratio of peaks in the CO-region, the ratio of the peaks proved the $C_{4v}$ symmetry of these complexes. In addition to experimental studies, the complexes of pentacarbonyl(4,6-dimethyl-2-mercaptopyrimidine)metal(0) were investigated theoretically by DFT computational method. After geometry optimizations, vibrational frequencies computed by calculating the 47 harmonic vibrational frequencies of complexes and compared with experimental spectra of the complexes. It was seen that vibrational spectra values were in a good aggrement with experimental data. Also DFT calculated proton shifts compared with both free ligand and experimental results confirmed that there is an successful application of DFT to proton chemical shifts.

**Competing Interest / Conflict of Interest**

The authors declare that they have no competing interests.

**Author Contribution**

We declare that all Authors equally contribute.

**6. References**

[1] Bhatt, V., (2016). Metal Carbonyls. Essentials of Coordination Chemistry, 1st ed. London, UK: Elsevier, 8: 191–236.

[2] Turner, J.J., George, M.W., Poliakoff, M., and Perutz, R.N., (2022). Photochemistry of transition metal carbonyls. Chemical Society Reviews. 51: 5300-5329.

[3] Bistoni, G., Rampino, S., Scafuri, N., Ciancaleoni, G., Zuccaccia, D., Belpassi, L., Tarantelli, F., (2016). How p back-donation quantitatively controls the CO stretching response in classical and non-classical metal carbonyl complexes. Chemical Science. 7(2): 1174-1184.

[4] Mohamed, R.G., Elantabli, F. M., Helal, N. H., El-Medani, S. M., (2015). New group 6 metal carbonyl complexes with 4,5-dimethyl-N,Nbis(pyridine-2-yl-methylene)benzene-1,2-diimine Schiff base: Synthesis, spectral, cyclic voltammetry and biological activity studies. Spectrochimica Acta Part A: Molecular and Biomolecular Spectroscopy. 141: 316–326.

[5] Erkan, S., Karakas, D., (2020). Computational investigation of structural, nonlinear optical and anti-tumor properties of dinuclear metal carbonyls bridged by pyridyl ligands with alkyne unit. Journal of Molecular Structure. 1199:127054.

[6] Yaman, Ş.Ö., Esentürk, E., Kayran, C., and Önal, A.M., (2002). Spectroelectrochemical Investigation of Pentacarbonyl(pyrazine)metal(0) (Metal = Cr, Mo, W) Complexes of Group 6 Elements. Zeitschrift für Naturforschung. 57(1): 92-98.

[7] Grevels, F. W., Jacke, J., and Ozkar, S., (1987). Photoreactions of Group 6 metal carbonyls with ethene: syntheses of trans-(.eta.2-ethene)2M(CO)$_4$ (M = chromium, molybdenum, tungsten. Journal of the American Chemical Society. 109(24): 7536–7537.

[8] Morkan, I. A., Güven, K., and Özkar, S., (2004). Pentacarbonyl(2,6-diaminopyridine)chromium(0): Synthesis and molecular structure. Journal of Organometallic Chemistry. 689(14): 2319–2323.

[9] Tuç, C., Morkan, I. A., and Özkar, S., (2007). Synthesis and spectroscopic characterization of group 6 pentacarbonyl(4-substituted pyridine)metal(0) complexes. Transition Metal Chemistry. 32(6): 727–731.

[10] Mashima, K., (1998) Group 4 (Ti, Zr, Hf) Metal Compounds. Synthesis of Organometallic Compounds, 1st ed. West Sussex, UK: John Wiley & Sons, Inc., ch. 6: 75-98.

[11] Braterman, P.S., Harril, R.W., and Kaesz, H.D., (1967). Spectroscopic studies of isotopically substituted metal carbonyls. II. Assignment of carbonyl stretching absorptions and their interaction with metal-hydrogen stretching modes in pentacarbonyl hydrides. Journal of the American Chemical Society. 89(12): 2851–2855.

[12] Crabtree, R. H., (2005). Carbonyls, Phosphines, And Substitution. The Organometallic Chemistry of The Transition Metals, 6th ed., Hoboken, New Jersey, USA, John Wiley, ch. 4(1): 98-108.

[13] Akrivos, A. D., (2001). Recent studies in the coordination chemistry of heterocyclic thiones and thionates. Coordination Chemistry Reviews. 213(1): 181–210.

[14] Dennenberg, R. J., and Darensbourg, D.J., (1972). Infrared and kinetic studies of Group VI metal pentacarbonyl amine compounds. Inorganic Chemistry,. 11(1): 72–77.

[15] Schwenzer, G., Darensbourg, M.Y., and Darensbourg, D. J., (1972). Photochemical substitution reactions of substituted Group VI metal carbonyls. Inorganic Chemistry. 11(8): 1967–1970.

[16] Darensbourg, D. J., Frost, B. J., Larkins, D. L., and Reibenspies, J. H., (2000). Organometallic Complexes of Uracil and Orotic Acid Derivatives: Coordination Mode, Structure, and Reactivity. European Journal of Inorganic Chemistry. 2000(12): 2487–2495.

[17] Vielhaber, T., Faust, K., and Topf, C., (2020). Group 6 Metal Carbonyl Complexes Supported by a Bidentate PN Ligand: Syntheses, Characterization, and Catalytic Hydrogenation Activity. Organometallics. 39(24): 4535-4543.

[18] Gonzales, M.A., Mascharak, P.K., (2014). Photoactive metal carbonyl complexes as potential agents for targeted CO delivery. Journal of Inorganic Biochemistry. 133: 127–135.

[19] Taqui Khan, B., and Zakeeruddin, S.M., (1986). Metal complexes of substituted pyrimidines. Inorganica Chimica Acta. 124(1): 5–11.

[20] Grigoryan, L.A., Kaldrikyan, M.A., Melik-Ogandzhanyan, R.G., Arsenyan, F.G., Stepanyan, G.M., and Garibdzhanyan, B.G., (2005). Synthesis and Antitumor Activity of 2-S-Substituted Pyrimidine Derivatives. Pharmaceutical Chemistry Journal. 39(9): 468–472.

[21] Fandos, R., Lanfranchi, M., Otero, A., Pellinghelli, M., Ruiz, M. and Terreros, P., (1996). Zirconium Alkyl Thiolate Complexes:Synthesis and Reactivity.Molecular Structures of $[Zr(H_5\text{-}C_5H_5)_2(\eta^2\text{-}C_6H_7N_2S)(Me)]$and$[Zr(H_5\text{-}C_5H_5)_2(H_1\text{-}C_6H_7N\ _2S)$. Organometallics. 15(22): 4725–4730.

[22] Antiñolo, A., Carrillo-Hermosilla, F., Corrochano, A. E., Fandos, R., Fernández-Baeza, J., Rodríguez, A.M., Ruiz, M.J., and Otero, A., (1999). New Monocyclopentadienyl Complexes of Titanium(IV) and Zirconium(IV) with Chelating Pyrimidinethiolate, Oxypyrimidine, and Oxypyridine Ligands. Molecular Structure of $[Zr(\eta^5\text{-}C_5Me_5)(\eta^2\text{-}O,N\text{-}ON_2C_6H_7)_3]$.Organometallics. 18(25): 5219–5224.

[23] Martos-Calvente, R., De la Peña O'Shea, V.A., Campos-Martin, J.M., Fierro, J.L.G., (2003). The Usefulness of Density Functional Theory To Describe the Tautomeric Equilibrium of 4,6-Dimethyl-2-mercaptopyrimidine in Solution. The Journal of Physical Chemistry A. 107(38): 7490–7495.

[24] Waheed, A., Alorainy, M.S., Alghasham, A.A., Khan, S.A., and Raza, M., (2008). Synthesis of a new series of substituted pyrimidines and its evaluation for antibacterial and antinociceptive effects. International Journal of Health Sciences. 2(1): 39–48.

[25] Ajibade, P.A., and Idemudia, O.G., (2013). Synthesis, Characterization, and Antibacterial Studies of Pd(II) and Pt(II) Complexes of Some Diaminopyrimidine Derivatives. Bioinorganic Chemistry and Applications. 2013: 549549.

[26] Creaser, C.S., Fey, M.A., and Stephenson, G.R., (1994). Environment sensitivity of IR-active metal carbonyl probe groups. Spectrochimica Acta Part A: Molecular and Biomolecular Spectroscopy. 50(7): 1295–1299.

doi:10.55385/kastamonujes.1177807 KUJES 8(2):116-121, 2022

Kastamonu University
Journal of Engineering and Sciences
e-ISSN 2667-8209
http://dergipark.gov.tr/kastamonujes

# Urban Public Spaces, Public Health, and Heavy Metal Pollution Threatening in Ankara City Center: Strategies for Urban Planning

**Öznur Işınkaralar[a, *], Emine Pirinç Bayraktar[b]**

[a] Department of Landscape Architecture, Faculty of Engineering and Agriculture, Kastamonu University, Kastamonu, Türkiye
[b] Department of Elderly Care, Vocational High School of Health Services, Lokman Hekim University, Ankara, Turkiye
***Corresponding Author:** obulan@kastamonu.edu.tr

Received: **September 20, 2022** ◆ Accepted: **December 05, 2022** ◆ Published Online: **December 26, 2022**

**Abstract:** In the last century, population growth and concentration in urban areas have caused many problems, especially in the central regions of metropolitan cities worldwide. One of these problems is air pollution. It reduces the quality of life of the citizens and threatens public health. Among the components of air pollution, heavy metals are the most dangerous because they accumulate in metabolism. Some are toxic and poisonous even at low concentrations and deadly for human health at high concentrations. Studies on the determination of air pollution are limited to revealing the current situation and do not offer solutions for urban planning. In this context, the accumulation of copper elements, which is extremely dangerous for public health, in the city center was investigated using landscape plants as a tool in the research. Within the scope of the study, the change of copper concentration in five plant species grown in areas with no vehicle density, less dense, and dense regions were investigated. As a result of the research, the increase in the concentration of copper in the air due to traffic has been revealed statistically. The study emphasizes the relationship between heavy metal pollution, which poses a severe threat to public health, and urban planning, and shows the basic strategies in terms of urban planning.

**Keywords:** City centers, Urban quality of life, Public health, Air pollution, Ankara

**Öz:** Son yüzyılda dünya genelinde nüfus artışı ve nüfusun kentsel alanlarda yoğunlaşması, özellikle metropol kentlerin merkezi alanlarında pek çok soruna neden olmaktadır. Bu sorunların başında kentlinin yaşam kalitesini düşüren ve halk sağlığını tehdit eden hava kirliliği gelmektedir. Hava kirliliği bileşenleri içerisinde ise ağır metaller, metabolizmada birikmeleri, bazılarının düşük konsantrasyonlarda bile, toksik ve zehirli olmaları, yüksek konsantrasyonlarda insan sağlığı için ölümcül olmaları nedeniyle en tehlikeli olanlarıdır. Hava kirliliğinin tespitine yönelik çalışmalar mevcut durumu ortaya koymakla sınırlı kalmakta ve şehir planlama açısından çözüme yönelik stratejiler sunmamaktadır. Bu kapsamda araştırmada peyzaj bitkileri bir araç olarak kullanılarak halk sağlığı açısından son derece tehlikeli olan bakır elementinin kent merkezinde yer alan bitkilerdeki birikimi araştırılmıştır. Çalışma kapsamında taşıt yoğunluğunun olmadığı, az yoğun olduğu ve yoğun olduğu alanlarda yetiştirilen beş bitki türündeki bakır konsantrasyonunun değişimi incelenmiştir. Çalışma sonucunda havadaki bakır konsantrasyonunun trafik kaynaklı olarak artışı istatistiki olarak ortaya konulmuştur. Araştırma halk sağlığına ciddi tehdit oluşturan ağır metal kirliliği ile kent planlama ilişkisine vurgu yaparak, kentsel planlama açısından temel stratejileri ortaya koymaktadır.

**Anahtar Kelimeler:** Kent merkezleri, Kentsel yaşam kalitesi, Halk sağlığı, Hava kirliliği, Ankara

## 1. Introduction

The World Health Organization (WHO) draws attention to the fact that air pollution is defined as one of the biggest environmental threats to human health [1]. The production mechanism that emerged in urban areas in response to the intense consumption demand of today's world [2] has transformed urban areas into areas with high human, building, and vehicle density and continues to change them, especially in developing countries [3,4]. The metropolitan structure and density of urban areas make it difficult to deal with cities in terms of urban economy, design, planning, environment, and aesthetics [5,6]. Difficulties in urban management bring along some problems, such as accessibility, a decrease in quality of life due to density, and the emergence of pollution [7-10]. One of the most significant of these problems is environmental pollution because it threatens the citizens' health [11-12]. Today, it is reported that 92% of the world's population lives in regions with low air quality [13], deaths directly caused by air pollution are increasing [14-16], and the role of water pollution, especially in epidemics [17]. Reports of international organizations reflect environmental concerns [18]. However, even the basic needs of the increasing population, such as heating and shelter, require energy [19]. The world's energy need is provided by fossil fuels with intense carbon content and the gases that emerge after energy production increase carbon emissions [20]. The resulting greenhouse gases are considered to be one of the main culprits of urban heat island formation [21].

The gases produced adversely affect the outdoor air quality [22]. However, air quality can be managed with sustainable planning decisions in terms of air quality by making use of energy-efficient planning approaches based on environmental and social sustainability. Spatially open urban air quality knowledge is essential for developing effective strategies and measures. Monitoring systems are challenging to measure urban air quality with global technics [23]. Since air pollution components are not closed and traceable mechanisms, determining their sources is a multidimensional structure, and the determination of these factors is quite complex [24]. In studies, measurements are generally applied with sparsely placed fixed monitor networks. However, the difficulties in using these devices in outdoor conditions, their economic unsustainability, and their analysis processes limit air quality research, so some researchers try to sample large scales with closed setups [25]. Air quality components are monitored by different methods [26-27]. Since heavy metals from these pollutants are not eliminated from metabolism, they accumulate in the body. Based on this, the biomonitoring technique, which is applied using structures belonging to living things, is widely preferred because it has less cost [28] and has a wide application area compared to other methods [29]. The research, using five species (*Acer negundo, Aesculus hippocastanum, Tilia platyphyllos, Prunus ceracifera, Ailanthus altissima*) that are commonly preferred in urban open green areas, determine the heavy metal accumulation levels due to vehicle density in Ankara city center and producing planning strategies for metropolitan areas. Accordingly, the study seeks to answer two basic research questions:

- Do different plant species and different organs of plants differ significantly in terms of heavy metal accumulation levels?
- Does traffic density affect the deposition level of copper metal?

## 2. Material and Method

The study was carried out in the city center of Ankara, one of the most crowded cities in Türkiye. The city where the first zoning plan of the country was made after it was declared the capital city. Urban arrangements reflecting the republican ideology were produced by planners, urban designers, and architects. The modernization process of the city began to take place with this development. The city's development continued with the implementation of the modernity project, separating squares, parks, and boulevards as components of contemporary community life [30]. In this process, Atatürk Boulevard has assumed the role of a publicity image located at the city's core beyond its transportation function. It has formed the main backbone of public open spaces such as Youth Park, Guvenpark, Kurtulus Park, and Zafer Square, where the society comes together and communicates. As the Jansen Plan of Ankara aimed, it lived for a while as a field of communication and action where individuals saw, heard, and interacted with each other. However, with the arrangements made around the area, it lost its publicity role. The boulevard, which turned into a speedway that moved away from the human scale on the city's axis, with the road widening works at the beginning, turned into a speedway with the open green spaces that define social life away from publicity over time.

The processes experienced have triggered the transformation of the social space that holds the society together in the city center into a physical space that has the characteristics of a transition point. The loss of the central function of the Ankara city center points to a planning problem such as the search for a center. However, one of the negative effects of the implemented decisions is the emission emissions that threaten public health due to the exposure of the public spaces network in the city center to vehicle density. These gases, which affect the air quality, reduce the quality of life in society and not only, but also pose a severe threat to public health. Therefore, in urban planning, the pollution levels in the city center of Ankara were measured and analyzed statistically to reveal the city center's heavy metal pollution and emphasize its significance in terms of public health. Based on these findings, it is aimed to question the decisions produced for the city center. In this context, it was conducted on *Acer negundo, Aesculus hippocastanum, Tilia platyphyllos, Prunus ceracifera*, and *Ailanthus altissima* species, which are the most frequently used plants in landscape studies in urban centers. The samples that are the subject of the study were collected from the species that grow in the city center of Ankara, one of the most crowded cities of Türkiye, in areas with heavy traffic, low density, and almost no traffic (at least 100 m near there is no highway). The specimens were cut from the last year's shoot with pruning shears, packaged, labeled, and brought to the laboratory. The samples obtained in the laboratory were first subjected to the dissection process, then they were cut into pieces, marked, and placed in glass Petri dishes so they could dry quickly. For the samples to become room dry for 15 days and then to dry completely, they were dried in an oven at 45 °C for seven days.

Completely dried samples were ground into powder, 0.5 g was weighed, placed in tubes designed for microwave use, and 10 mL of 65% $HNO_3$ was added. The samples were then burned in a microwave device at 280 PSI and 180 ºC for 20 minutes. After the combustion process was completed, the tubes were removed from the microwave and allowed to cool. Deionized water was added to the cooled samples, made up to 50 ml, and filtered through filter paper. Samples prepared in this way were read at appropriate wavelengths in the ICP-OES device. This method is one of the most used methods in heavy metal analysis in plants, and many studies have been carried out using this method in recent years [31, 32].

The data obtained as a result of the study were evaluated with the help of the SPSS 23.0 statistical package program, analysis of variance was applied to the data, and homogeneous groups were obtained by using the Duncan test to the data with significant differences of at least 95% confidence level ($p$<0.05). The data obtained were organized according to the scope of the research, and the importance of the findings was interpreted within the framework of decisions and strategies.

## 3. Result and Discussion

There is the change in copper concentration in the samples subject to the study in areas where there is no traffic, where there is little or no traffic, and based on species and organs in Table 1. As a result of the analysis of variance, it was determined that the change of copper concentration based on organs in all traffic densities differed statistically at the 99.9% confidence level ($p$<0.001).

**Table 1.** Variation of copper concentration (ppm) by species and organs

| Species | Organs | Traffic Density | | |
|---|---|---|---|---|
| | | None | Slightly intense | Intensive |
| ***Acer negundo*** | Leef | 5.13 bc | 0.70 a | 1.86 a |
| | Seed | 5.80 cd | 6.16 d | 52.33 c |
| | Branch | 1.20 a | 10.60 h | 15.53 a |
| ***Aesculus hippocastanum*** | Leef | 7.13 d | 1.83 b | 23.83 ab |
| | Seed | 0.40 a | 0.93 a | 3.33 a |
| | Branch | 3.70 b | 8.96 f | 10.10 a |
| ***Tilia platyphyllos*** | Leef | 0.63 a | 0.76 a | 13.03 a |
| | Seed | 15.46 f | 19.16 j | 330.66 d |
| | Branch | 7.16 d | 7.26 e | 2.86 a |
| ***Prunus ceracifera*** | Leef | 8.73 e | 12.16 i | 42.63 bc |
| | Seed | 9.30 e | 10.00 g | 10.66 a |
| | Branch | 6.43 cd | 0.53 a | 19.16 a |
| ***Ailanthus altissima*** | Leef | 3.83 b | 4.13 c | 8.26 a |
| | Seed | 16.60 f | 20.00 k | 23.16 ab |
| | Branch | 5.60 cd | 9.13 f | 13.40 a |
| **F Value** | | 89.16*** | 1892.71*** | 132.42*** |

The relationship between traffic density and copper accumulation is questioned in the study. In this context, the lowest values from the Duncan test were obtained in *Aesculus hippocastanum* seeds in areas with no traffic, *Prunus ceracifera* branches in areas with low traffic density, and *Acer negundo* leaves in areas with heavy traffic. The highest values were obtained from *Ailanthus altissima* seeds in areas with less traffic and less intense areas and *Tilia platyphyllos* seeds in areas with heavy traffic. The variation of copper concentration depending on traffic density is given in Table 2.

**Table 2.** Variation of copper concentration (ppm) depending on traffic density

| Species | Organs | Traffic Density | | | F Value |
|---|---|---|---|---|---|
| | | None | Slightly intense | Intensive | |
| ***Acer negundo*** | Leef | 5.13 c | 0.70 a | 1.86 b | 2851.80*** |
| | Seed | 5.80 a | 6.16 a | 52.33 b | 31.71** |
| | Branch | 1.20 a | 10.60 b | 15.53 c | 5113.00*** |
| ***Aesculus hippocastanum*** | Leef | 7.13 b | 1.83 a | 23.83 c | 11864.70*** |
| | Seed | 0.40 a | 0.93 a | 3.33 b | 71.65*** |
| | Branch | 3.70 a | 8.96 b | 10.10 c | 149.25*** |
| ***Tilia platyphyllos*** | Leef | 0.63 a | 0.76 a | 13.03 b | 9127.46*** |
| | Seed | 15.46 a | 19.16 a | 330.66 b | 140.18*** |
| | Branch | 7.16 b | 7.26 b | 2.86 a | 246.91*** |
| ***Prunus ceracifera*** | Leef | 8.73 a | 12.16 b | 42.63 c | 156691.2*** |
| | Seed | 9.30 a | 10.00 b | 10.66 c | 21.74** |
| | Branch | 6.43 b | 0.53 a | 19.16 c | 2814.56*** |
| ***Ailanthus altissima*** | Leef | 3.83 a | 4.13 a | 8.26 b | 789.19*** |
| | Seed | 16.60 a | 20.00 b | 23.16 c | 529.43*** |
| | Branch | 5.60 a | 9.13 b | 13.40 c | 840.57*** |

As a result of the analysis of variance, it was determined that the change of copper concentration in all organs, depending on the traffic density, differed significantly, at least at the 99% confidence level ($p$<0.001). As a result of the Duncan test, the lowest values were obtained in 11 of the 15 organs subject to the study in areas without traffic, while the highest values were obtained in areas with heavy traffic in 13 of them. Copper concentration in 11 organs increases with traffic density. This value shows that the copper concentration is directly related to traffic density. It was determined that the copper concentration increased in all organs of *Ailanthus altissima* depending on the traffic density.

Firstly, the changes in copper concentration depending on the organ and traffic density were determined as a result of the study. Copper is an essential trace element for human and animal metabolism and is an indispensable part of red blood

cells and many oxidation and reduction processes in animals and humans. However, when taken in excess, it is harmful to a life-threatening level. Therefore, monitoring and reducing copper pollution is a necessity. The study results show that the copper concentration increased depending on the traffic density. This finding indicates that traffic is an essential source of copper pollutants. Numerous studies show that heavy metals are emitted mainly into the atmosphere from anthropogenic sources such as mining activities, industry, and traffic [32-34]. It is emphasized that the most significant heavy metal source, especially in urban areas, is traffic. However, there are still not enough studies on the relationship between pollution levels, traffic, and urban planning, with different land uses and transportation types. Increasing the number of studies on heavy metals, which are extremely dangerous for human health, even at low concentrations, is of great importance in monitoring the change in heavy metal pollution, reducing pollution, and protecting and improving public health.

City centers can be defined as the most complex area of the city by nature and it is very difficult to explain their dynamic relationships [8, 35-38]. The public spaces in the city centers can be accepted as the primary communication object of society. At the same time, these areas are the building blocks of urban life quality and urban identity. The relationship that the city centers establish with the city is an essential criterion for the identity of a contemporary capital. However, Atatürk Boulevard and its surroundings, which were chosen as the research area, moved away from being a part of the social life due to the decisions taken and became a passageway that divides the public uses in the center that pedestrians find it difficult to overcome. The research focuses on the level of air quality in the context of its quality of life. The findings reveal the accumulation of plants as a striking result of traffic concentration in the city center. Accordingly, the recommendations can be listed as follows: it is of great significance in terms of protection and development.

## 4. Conclusions

The limitation of urban air corridors with high-rise buildings and the construction of the open green space pattern is effective based on air pollution in the city center. The density of vehicles in the city center is mainly due to the density of cars on the existing axes connecting to the center. Using the city center for transit purposes encourages the transfer of journeys produced in urban development and expansion areas by using the city center. But the trips to residential districts can be reduced through spatial decisions and demand management. It is known that this vehicle density is primarily due to individual use. The number of vehicles using the city center can be reduced by encouraging alternative and public transportation modes.

However, with access control strategies (taxation in different zones, parking costs, etc.) in developed countries, measures can be taken to discourage private vehicle use. Working areas other than the uses bearing the identity of the city center can be planned in development areas. In addition to these, pedestrian spaces can be revitalized, and approaches to strengthen pedestrian mobility (traffic clarification, level crossings, etc.) can be developed. Among the species subject to this research, which was developed based on air quality, the highest copper concentrations were obtained in *Tilia platyphyllos* and *Acer negundo*. Therefore, these species can be used in different areas to reduce copper concentration in the air and to monitor copper pollution. It is essential to increase the research related to monitoring air quality in cities in a way that is related to planning and developing alternative methods.

## Competing Interest

The authors declare that they no conflict of interest. The none of the authors have any competing interests in the manuscript.

## Author Contribution

There is no financial support and commercial support.

## Acknowledgements

We There is no financial support and commercial support. We declare that all Authors equally contribute.

## 5. References

[1] Maione, M., Mocca, E., Eisfeld, K., Kazepov, Y. and Fuzzi, S. (2021). Public perception of air pollution sources across Europe. Ambio, 50(6), 1150-1158.

[2] Javed, A. R., Shahzad, F., ur Rehman, S., Zikria, Y. B., Razzak, I., Jalil, Z. and Xu, G. (2022). Future smart cities requirements, emerging technologies, applications, challenges, and future aspects. Cities, 129, 103794.

[3] Yigitcanlar, T., Degirmenci, K., Butler, L. and Desouza, K. C. (2022). What are the key factors affecting smart city transformation readiness? Evidence from Australian cities. Cities, 120, 103434.

[4] Wang, Q. and Li, L. (2021). The effects of population aging, life expectancy, unemployment rate, population density, per capita GDP, urbanization on per capita carbon emissions. Sustainable Production and Consumption, 28, 760-774.

[5] Oztas, Ç. Ç. (2021). How to Best Classify Rural in Metropolitan Areas? The Turkish Case. Planning Practice and Research, 36(4), 456-466.

[6] Rahman, M. M., Najaf, P., Fields, M. G. and Thill, J. C. (2022). Traffic congestion and its urban scale factors: Empirical evidence from American urban areas. International Journal of Sustainable Transportation, 16(5), 406-421.

[7] Haque, A. B., Bhushan, B. and Dhiman, G. (2022). Conceptualizing smart city applications: Requirements, architecture, security issues, and emerging trends. Expert Systems, 39(5), e12753.

[8] Isinkaralar, O., Varol, C. and Yilmaz, D. (2022). Digital mapping and predicting the urban growth: integrating scenarios into cellular automata—Markov chain modeling. Applied Geomatics, 1-11.

[9] Meydan, K., Vural, O., Oztürk, S. and Isinkaralar, O. Development of Ecotourism Resource Values Using Rapid Rural Assessment Method: The Case of Ilıca Village. Sciences, 10(1), 1-14.

[10] Cakir, C., Isinkaralar, Ö. and Oztürk, S. Geographical accessibility of health care network via GIS in Kastamonu. Kastamonu University Journal of Engineering and Sciences, 8(1), 60-68.

[11] Bayraktar, E. P., Isinkaralar, O. and Isinkaralar, K. (2022). Usability of several species for monitoring and reducing the heavy metal pollution threatening the public health in urban environment of Ankara. World Journal of Advanced Research and Reviews, 14(3), 276-283.

[12] Sulhan, O. F., Sevik, H., and Isinkaralar, K. (2022). Assessment of Cr and Zn deposition on Picea pungens Engelm. in urban air of Ankara, Türkiye. Environment, Development and Sustainability, 1-20.

[13] Popov, O., Iatsyshyn, A., Kovach, V., Artemchuk, V., Kameneva, I., Taraduda, D. and Yatsyshyn, T. (2020). Risk assessment for the population of Kyiv, Ukraine as a result of atmospheric air pollution. Journal of Health and Pollution, 10(25).

[14] Clancy, L., Goodman, P., Sinclair, H., and Dockery, D. W. (2002). Effect of air-pollution control on death rates in Dublin, Ireland: an intervention study. The lancet, 360(9341), 1210-1214.

[15] Balakrishnan, K., Dey, S., Gupta, T., Dhaliwal, R. S., Brauer, M., Cohen, A. J. and Dandona, L. (2019). The impact of air pollution on deaths, disease burden, and life expectancy across the states of India: the Global Burden of Disease Study 2017. The Lancet Planetary Health, 3(1), e26-e39.

[16] Austin, K. F. and Mejia, M. T. (2017). Household air pollution as a silent killer: women's status and solid fuel use in developing nations. Population and Environment, 39(1), 1-25.

[17] Skip, B. (2009). Water pollution impact on immune status of human organism and typical epidemic processes: mathematic model, obtaining results, their analysis and proposals to manage risk factors. In Risk Management of Water Supply and Sanitation Systems (pp. 199-204). Springer, Dordrecht.

[18] Golob, U. and Bartlett, J. L. (2007). Communicating about corporate social responsibility: A comparative study of CSR reporting in Australia and Slovenia. Public relations review, 33(1), 1-9.

[19] Woo, S., Yoon, S., Kim, J., Hwang, S. W. and Kweon, S. J. (2021). Optimal cooling shelter assignment during heat waves using real-time mobile-based floating population data. Urban Climate, 38, 100874.

[20] Moyer, J. D. and Hughes, B. B. (2012). ICTs: do they contribute to increased carbon emissions?. Technological Forecasting and Social Change, 79(5), 919-931.

[21] Mohajerani, A., Bakaric, J. and Jeffrey-Bailey, T. (2017). The urban heat island effect, its causes, and mitigation, with reference to the thermal properties of asphalt concrete. Journal of environmental management, 197, 522-538.

[22] Curtis, L., Rea, W., Smith-Willis, P., Fenyves, E. and Pan, Y. (2006). Adverse health effects of outdoor air pollutants. Environment international, 32(6), 815-830.

[23] Chen, F., Kusaka, H., Bornstein, R., Ching, J., Grimmond, C. S. B., Grossman-Clarke, S. and Zhang, C. (2011). The integrated WRF/urban modelling system: development, evaluation, and applications to urban environmental problems. International Journal of Climatology, 31(2), 273-288.

[24] Taylan, O. (2017). Modelling and analysis of ozone concentration by artificial intelligent techniques for estimating air quality. Atmospheric environment, 150, 356-365.

[25] Spengler, J. D. and Chen, Q. (2000). Indoor air quality factors in designing a healthy building. Annual Review of Energy and the Environment, 25(1), 567-600.

[26] Lu, W. Z., He, H. D. and Dong, L. Y. (2011). Performance assessment of air quality monitoring networks using principal component analysis and cluster analysis. Building and Environment, 46(3), 577-583.

[27] Harkat, M. F., Mourot, G. and Ragot, J. (2006). An improved PCA scheme for sensor FDI: Application to an air quality monitoring network. Journal of Process Control, 16(6), 625-634.

[28] Giordano, S., Spagnuolo, V. and Capozzi, F. (2021). Biomonitoring of Air Pollution. Atmosphere, 12(4), 433.

[29] Savas, D. S., Sevik, H., Isinkaralar, K., Turkyilmaz, A. and Cetin, M. (2021). The potential of using Cedrus atlantica as a biomonitor in the concentrations of Cr and Mn. Environmental Science and Pollution Research, 28(39), 55446-55453.

[30] Tekeli, İ. (2008). Göç ve Ötesi. İstanbul: Tarih Vakfı Yurt Yayınları.

[31] Saleh, E. A. A. and Işınkaralar, Ö. (2022). Analysis of trace elements accumulation in some landscape plants as an indicator of pollution in an urban environment: Case of Ankara. Kastamonu University Journal of Engineering and Sciences, 8(1), 1-5.

[32] Yayla, E. E., Sevik, H. and Isinkaralar, K. (2022). Detection of landscape species as a low-cost biomonitoring study: Cr, Mn, and Zn pollution in an urban air quality. Environmental Monitoring and Assessment, 194(10), 1-10.

[33] Isinkaralar, K. (2022). Atmospheric deposition of Pb and Cd in the Cedrus atlantica for environmental biomonitoring. Landscape and Ecological Engineering, 1-10.

[34] Turkyilmaz, A., Cetin, M., Sevik, H., Isinkaralar, K. and Saleh, E. A. A. (2020). Variation of heavy metal accumulation in certain landscaping plants due to traffic density. Environment, Development and Sustainability, 22(3), 2385-2398.

[35] Yilmaz, D., Öztürk, S., & Işinkaralar, Ö. (2022). Kent İmgesinin Yapıtaşı Olarak Sokaklarda Mekânsal Zenginliğin Fraktal Geometri ile Analizi. Kent Akademisi, 15(3), 1341-1358.

[36] Öztürk, S., and Işınkaralar, Ö. (2019). Kastamonu kent merkezinde otopark sorunsalı: Eleştirel bir değerlendirme. Uluslararası Sosyal Araştırmalar Dergisi, 12(67), 506-511.

[37] Isinkaralar, O., and Varol, C. (2023). A cellular automata-based approach for spatio-temporal modeling of the city center as a complex system: The case of Kastamonu, Türkiye. Cities, 132, 104073.

[38] Cetin, M., Onac, A. K., Sevik, H., and Sen, B. (2019). Temporal and regional change of some air pollution parameters in Bursa. Air Quality, Atmosphere & Health, 12(3), 311-316.

doi:10.55385/kastamonujes.1185210 KUJES 8(2):122-127, 2022

Kastamonu University
Journal of Engineering and Sciences
e-ISSN 2667-8209
http://dergipark.gov.tr/kastamonujes

# Change of Calcium Concentrations in Forest Soils by Plant Species and Soil Depth

**Ramazan Erdem**

Department of Forestry, Programs of Forestry and Forestry Products, Arac Rafet Vergili Vocational School Kastamonu University, Kastamonu, Türkiye
***Corresponding Author:** rerdem@kastamonu.edu.tr

Received: **October 06, 2022** ◆ Accepted: **December 12, 2022** ◆ Published Online: **December 26, 2022**

**Abstract:** One of the most important factors playing role in plant development is the nutrient element content of the soil. Being one of the fundamentally necessary macronutrients for plant nourishment, calcium (Ca) plays an important role in the growth and development of a plant. Thus, even though many studies have been carried out on the change of Ca concentration in agricultural soils, the number of studies examining this subject for forest soils is very limited. In the present study, it was aimed to compare the concentrations of Ca in soil and plant organs for the soils, where different forest trees are grown. Within this scope, leaf, bark, wood, cone, and root samples were collected from Turkish fir, black pine, Scotch pine, and Oriental beech species and soil samples were taken from the surface, mid-deep, and deep soil levels. Then, the Ca concentrations were compared. As a result, it was determined that Ca concentrations statistically significantly vary between leaves, roots, and woods of plants and between mid-deep and deep soils by species ($p<0.05$).

**Keywords:** Soil, Forest, Nutrient Element, Ca

**Öz:** Bitki gelişiminde rol oynayan en önemli faktörlerden biri toprağın besin element içeriğidir. Bitki beslenmesi için temel olarak gerekli makro besinlerden biri olan kalsiyum (Ca), bitkinin büyüme ve gelişmesinde önemli bir rol oynar. Bu nedenle tarım topraklarında Ca konsantrasyonunun değişimi ile ilgili birçok çalışma yapılmış olmasına rağmen orman toprakları için bu konuyu inceleyen çalışma sayısı oldukça sınırlıdır. Bu çalışmada, farklı orman ağaçlarının yetiştirildiği topraklar için toprak ve bitki organlarındaki Ca konsantrasyonlarının karşılaştırılması amaçlanmıştır. Bu kapsamda köknar, karaçam, sarıçam ve doğu kayını türlerinden yaprak, ağaç kabuğu, odun, koni ve kök örnekleri toplanmış ve yüzey, orta-derin ve derin toprak seviyelerinden toprak örnekleri alınmıştır. Daha sonra Ca konsantrasyonları karşılaştırıldı. Sonuç olarak, Ca konsantrasyonlarının bitkilerin yaprak, kök ve odunları arasında ve türlere göre orta-derin ve derin topraklar arasında istatistiksel olarak anlamlı farklılık gösterdiği belirlenmiştir ($p<0.05$).

**Anahtar Kelimeler:** Toprak, Orman, Besin Elementi, Ca

## 1. Introduction

Plants are grown and perform on the soil where they photosynthesis by using the sunlight and produce the nutrients that are required by other organisms [1, 2]. Thus, the entire organic life is directly or indirectly dependent upon the plants [3]. For the plants, offering the benefits they are supposed to offer depends on their healthy growth and development [4-6]. Plant development depends mainly on climatic [7-9] and edaphic factors [10-12] and nutrient elements are among the factors influencing the plant development the most [13-14].

In plant nourishment, there are 16 fundamental nutrient elements that are required and, being one of these elements, calcium (Ca) is among the elements that are required for plant growth and development [15]. Ca plays an important role in growth and development of cells, in arranging the membrane permeability, in stabilization of tissues, and also in quality of plants. Moreover, it has also important effects on the chemical characteristics of the soil. Thus, it is of an inevitable importance for fauna, microflora, plant, and soil. In case of Ca deficiency, besides a decrease in plant yield, also the quality decreases generally [15-17].

Ca is also a heavy metal. Some of the heavy metals (such as Pb, Cr, Ni, and Hg) are toxic, carcinogenic, and harmful for organisms even when at low concentrations [18-21] and the ones that are necessary as plant nutrient elements can be harmful for organisms when at high concentrations [22-24]. Hence, it is very important to monitor the concentrations of heavy metals in air, soil, and water [25-27]. In the present study, in order to understand the interaction of Ca in soil and plant organs, the change of Ca concentrations in soil and plant organs was examined in soils, where different forest trees are grown.

## 2. Material and Method

The main objective of the present study is to investigate the variance in Ca concentration by the plant species grown in soils forming on the same bedrock. Thus, an area, where different forest trees are grown but the environmental factors are similar, was chosen as the study material. The study area, which is a plain field, is in the Araç district of Kastamonu province and the environmental factors other than the plant species are similar. Thus, it was accepted that the main factor altering the soil structure was the plant species.

Within the scope of this study, leaf, bark, wood, cone, and root samples were collected from Turkish fir (*Abies nordmanniana* subsp. bornmülleriana Mattf), black pine, (*Pinus nigra* Arnold.), Scotch pine, (*Pinus sylvestris* L.), and Oriental beech (*Fagus orientalis* Libsky.) species grown in places, which were close to each other, whereas the soil samples were taken from surface (0-5 cm), mid-depth (20-30 cm), and deep (50-60 cm) levels under each trees. Ca analyses were performed using the ICP-OES device. This method is one of the most widely used methods preferred in many studies in recent years [28-31]. The data obtained were analyzed using Variance analysis and Duncan's test by making use of SPSS package software. The data were interpreted after simplifying and tabularizing them.

## 3. Result and Discussion

The data and statistical analysis results regarding the change of Ca concentration in plant organs are presented in Table 1.

**Table 1.** Change of Ca concentration between plant organs

| Species | Organ | | | | | F Values | Average |
|---|---|---|---|---|---|---|---|
| | Leaf | Bark | Cone | Wood | Root | | |
| Tf | 8164.4 Db | 5901.4 C | 3803.6 B | 1614.8 Aa | 7881.9 CDb | 14.4*** | 5473.2 |
| Bp | 6624.7 Ca | 5574.8 B | 1458.3 A | 4517.4 Bb | 3695.7 Ba | 7.97*** | 4374.2 |
| Sp | 6880.2 Ba | 8047.9 B | 1773.0 A | 1547.1 Aa | 7146.3 Bb | 63.89*** | 5078.9 |
| Ob | 8205.6 Cb | 4999.7 A | - | 3907.9 Ab | 6599.1 Bb | 14.90*** | 5928.1 |
| F Values | 9.36*** | 2.20 ns | 2.80 ns | 12.59*** | 15.85*** | | 2.19 ns |
| Average | 7468.7 C | 6130.9 B | 2344.9 A | 2896.8 A | 6330.8 B | 37.59*** | |

Variance analysis results showed that the change of Ca concentration by organ was statistically significant in all the species at the confidence level of 99.9%. Given the data, it can be seen that the lowest values were obtained from the woods and cones, whereas the highest values were obtained from the leaves. Examining by the species, the change of Ca concentration was not statistically significant in barks and cones ($p>0.05$). Considering the leaves, the lowest values were obtained from the pine varieties, whereas the highest ones were obtained from beech and fir species. The changes of Ca concentration in soil samples are presented in Table 2.

**Table 2.** Change of Ca concentration in soils

| Species | Soil depth | | | F Values | Average |
|---|---|---|---|---|---|
| | Upper | Medium | Lower | | |
| Tf | 8855.75 | 8695.33 b | 8993.38 bc | 0.08 ns | 8848.15 b |
| Bp | 8858.86 A | 10105.41 Bc | 7673.16 Ab | 4.34* | 8879.14 b |
| Sp | 9209.50 | 9606.77 bc | 9594.08 c | 0.42 ns | 9470.12 b |
| Ob | 8770.61 B | 5014.27 Aa | 5635.52 Aa | 17.65*** | 6473.47 a |
| F Values | 0.12 ns | 48.19*** | 10.55*** | | 16.14*** |
| Average | 8923.68 | 8355.45 | 7974.04 | 1.99 ns | |

As can be seen in Table 2, the change of Ca concentration by the soil depth was statistically significant for only soils, where Bp and Ob were grown ($p>0.05$). Besides that, the change of Ca concentration was not statistically significant for the surface level but statistically significant for mid-depth and deep levels. In mid-depth level, the lowest value was obtained from the soils where Ob was grown, whereas the highest values were obtained from the soils where pine varieties were grown. Considering the deep level, the lowest values were obtained from the soils where Ob was grown, whereas the highest values were obtained from the soils where Tf and Sp were grown.

## 4. Discussion and Conclusion

The results obtained here showed that Ca concentration in plant organs and in soils, where the species examined here are grown, might change depending on the plant species. It suggests that Ca nutrient element in soils is used at different levels by different plants. Therefore, plants significantly alter the nutrient element content in the soils, where they are grown. The nutrient element content of the soil is one of the most important factors influencing the root development of plants

[32-34]. As with all other organisms, the phenotypical characteristics and development of plants are shaped under the effects of plants' genetic structures [35-37] and environmental factors [38-41].

Among the environmental factors, one of the main factors influencing the plant development is the soil structure. Many factors such as nutrient content of soil, soil depth, enzymatic activities, microorganism status, soil structure, and soil texture influence the plant development [13, 42]. In fact, although the main factors influencing the plant development are the climatic [43-46] and edaphic [47-49] factors, previous studies showed that microclimatic and microedaphic factors affected the development and phenotypical characteristics of plants more than macro factors did [50-51] because plants get stressed due to various factors such as temperature, water deficiency, frost, UV-B, diseases and pests, and air pollution and it significantly affects plant development and phenotypical characteristics [52-61]. Among these factors, one of the ones influencing the plant development the most is the soil composition, which indicates the nutrient content of the soil [13,32].

Plants utilize the nutrient elements, which are necessary for their development, by taking them from the soil through their roots. As a result, the amount of nutrient content in the soil decreases and it affects the plant development. In agricultural soils, the deficiency of nutrient elements in the soil can be compensated through fertilization. However, since no fertilization can be performed in forest soils and it is necessary to carefully select the tree species to be grown by considering the nutrient content in the soil. But the number of studies examining to what extent the forest trees utilize which nutrient elements to what extent is very limited.

To date, many studies were carried out examining the concentrations of various nutrient elements in plant organs [62-64] and the soils [33-34]. However, the intake of nutrient elements into plants occurs through roots and aboveground roots. The knowledge of which sources the nutrient elements in plant organs are taken into plant body from is very limited [65]. Similarly, the information about the transfer of nutrient elements within the plant after the intake from soil or air is also limited [66-68]. Thus, to provide important information, it is necessary to determine the amounts of nutrient elements in soil and to perform comparative evaluations. Hence, it is recommended to carry out and diversify the studies examining this subject.

**Competing Interest / Conflict of Interest**

The authors declare that they have no competing interests.

**Author Contribution**

We declare that all Authors equally contribute.

**5. References**

[1] Yigit, N., Cetin, M., Ozturk, A., Sevik, H., & Cetin, S. (2019). Varitation of stomatal characteristics in broad leaved species based on habitat. Applied Ecology and Environmental Research, 17(6),12859-12868.

[2] Ozel, H. B., Donduran, B., Cakmakli, E., & Sevik, H. (2020). Factors affecting success in natural regeneration works of cedar (*Cedrus libani* A. Rich.) In Kas region of Antalya. World Journal of Advanced Research and Reviews, 6(2), 054-059.

[3] Cesur, A., Zeren Cetin, I., Abo Aisha, A. E. S., Alrabiti, O. B. M., Aljama, A. M. O., Jawed, A. A., Cetin, M., Sevik, H., Ozel, H. B. (2021). The usability of *Cupressus arizonica* annual rings in monitoring the changes in heavy metal concentration in air. Environmental Science and Pollution Research, 8(27), 35642-35648.

[4] Aricak, B., Cetin, M., Erdem, R., Sevik, H., & Cometen, H. (2019). The change of some heavy metal concentrations in Scotch pine (*Pinus sylvestris*) depending on traffic density, organelle and washing. Applied Ecology and Environmental Research, 17(3), 6723-6734.

[5] Sevik, H., Cetin, M., Kapucu, O., Aricak, B., & Canturk, U. (2017). Effects of light on morphologic and stomatal characteristics of Turkish Fir needles (*Abies nordmanniana* subsp. *bornmulleriana* Mattf.). Fresenius Environmental Bulletin, 26(11), 6579-6587.

[6] Yucedag, C., Ozel, H. B., Cetin, M., & Sevik, H. (2019). Variability in morphological traits of seedlings from five *Euonymus japonicus* cultivars. Environmental Monitoring and Assessment, 191(5), 1-4.

[7] Koç, İ. (2021). Changes that may occur in temperature, rain, and climate types due to global climate change: the example of Düzce. Turkish Journal of Agriculture-Food Science and Technology, 9(8), 1545-1554.

[8] Koç, İ. (2022). Determining the biocomfort zones in near future under global climate change scenarios in Antalya. Kastamonu University Journal of Engineering and Sciences, 8(1), 6-17.

[9] Zeren Cetin, I., Varol, T., Ozel, H. B. & Sevik H. (2022). The effects of climate on land use/cover: a case study in Turkey by using remote sensing data. Environmental Science and Pollution Research, 1-12.

[10] Varol, T., Ozel, H. B., Ertugrul, M., Emir, T., Tunay, M., Cetin, M., & Sevik, H. (2021). Prediction of soil-bearing capacity on forest roads by statistical approaches. Environmental Monitoring and Assessment, 193(8), 527.

[11] Sevik, H., Cetin, M., Ozel, H. B., & Pinar, B. (2019). Determining toxic metal concentration changes in landscaping plants based on some factors. Air Quality, Atmosphere & Health, 12(8), 983-991.

[12] Shults, P., Nzokou, P., & Koc, I. (2020). Nitrogen contributions of alley cropped Trifolium pratense may sustain short rotation woody crop yields on marginal lands. Nutrient Cycling in Agroecosystems, 117(2), 261-272.

[13] Kravkaz Kuscu, I. S., Cetin, M., Yigit, N., Savaci, G., & Sevik, H. (2018). Relationship between enzyme activity (Urease-Catalase) and nutrient element in soil use. Polish Journal of Environmental Studies, 27(5), 2107-2112.

[14] Erdem, R. (2021). Change of Several Plant Nutrient Elements by Plant Species and Organ. Turkish Journal of Agriculture-Food Science and Technology, 9(12), 2319-2324.

[15] Tuna, L. A. & Özer, Ö. (2005). Effect of different calcium compounds on the fruit yield, nutrition and some quality properties of watermelon (*Citrullus lanatus*) plant. Journal of Ege University Faculty of Agriculture, 42(1), 203-212.

[16] Mossi, M. M. M. (2018). Determination of heavy metal accumulation ın some shrub formed landscape plants. Kastamonu University, Institute of Science Department of Forest Engineering, PhD. Thesis. 141 pages.

[17] Cetin, M., Sevik, H., & Cobanoglu, O. (2020). Ca, Cu, and Li in washed and unwashed specimens of needles, bark, and branches of the blue spruce (Picea pungens) in the city of Ankara. Environmental Science and Pollution Research, 27(17), 21816-21825.

[18] Isinkaralar K. (2022). Some atmospheric trace metals deposition in selected trees as a possible biomonitor. Romanian Biotechnological Letters, 27(1), 3227-3236.

[19] Kuzmina, N., Menshchikov, S., Mohnachev, P., Zavyalov, K., Petrova, I., Ozel, H.B., Aricak, B., Onat, S. M., & Sevik, H. (2022). Change of aluminum concentrations in specific plants by species, organ, washing, and traffic density. BioResources, (InPress)

[20] Isinkaralar, K. (2022). Atmospheric deposition of Pb and Cd in the *Cedrus atlantica* for environmental biomonitoring. Landscape and Ecological Engineering, 1-10.

[21] Sevik, H., Cetin, M., Ozturk, A., Ozel, H. B., & Pinar, B. (2019). Changes in Pb, Cr and Cu concentrations in some bioindicators depending on traffic density on the basis of species and organs. Applied Ecology and Environmental Research, 17(6),12843-12857.

[22] Elajail, I. S. I., Sevik, H., Ozel, H. B., & Isik, B. (2022). Examining the chemical compositions of mineral concrete agents in terms of their environmental effects, Feb-Fresenius Environmental Bulletin. (InPress).

[23] Ghoma, W., Sevik, H. & Isinkaralar, K. (2022). Using indoor plants as biomonitors for detection of toxic metals by tobacco smoke. Air Quality, Atmosphere & Health, 15, 415-424.

[24] Isinkaralar, K., Erdem, R. (2021), Landscape plants as biomonitors for magnesium concentration in some species. International Journal of Progressive Sciences and Technologies, 29(2), 468-473.

[25] Isinkaralar, K., Koc, I., Erdem, R., Sevik, H. (2022). Atmospheric Cd, Cr, and Zn deposition in several landscape plants in Mersin, Türkiye. Water, Air, & Soil Pollution, 233(4), 1-10.

[26] Koç, İ. (2021). Using *Cedrus atlantica*'s annual rings as a biomonitor in observing the changes of Ni and Co concentrations in the atmosphere. Environmental Science and Pollution Research, 28(27), 35880–35886.

[27] Ucun Ozel, H., Ozel, H. B., Cetin, M., Sevik, H., Gemici, B. T., & Varol, T. (2019). Base alteration of some heavy metal concentrations on local and seasonal in Bartin River. Environmental Monitoring and Assessment, 191(9), 594.

[28] Sevik, H., Ozel, H. B., Cetin, M., Özel, H. U., & Erdem, T. (2019). Determination of changes in heavy metal accumulation depending on plant species, plant organism, and traffic density in some landscape plants. Air Quality, Atmosphere & Health, 12(2), 189-195.

[29] Sulhan, O.F., Sevik, H. & Isinkaralar, K. (2022). Assessment of Cr and Zn deposition on *Picea pungens* Engelm. in urban air of Ankara, Türkiye. Environment, Development and Sustainability, 1-20.

[30] Isinkaralar, K. (2022). Temporal variability of trace metal evidence in Cupressus arizonica, Platanus orientalis, and Robinia pseudoacacia as pollution-resistant species at an industrial site. Water, Air, & Soil Pollution, 233(7), 1-12.

[31] Isinkaralar, K., Isinkaralar, O., Sevik, H. (2022). Usability of some landscape plants in biomonitoring technique: an anaysis with special regard to heavy metals. Kent Akademisi Dergisi, 15(3),1413-1421.

[32] Kravkaz-Kuscu, I. S., Sariyildiz, T., Cetin, M., Yigit, N., Sevik, H., & Savaci, G. (2018). Evaluation of the soil properties and primary forest tree species in Taskopru (Kastamonu) district. Fresenius Environmental Bulletin, 27 (3), 1613-1617.

[33] Isinkaralar, K. (2022). Theoretical removal study of gas form BTEX onto activated carbon produced from Digitalis purpurea L. biomass. Biomass Conversion and Biorefinery, 1-11.

[34] Cetin, M., Aljama, A. M. O., Alrabiti, O. B. M. Adiguzel, F., Sevik, H., & Zeren Cetin, I. (2022). Using topsoil analysis to determine and map changes in Ni, Co pollution. Water, Air and Soil Pollution, 233, 293.

[35] Sevik, H., Yahyaoglu, Z., & Turna, I. (2012). Determination of genetic variation between populations of *Abies nordmanniana* subsp. *bornmulleriana* Mattf according to some seed characteristics, genetic diversity in plants. Chapter, 12, 231-248.

[36] Kurz, M., Koelz, A., Gorges, J., Carmona, B. P., Brang, P., Vitasse, Y., ... & Csillery, K. (2022). Tracing the origin of Oriental beech stands across Western Europe and reporting hybridization with European beech-implications for assisted gene flow. bioRxiv.

[37] Koç, İ (2021). Examination of gas exchange parameters of *Abies balsamea* (L.) Mill. and Abies concolor saplings, grown under various water regime, exposed to extreme drought stress at the end of the growing season. Turkish Journal of Forest Science, 5(2), 592-605.

[38] Bayraktar, E. P., Isinkaralar, O., & Isinkaralar, K. (2022). Usability of several species for monitoring and reducing the heavy metal pollution threatening the public health in urban environment of Ankara. World Journal of Advanced Research and Reviews, 14(3), 276-283.

[39] Isinkaralar, O., & Varol, C. (2023). A cellular automata-based approach for spatio-temporal modeling of the city center as a complex system: The case of Kastamonu, Türkiye. Cities, 132, 104073.

[40] Koç, İ. (2022). Determining the near-future biocomfort zones in Samsun province by the global climate change scenarios. Kastamonu University Journal of Forestry Faculty, 22(2), 181-192.

[41] Sevik, H., Cetin, M., & Kapucu, O. (2016). Effect of light on young structures of Turkish fir (*Abies nordmanniana* subsp. *bornmulleriana*). Oxidation Communications, 39(1), 485-492.

[42] Koç, İ., Nzokou, P., Cregg B. (2021). Biomass allocation and nutrient use efficiency in response to water stress: Insight from experimental manipulation of balsam fir, concolor fir and white pine transplants. New Forests, 53(5), 915-933.

[43] Isinkaralar, O., Varol, C., & Yilmaz, D. (2022). Digital mapping and predicting the urban growth: integrating scenarios into cellular automata—Markov chain modeling. Applied Geomatics, 1-11.

[44] Koç, İ. (2021). Examining seed germination rate and seedlings gas exchange performances of some Turkish Red pine provenances under water stress. Düzce University Journal of Science & Technology, 9(3), 48-60.

[45] Zeren Cetin, I. & Sevik, H. (2020). Investigation of the relationship between bioclimatic comfort and land use by using GIS and RS techniques in Trabzon. Environmental Monitoring and Assessment, 192 (2), 71.

[46] Tekin, O., Cetin, M., Varol, T., Ozel, H. B., Sevik, H., Zeren Cetin, I. (2022). Altitudinal migration of species of Fir (Abies spp.) in adaptation to climate change. Water, Air, & Soil Pollution, 233, 385 (2022).

[47] Varol, T., Emir, T., Akgul, M., Ozel, H. B., Acar, H. H., & Cetin, M. (2020). Impacts of small-scale mechanized logging equipment on soil compaction in forests. Journal of Soil Science and Plant Nutrition, 1-11.

[48] Işınkaralar, K. & Erdem, R. (2022). The effect of atmospheric deposition on potassium accumulation in several tree species as a biomonitor. Environmental Research and Technology, 5(1), 94-100.

[49] Karacocuk, T., Sevik, H., Isinkaralar, K. Turkyilmaz, A., Cetin, M. (2022). The change of Cr and Mn concentrations in selected plants in Samsun city center depending on traffic density. Landscape and Ecological Engineering, 18, 75-83.

[50] Yigit, N., Mutevelli, Z., Sevik, H., Onat, S. M., Ozel, H. B., Cetin, M., Olgun, C. (2021). Identification of some fiber characteristics in Rosa sp. and Nerium oleander L. wood grown under different ecological conditions. BioResources, 16(3), 5862-5874.

[51] Sevik, H., Cetin, M., Ozel, H. B., Erbek, A., & Cetin, I. Z. (2021). The effect of climate on leaf micromorphological characteristics in some broad-leaved species. Environment, Development and Sustainability, 23(4), 6395-6407.

[52] Ozel, H. B., Cetin, M., Sevik, H., Varol, T., Isik, B., Yaman, B. (2021). The effects of base station as an electromagnetic radiation source on flower and cone yield and germination percentage in Pinus brutia Ten. Biologia Futura. https://doi.org/10.1007/s42977-021-00085-1

[53] Yigit, N., Cetin, M., & Sevik, H. (2018). The of *Prunus laurocerasus* L. species by their habitat. Turkish Journal of Agriculture-Food Science and Technology, 6 (11), 1517-1521.

[54] Koç, İ. (2021). Examining of seed germination rate and seedlings gas exchange performances of Anatolian black pine under water stress. International Karabakh Applied Science Conference. Khazar Univeristy, June 17-19, 2021. (Conference paper).

[55] Işınkaralar, K. (2021). Changes in cadmium (Cd) concentrations in some plants depending on traffic density. New Trends and Issues Proceedings on Advances in Pure and Applied Sciences, (14), 63-70.

[56] Guney, K., Cetin, M., Sevik, H., Guney K. B. (2016). Influence of germination percentage and morphological properties of some hormones practice on *Lilium martagon* L. seeds. Oxidation Communications, 39(1-II), 466-474.

[57] Cesur, A., Zeren Cetin, I., Cetin, M., Sevik, H., Ozel, H. B. (2022). The use of *Cupressus arizonica* as a biomonitor of Li, Fe, and Cr pollution in Kastamonu. Water, Air and Soil Pollution, 233, 193.

[58] Koc, I., & Nzokou, P. (2018). Effects of water stress and cold treatments on the germination of two conifers (*Pinus nigr*a and *Pinus brutia*) species from Turkey. Hortscience, 53(9), 259-259.

[59] Sevik, H., & Erturk, N. (2015). Effects of drought stress on germination in fourteen provenances of *Pinus brutia* Ten. seeds in Turkey. Turkish Journal of Agriculture-Food Science and Technology, 3(5), 294-299.

[60] Sevik, H., & Karaca, U. (2016). Determining the resistances of some plant species to frost stress through ion leakage method. Feb-Fresenius Environmental Bulletin, 25(8), 2745-2750.

[61] Varol, T., Cetin, M., Ozel, H. B., Sevik, H., Zeren Cetin, I. (2022). The effects of climate change scenarios on *Carpinus betulus* and *Carpinus orientalis* in Europe. Water, Air and Soil Pollution, 233, 45.

[62] Savas, D.S., Sevik, H., Isinkaralar, K. Turkyilmaz, A. & Cetin, M. (2021). The potential of using *Cedrus atlantica* as a biomonitor in the concentrations of Cr and Mn. Environmental Science and Pollution Research, 28(39), 55446-55453.

[63] Turkyilmaz, A., Cetin, M., Sevik, H., Isinkaralar, K., & Saleh, E. A. A. (2020). Variation of heavy metal accumulation in certain landscaping plants due to traffic density. Environment, Development and Sustainability, 22(3), 2385-2398.

[64] Sevik, H., Cetin, M., Ozel, H. B., Ozel, S., & Cetin, I. Z. (2020). Changes in heavy metal accumulation in some edible landscape plants depending on traffic density. Environmental Monitoring and Assessment, 192(2), 78.

[65] Shahid, M., Dumat, C., Khalid, S., Schreck, E., Xiong, T., & Niazi, N. K. (2017). Foliar heavy metal uptake, toxicity and detoxification in plants: A comparison of foliar and root metal uptake. Journal of Hazardous Materials, 325, 36-58.

[66] Key, K., & Kulaç, Ş. (2022). Proof of concept to characterize historical heavy metal concentrations from annual rings of *Corylus colurna*: determining the changes of Pb, Cr, and Zn concentrations in atmosphere in 180 years in North Turkey. Air Quality, Atmosphere & Health, 1-11.

[67] Turkyilmaz, A., Sevik H., Isinkaralar K, & Cetin M. (2019). Use of tree rings as a bioindicator to observe atmospheric heavy metal deposition, Environmental Science and Pollution Research, 26(5), 5122-5130.

[68] Yayla, E. E., Sevik, H., & Isinkaralar, K. (2022). Detection of landscape species as a low-cost biomonitoring study: Cr, Mn, and Zn pollution in an urban air quality. Environmental Monitoring and Assessment, 194(10), 1-10.

doi:10.55385/kastamonujes.1185217 KUJES 8(2):128-134, 2022

Kastamonu University
Journal of Engineering and Sciences
e-ISSN 2667-8209
http://dergipark.gov.tr/kastamonujes

# Assessing the Co, Bi, and Mg Contents of Some Mineral Concrete Additives in terms of Environmental Effects

**Ibrahim Saleh Ibrahim Elajail [a], Hakan Sevik [b *]**

[a] Department of Material Science and Engineering, Institute of Science, Kastamonu University, Türkiye.
[b] Department of Environmental Engineering, Faculty of Engineering and Architecture, Kastamonu University, Kastamonu, Türkiye.
***Corresponding Author:** hsevik@kastamonu.edu.tr

Received: **October 06, 2022** ◆ Accepted: **December 14, 2022** ◆ Published Online: **December 26, 2022**

**Abstract:** Concrete additives started to be used commonly in order to reduce the cost of concrete, which is widely used in construction industry, and to recycle some wastes that are harmful to the environment. However, these additives might include heavy metals that are very harmful to human and environmental health and the number of studies on this subject is very limited. Besides the health of individuals working in this industry, it also creates a lack of knowledge about the environmental effects of construction activities. In the present study, among the heavy metals that can be very harmful to human and environmental health, Co, Bi, and Mg concentrations in some concrete additives were examined. The results showed that heavy metal concentrations in various concrete additives including copper slag, vermiculite, brick dust, Cem III cement, and blast furnace slag were very high. It might pose a risk to the health of individuals working in this industry, as well as the environmental health.

**Keywords:** Concrete, Additive, Cobalt, Bismuth, Magnesium

**Öz:** İnşaat sektöründe yaygın olarak kullanılan betonun maliyetini düşürmek ve çevreye zararlı bazı atıkların geri dönüştürülmesi amacıyla beton katkı maddeleri yaygın olarak kullanılmaya başlanmıştır. Ancak bu katkı maddeleri insan ve çevre sağlığına çok zararlı ağır metaller içerebilir ve bu konudaki çalışma sayısı oldukça sınırlı olduğu bilinmektedir. Bu sektörde çalışan bireylerin sağlığının yanı sıra inşaat faaliyetlerinin çevresel etkileri hakkında bilgi eksikliği de yaratmaktadır. Bu çalışmada insan ve çevre sağlığına çok zararlı olabilecek ağır metallerden bazı beton katkı maddelerindeki Co, Bi ve Mg konsantrasyonları incelenmiştir. Sonuçlar, bakır cürufu, vermikülit, tuğla tozu, Cem III çimentosu ve yüksek fırın cürufu gibi çeşitli beton katkı maddelerindeki ağır metal konsantrasyonlarının çok yüksek olduğunu göstermiştir. Bu sektörde çalışan bireylerin sağlığı ve çevre sağlığı açısından risk oluşturabilir.

**Anahtar Kelimeler:** Beton, Katkı, Kobalt, Bizmut, Magnezyum

## 1. Introduction

Social life and demographic structure on the earth have significantly changed in the last century due to the direct and indirect effects of the industrial activities. The most obvious effects of this change include global climate change, urbanization, and environmental health, which are among the most important problems worldwide. Increasing population density in urban areas necessitated the construction of multilayered buildings hosting more individuals in the unit area. Besides the construction of new buildings, also the replacement of old buildings with new ones requires the use of concrete at high amounts [1-8]

Concrete is the second-most used construction material (following the water) and it is the main constituent of buildings [9-11]. Thus, the content of concrete is very important from the aspect of environmental effects because it was reported that construction activities are among the factors affecting the amount of particles in the air during both construction and destruction phases [12]. Particle materials are among the ones determining the air quality [13] and the chemical structure of the particles in concrete composition is important for the environmental pollution [14-16]. Hence, the chemicals in the concrete additives might pose risk to workers working during the construction of building, individuals living in those buildings, and also the entire environment during the destruction [12]. For this reason, it is very important to determine the harmful element content of the additives constituting the concrete.

The scope of this study, Co, Bi, and Mg concentrations of some concrete additives were compared. Among the elements examined here, cobalt (Co) is an element that has toxic effects and, when inhaled, it causes alveoli, bronchus tumors, acute inflammation, alveoli epithelial hyperplasia, bronchial necrosis, and lung cancer [17]. Inhalation of bismuth (Bi) results in airway irritation and gingivitis, whereas oral intake of this element causes nausea, loss of appetite and weight, weariness, albuminuria, diarrhea, skin reactions, headache, fever, sleeplessness, and depression due to sulfur

accumulation [18]. The least harmful among the elements examined here is Magnesium (Mg) and Mg is the central atom of chlorophyll and plays a vital role in photosynthesis. The surplus of magnesium prevents the intake of potassium and negatively affects the root development of trees [19]. However, Mg is one of the heavy metals and previous studies showed that even the heavy metals, which are necessary as nutrient elements for organisms, are harmful when at high concentrations [20-23]. Moreover, it is known that inhaled heavy metals are very harmful to the human organism [24].

Even though these elements are very important for human and environmental health, the number of studies examining the chemical contents of concrete additives is not enough. In the present study, it was aimed to compare the Co, Bi, and Mg contents, which can be very harmful to human and environmental health, in some concrete additives.

## 2. Material and Method

Within the scope of this study, it was aimed to compare Co, Bi, and Mg contents of some mineral concrete additives. For this purpose, the mineral additives used as concrete additives most widely, especially the cement that is the main ingredient of concrete, were determined and samples were taken from recycling aggregate, blast furnace slag, fly ash, lime, wood ash, plaster, crushed stone, pumice, bottom ash, silica sand, brick dust, silica fume, copper slag, Cem I, Cem II, Cem II and Cem IV Cement, vermiculite, diatomite, rubber powder, marble powder, zeolite, perlite, and red pumice.

The materials obtained within the scope of this study were prepared for preliminary analyses. At this step, these materials were ground and sieved. Then, they were kept under laboratory conditions for 2 weeks until they became air-dried. Then, taking them into petri dishes, they were dried in drying oven at 45 °C for two weeks. Taking 0.5g from dried samples, they were taken into tubes designed specifically for microwave oven and added with 10 ml 65% $HNO_3$ and 2 ml 30% $H_2O_2$. These samples were combusted in a specifically designed microwave device under 280 PSI pressure at 180 ºC for 20 minutes. After cooling, the tubes taken out of the microwave were added with deionized water to fill to 50 ml. The samples were filtered using filter paper and then scanned using an ICP-OES (Inductive Coupled Plasma-Optic Emission Spectrometer) device at an appropriate wavelength. This method is among the ones used in elemental determination the most in recent years [25-31] and it is also used for analyzing the concrete additives [12].

In this study, all the measurements were repeated three times and the data obtained were analyzed using Variance Analysis and Duncan's test in SPSS package program. The results obtained from Variance Analysis and Duncan's test were simplified, tabularized, and then interpreted.

## 3. Result and Discussion

Figure The mean values for Co, Bi, and Mg elements examined here and the statistical analysis results are presented in Table 1.

**Table 1.** Elemental contents of solid materials

| Materials | Co (ppb) | Bi (ppb) | Mg (ppm) |
|---|---|---|---|
| Recycling aggregate | 2294.8 d | 1502.3 ab | 3344.3 i |
| Blast Furnace Slag | 7461.8 l | 9382.7 g | 15347.1 v |
| Fly ash | 5037.8 i | UnLim | 2113.6 f |
| Lime | 856.4 a | 2703.1 cd | 5821.7 k |
| Wood ash | 8165.4 m | 3375.9 d | 10286.8 p |
| Gypsum | 707.2 a | 1759.9 abc | 4530.8 j |
| Crushed Stone | 806.6 a | 2553.3 bcd | 1332.3 e |
| Pumice | 4017.4 g | 684.7 a | 762.0 c |
| Bottom ash | 4351.3 h | 1103.3 a | 2091.4 f |
| Silica sand | 1594.6 c | 1124.9 a | 420.6 b |
| Brick powder | 23830.8 r | 5679.2 e | 10630.6 r |
| Silica fume | 1126.8 b | UnLim | 1067.8 d |
| Copper slag | 82648.0 t | 158643.2 i | 6434.2 m |
| Cem II Cement | 7028 k | 5554.7 e | 8481.2 o |
| Vermiculite | 25195.3 s | 4574.6 e | 15246.2 u |
| Cem IV Cement | 6208.3 j | 4739.5 e | 8166.3 n |
| Diatomite | 2982.7 f | 1018.8 a | 6083.1 l |
| Cem III Cement | 10129 n | 11503.3 h | 15356.0 v |
| Cem I Cement | 7333.3 l | 7935.3 f | 12962.6 s |
| Tire dust | 11248.8 o | UnLim | 14.7 a |
| Marble powder | 2748.3 e | 1217.8 a | 2341 g |
| Zeolite | 1125.8 b | 741 a | 3198.3 h |
| Perlite | 695 a | UnLim | UnLim |
| Red Pumice | 18541.1 p | 5218.6 e | 15043.8 t |
| F Values | 71815.061*** | 8378.837*** | 70321.087*** |

letter refers to the vertical direction, UnLim: Under detection limits, *** significant at 0.001 level.

As a result of the study, it was determined that Co concentration ranged between 695 ppb and 82648 ppb, that the lowest values were obtained in perlite (695.0 ppb), plaster (707.2 ppb), and crushed stone (806.6 ppb), whereas the highest values were obtained from copper slag (82648.0 ppb), vermiculite (25195.3 ppb), and brick powder (23830.8 ppb). It is interesting that there was a difference higher than three folds between copper slag yielding the highest value and vermiculite yielding the second-highest value.

Bi concentration remained below the detectable limits in fly ash, silica fume, rubber powder, and perlite. The lowest Bi concentrations were found in pumice (684.7 ppb), zeolite (741.0 ppb), and diatomite (1018.8 ppb), whereas the highest values were found in copper slag (158643.2 ppb), Cem III cement (11503.3 ppb), and blast furnace slag (9382.7 ppb). As with Co element, there was a very high level of difference between the highest value (copper slag) and the second-highest value (Cem III cement) and the difference was higher than thirteen folds.

Mg, the other element examined here, remained below the detectable limits in perlite and ranged between 14.7 ppm and 15356.0 ppm in other samples. The lowest Mg concentrations were obtained from rubber powder (14.7 ppm), silica sand (420.6 ppm), and pumice (762.0 ppm), whereas the highest concentrations were obtained from Cem III cement (15356.0 ppm), blast furnace slag (15347.1 ppm), and vermiculite (15246.2 ppm).

## 4. Discussion and Conclusion

As a result of the study, it was determined that the elements examined here were at very high concentrations in some concrete additives. These elements are classified as heavy elements and, from the aspect of health, many of heavy elements are toxic, harmful, and carcinogenic even at low concentrations [32]. Co, one of these elements, is in the preliminary pollutant list of ATSDR (Agency for Toxic Substances and Disease Registry) [33] and is harmful to organisms even when at low concentrations [34]. Thus, many studies were carried out in order to determine the concentration of Co in various environments [35-38]. However, Bi and Mg, the other elements examined in the present study, are among the ignored elements. On the other hand, it is emphasized that these elements might be harmful to health. For instance, Bi can cause diarrhea, headache, fever, and liver and kidney diseases [18], while it was stated that all heavy metals could cause severe disorders when inhaled [24].

Moreover, previous studies showed that even the heavy metals that are necessary as nutrient element for organic development might be harmful to health when at high concentrations [35-38]. For this reason, many studies have examined the concentrations of heavy metals in soil [39, 40], water [41-43], and air [44-49]. In recent years, the studies carried out on heavy metals were diversified more and many studies were carried out on heavy metal pollution caused by heavy metal sources such as traffic [50-53], industry [54], urban areas [55], and mining fields [56].

Remaining undegraded in nature for a long time since it has a long half-life, heavy metals that accumulate in bodies of organisms and can be toxic or carcinogenic even when at low concentrations are considered as one of the most dangerous environmental pollution factors [57-60]. For this reason, use of waste materials (especially heavy metals), many of which are important environmental pollutants, as a concrete additive is very important since it decreases the cost of concrete and it contributes to the reduction of environmental pollution by eliminating the environmental pollutants through recycling [61-64]. For this reason, many studies examining the use of various waste materials as concrete additives were carried out in recent years [65-67]. However, almost all those studies investigated the effects of those additives on concrete characteristics [68-71]. Yet, the number of studies on the chemical compositions of those additives is very limited.

## 5. Suggestions

As a result of this study, it was determined that the concentrations of Co, Bi, and Mg were very high in some concrete additives. Inhalation of additives, which were examined here, by workers while they are used as concrete additives might cause severe health risks. For this reason, attention should be paid to the use of copper slag, vermiculite, brick powder, Cem III cement, and blast furnace slag, in which the heavy metal pollutions were found to be high. Workers should be warned about the risks of these materials and necessary measures should be taken.

Among the additives examined here, the ones such as blast furnace slag and copper slag are the wastes of industrial facilities. The materials such as vermiculite are used in agriculture, and brick is used in various fields. Thus, the individuals working in these industries are exposed to the powders of these materials. The individuals working in other industries, where these materials are used, should be warned and it should be ensured that necessary measures would be taken.

## Competing Interest / Conflict of Interest

The authors declare that they have no competing interests.

## Author Contribution

We declare that all Authors equally contribute.

**Acknowledgements**

This study was produced from a Doctoral study at Kastamonu University, Institute of Science Graduate Studies Research Projects (Ph.D.). Thank you for advisor and Kastamonu University Institute of Science Department of Material Science and Engineering for Ph.D. thesis

**6. References**

[1] Koç, İ. (2022). determining the near-future biocomfort zones in samsun province by the global climate change scenarios. Kastamonu University Journal of Forestry Faculty, 22(2), 181-192.

[2] Isinkaralar, O., & Varol, C. (2023). A cellular automata-based approach for spatio-temporal modeling of the city center as a complex system: The case of Kastamonu, Türkiye. Cities, 132, 104073.

[3] Isinkaralar, O., Varol, C., & Yilmaz, D. (2022). Digital mapping and predicting the urban growth: integrating scenarios into cellular automata—Markov chain modeling. Applied Geomatics, 1-11.

[4] Isinkaralar, K. (2022). Theoretical removal study of gas form BTEX onto activated carbon produced from *Digitalis purpurea* L. biomass. Biomass Conversion and Biorefinery, 1-11.

[5] Kalayci Onac, A., Cetin, M., Sevik, H., Orman, P., Karci, A., Gonullu Sutcuoglu, G. (2021). Rethinking the campus transportation network in the scope of ecological design principles: case study of İzmir Katip Çelebi University Çiğli Campus Environmental Science and Pollution Research, 28(36), 50847-50866.

[6] Zeren Cetin, I., Varol, T., Ozel, H. B., & Sevik, H. (2022). The effects of climate on land use/cover: a case study in Turkey by using remote sensing data. Environmental Science and Pollution Research, 1-12.

[7] Varol, T., Canturk, U., Cetin, M., Ozel, H. B., Sevik, H., & Zeren Cetin, I. (2022). Identifying the suitable habitats for Anatolian boxwood (*Buxus sempervirens* L.) for the future regarding the climate change. Theoretical and Applied Climatology, 150(1), 637-647.

[8] Tekin, O., Cetin, M., Varol, T., Ozel, H. B., Sevik, H., & Zeren Cetin, I. (2022). Altitudinal migration of species of fir (Abies spp.) in adaptation to climate change. Water, Air, & Soil Pollution, 233(9), 1-16.

[9] Gencel, O., Sarı, A., Kaplan, G., Ustaoglu, A., Hekimoğlu, G., Bayraktar, O. Y., & Ozbakkaloglu, T. (2022). Properties of eco-friendly foam concrete containing PCM impregnated rice husk ash for thermal management of buildings. Journal of Building Engineering, 58, 104961.

[10] Bayraktar, O. Y., Soylemez, H., Kaplan, G., Benli, A., Gencel, O., & Turkoglu, M. (2021). Effect of cement dosage and waste tire rubber on the mechanical, transport and abrasion characteristics of foam concretes subjected to H2SO4 and freeze–thaw. Construction and Building Materials, 302,124229.

[11] Altera, A. Z. A., Bayraktar, O. Y., & Soylemez, H. (2019). Investigation of the effects of modified bitumen on asphalt concrete performance by industrial waste. Kastamonu University Journal of Engineering and Sciences, 5(2),93-100.

[12] Elajail, I. S. I., Sevik, H., Ozel, H. B., Isik, B. (2022). Examining the chemical compositions of mineral concrete agents in terms of their environmental effects. Feb-Fresenius Environmental Bulletin, 31(9), 9784-9790.

[13] Cetin, M., Sevik, H., & Isinkaralar, K. (2017). Changes in the particulate matter and CO2 concentrations based on the time and weather conditions: the case of Kastamonu. Oxidation Communications, 40(1-II), 477-485.

[14] Amran, M., Huang, S. S., Onaizi, A. M., Makul, N., Abdelgader, H. S., & Ozbakkaloglu, T. (2022). Recent trends in ultra-high performance concrete (UHPC): Current status, challenges, and future prospects. Construction and Building Materials, 352, 129029.

[15] Wang, H., Wu, Y., & Cheng, B. (2022). Mechanical properties of alkali-activated concrete containing crumb rubber particles. Case Studies in Construction Materials, 16, e00803.

[16] Surendranath, A., & Ramana, P. V. (2022). Valorization of bakelite plastic waste aimed at auxiliary comprehensive concrete. Construction and Building Materials, 325, 126851.

[17] Suh, M., Thompson, C. M., Brorby, G. P., Mittal, L., & Proctor, D. M. (2016). Inhalation cancer risk assessment of cobalt metal. Regulatory Toxicology and Pharmacology, 79, 74-82.

[18] Bakırcı, S. (2019). Aydın ilinde üretimi yapılan bazı arı ürünlerindeki ağır metal düzeylerinin karşılaştırılması. Adnan Menderes University Institute of Health Sciences (Veterinary Medicine) Departman of Biochemistry, Master's Thesis, p. 108.

[19] Ozel, H. B., Varol, H.N., Sevik, H. (2021). Change of Mg concentration in several plants depending on plant species, washing status, and traffic density, World Journal of Advanced Research and Reviews, 12(01), 447–453

[20] Sevik, H., Cetin, M., Ozel, H. U., Ozel, H. B., Mossi, M. M. M., & Cetin, I. Z. (2020). Determination of Pb and Mg accumulation in some of the landscape plants in shrub forms. Environmental Science and Pollution Research, 27(2), 2423-2431.

[21] Ozel, H. B., Sen, M., Sevik, H. (2021). Change of Ba concentration by species and organ in several fruits grown in city centers, World Journal of Advanced Research and Reviews, 12(03), 143–150.

[22] Işınkaralar, K. (2021). Changes in cadmium (Cd) concentrations in some plants depending on traffic density. New Trends and Issues Proceedings on Advances in Pure and Applied Sciences, (14), 63-70.

[23] Yayla, E. E., Sevik, H., & Isinkaralar, K. (2022). Detection of landscape species as a low-cost biomonitoring study: Cr, Mn, and Zn pollution in an urban air quality. Environmental Monitoring and Assessment, 194(10), 1-10.

[24] Elajail, I.S.I., Sevik, H., (2022). Examining the chemical compositions of mineral concrete agents in terms of their environmental effects. Icontech International Journal, 6(3), 83-93.

[25] Çobanoğlu, H., Şevik, H., & Koç, İ. (2022). Availability of annual rings in the detection of ca concentration in the air and ıts relationship with traffic density. Icontech International Journal, 6(3), 94-106.

[26] Kuzmina, N., Menshchikov, S., Mohnachev, P., Zavyalov, K., Petrova, I., Ozel, H. B., Aricak, B., Onat, S. M., Sevik, H. (2022). Change of aluminum concentrations in specific plants by species, organ, washing, and traffic density. BioResources, (InPress)

[27] Isinkaralar, K. (2022). Temporal variability of trace metal evidence in Cupressus arizonica, Platanus orientalis, and Robinia pseudoacacia as pollution-resistant species at an industrial site. Water, Air, & Soil Pollution, 233(7), 1-12.

[28] Isinkaralar, K., Koc, I., Erdem, R., & Sevik, H. (2022). Atmospheric Cd, Cr, and Zn deposition in several landscape plants in Mersin, Türkiye. Water, Air, & Soil Pollution, 233(4), 1-10.

[29] Ghoma, W., Sevik, H. & Isinkaralar, K. (2022). Using indoor plants as biomonitors for detection of toxic metals by tobacco smoke. Air Quality Atmosphere and Health, 15, 415-424.

[30] Cesur, A., Zeren Cetin, I., Cetin, M., Sevik, H., Ozel, H. B. (2022). The use of Cupressus arizonica as a biomonitor of Li, Fe, and Cr pollution in Kastamonu. Water, Air and Soil Pollution, 233, 193.

[31] Aricak, B., Cetin, M., Erdem, R., Sevik, H., & Cometen, H. (2020). The usability of Scotch pine (Pinus sylvestris) as a biomonitor for traffic-originated heavy metal concentrations in Turkey. Polish Journal of Environmental Studies, 29 (2), 1051-1057.

[32] Sulhan, O. F., Sevik, H., & Isinkaralar, K. (2022). Assessment of Cr and Zn deposition on Picea pungens Engelm. in urban air of Ankara, Türkiye. Environment, Development and Sustainability, 1-20.

[33] Badea, M., Luzardo, O. P., González-Antuña, A., Zumbado, M., Rogozea, L., Floroian, L., Alexandrescu, D., Moga, M., Gaman, L.,Radoi, M., Boada, L.D. & Henríquez-Hernández, L. A. (2018). Body burden of toxic metals and rare earth elements in non-smokers, cigarette smokers and electronic cigarette users. Environmental research, 166, 269-275.

[34] Cetin, M., Aljama, A. M. O., Alrabiti, O. B. M. Adiguzel, F., Sevik, H., & Zeren Cetin, I. (2022). Using topsoil analysis to determine and map changes in Ni Co pollution. Water, Air and Soil Pollution, 233, 293 (2022).

[35] Sevik, H., Cetin, M., Ozel, H. B., Akarsu, H., & Cetin, I. Z. (2020). Analyzing of usability of tree-rings as biomonitors for monitoring heavy metal accumulation in the atmosphere in urban area: a case study of cedar tree (Cedrus sp.). Environmental Monitoring and Assessment, 192 (1), 23.

[36] Turkyilmaz, A., Sevik, H., & Cetin, M. (2018). The use of perennial needles as bio-monitors for recently accumulated heavy metals. Landsc Ecol Eng 14 (1):115–120.

[37] Turkyilmaz, A., Sevik H., Isinkaralar, K., & Cetin, M. (2019). Use of tree rings as a bioindicator to observe atmospheric heavy metal deposition. Environmental Science and Pollution Research, 26(5), 5122-5130.

[38] Kravkaz Kuşçu, İ. S., Kılıç Bayraktar, M., & Tunçer, B. (2022). Determination of heavy metal (Cr, Co, and Ni) accumulation in selected vegetables depending on traffic density. Water, Air and Soil Pollution, 233(6), 1-10.

[39] Cetin, M., Aljama, A. M. O., Alrabiti, O. B. M., Adiguzel, F., Sevik, H., & Zeren Cetin, I. (2022). Determination and mapping of regional change of Pb and Cr pollution in Ankara city center. Water, Air and Soil Pollution, 233(5), 1-10.

[40] Qin, G., Niu, Z., Yu, J., Li, Z., Ma, J., & Xiang, P. (2021). Soil heavy metal pollution and food safety in China: Effects, sources and removing technology. Chemosphere, 267, 129205.

[41] Demir, T., Mutlu, E., Aydın, S., & Gültepe, N. (2021). Physicochemical water quality of Karabel, Çaltı, and Tohma brooks and blood biochemical parameters of Barbus plebejus fish: assessment of heavy metal concentrations for potential health risks. Environmental Monitoring and Assessment, 193(11), 1-15.

[42] Tokatli, C., Mutlu, E., & Arslan, N. (2021). Assessment of the potentially toxic element contamination in water of Şehriban Stream (Black Sea Region, Turkey) by using statistical and ecological indicators. Water Environment Research, 93(10), 2060-2071.

[43] Ucun Ozel, H., Ozel, H. B., Cetin, M., Sevik, H., Gemici, B. T., & Varol, T. (2019). Base alteration of some heavy metal concentrations on local and seasonal in Bartin River. Environmental Monitoring And Assessment, 191(9), 594.

[44] Savas, D. S., Sevik, H., Isinkaralar, K., Turkyilmaz, A., & Cetin, M. (2021). The potential of using Cedrus atlantica as a biomonitor in the concentrations of Cr and Mn. Environmental Science and Pollution Research, 28(39), 55446-55453.

[45] Turkyilmaz, A., Cetin, M., Sevik, H., Isinkaralar, K., & Saleh, E. A. A. (2020). Variation of heavy metal accumulation in certain landscaping plants due to traffic density. Environment, Development and Sustainability, 22(3), 2385-2398.

[46] Sevik, H., Ozel, H. B., Cetin, M., Özel, H. U., & Erdem, T. (2019). Determination of changes in heavy metal accumulation depending on plant species, plant organism, and traffic density in some landscape plants. Air Quality, Atmosphere & Health, 12(2), 189-195.

[47] Key, K., & Kulaç, Ş. (2022). Proof of concept to characterize historical heavy metal concentrations from annual rings of Corylus colurna: determining the changes of Pb, Cr, and Zn concentrations in atmosphere in 180 years in North Turkey. Air Quality, Atmosphere & Health, 1-11.

[48] Isinkaralar, K., Isinkaralar, O., Sevik, H. (2022). Usability of some landscape plants in biomonitoring technique: an anaysis with special regard to heavy metals. Kent Akademisi Dergisi, 15(3),1413-1421.

[49] Cetin, M., Sevik, H., & Cobanoglu, O. (2020). Ca, Cu, and Li in washed and unwashed specimens of needles, bark, and branches of the blue spruce (Picea pungens) in the city of Ankara. Environmental Science and Pollution Research, 27(17), 21816-21825.

[50] Cesur, A., Zeren Cetin, I., Abo Aisha, A. E. S., Alrabiti, O. B. M., Aljama, A. M. O., Jawed, A. A., Cetim, M., Sevik, H., & Ozel, H. B. (2021). The usability of Cupressus arizonica annual rings in monitoring the changes in heavy metal concentration in air. Environmental Science and Pollution Research, 28(27), 35642-35648.

[51] Aricak, B., Cetin, M., Erdem, R., Sevik, H., & Cometen, H. (2019). The change of some heavy metal concentrations in Scotch pine (Pinus sylvestris) depending on traffic density, organelle and washing. Applied Ecology and Environmental Research, 17(3), 6723-6734.

[52] Isinkaralar, K. (2022). Atmospheric deposition of Pb and Cd in the Cedrus atlantica for environmental biomonitoring. Landscape and Ecological Engineering, 1-10.

[53] Sevik, H., Cetin, M., Ozel, H. B., & Pinar, B. (2019). Determining toxic metal concentration changes in landscaping plants based on some factors. Air Quality, Atmosphere & Health, 12(8), 983-991.

[54] Key, K., Kulaç, Ş., Koç, İ., & Sevik, H. (2022). Determining the 180-year Change of Cd, Fe, and Al concentrations in the air by using annual rings of Corylus colurna L. Water, Air, & Soil Pollution, 233(7), 1-13.

[55] Ucun Ozel, H., Gemici, B. T., Gemici, E., Ozel, H. B., Cetin, M., & Sevik, H. (2020). Application of artificial neural networks to predict the heavy metal contamination in the Bartin River. Environmental Science Pollution Research, 27,42495–42512

[56] Alaqouri, H. A. A., Ozer Genc, C., Aricak, B., Kuzmina, N., Menshikov, S., Cetin, M. (2020) The Possibility of Using Scots Pine (Pinus sylvestris L.) Needles as biomonitor in the determination of heavy metal accumulation. Applied Ecology and Environmental Research, 18(2), 3713-3727.

[57] Pirinc Bayraktar, E., Isinkaralar, O., & Isinkaralar, K. (2022). Usability of several species for monitoring and reducing the heavy metal pollution threatening the public health in urban environment of Ankara. World Journal of Advanced Research and Reviews, 14(3), 276-283.

[58] Isinkaralar, K. (2022). Some atmospheric trace metals deposition in selected trees as a possible biomonitor. Romanian Biotechnological Letters, 27(1), 3227-3236.

[59] Karacocuk, T., Sevik, H., Isinkaralar, K., Turkyilmaz, A., Cetin, M. (2022). The change of Cr and Mn concentrations in selected plants in Samsun city center depending on traffic density. Landscape and Ecological Engineering, 18,75-83.

[60] Koç, İ. (2021). Using Cedrus atlantica's annual rings as a biomonitor in observing the changes of Ni and Co concentrations in the atmosphere. Environmental Science and Pollution Research, 28(27), 35880–35886

[61] Bayraktar, O. Y., Yarar, G., Benli, A., Kaplan, G., Gencel, O., Sutcu, M., ... & Kadela, M. (2022). Basalt fiber reinforced foam concrete with marble waste and calcium aluminate cement. Structural Concrete.

[62] Gencel, O., Harja, M., Sarı, A., Hekimoğlu, G., Ustaoğlu, A., Sutcu, M., ... & Bayraktar, O. Y. (2022). Development, characterization, and performance analysis of shape-stabilized phase change material included-geopolymer for passive thermal management of buildings. International Journal of Energy Research.

[63] Kaplan, G., Turkoglu, M., Bodur, B., & Bayraktar, O. Y. (2022). Usage of recycled fine aggregates obtained from concretes with low w/c ratio in the production of masonry plaster and mortar. Environment, Development and Sustainability, 24(2), 2685-2714.

[64] Kursuncu, B., Gencel, O., Bayraktar, O. Y., Shi, J., Nematzadeh, M., & Kaplan, G. (2022). Optimization of foam concrete characteristics using response surface methodology and artificial neural networks. Construction and Building Materials, 337, 127575.

[65] Bayraktar, O. Y. (2020). Use of geosynthetics in road construction. Kastamonu University Journal of Engineering and Sciences, 6(2), 107-113.

[66] Gencel, O., Balci, B., Bayraktar, O. Y., Nodehi, M., Sarı, A., Kaplan, G., ... & Ozbakkaloglu, T. (2022). The effect of limestone and bottom ash sand with recycled fine aggregate in foam concrete. Journal of Building Engineering, 104689.

[67] Yaras, A., Ustaoglu, A., Gencel, O., Sarı, A., Hekimoğlu, G., Sutcu, M., ... & Bayraktar, O. Y. (2022). Characteristics, energy saving and carbon emission reduction potential of gypsum wallboard containing phase change material. Journal of Energy Storage, 55, 105685.

[68] Gencel, O., Nodehi, M., Bayraktar, O. Y., Kaplan, G., Benli, A., Gholampour, A., & Ozbakkaloglu, T. (2022). Basalt fiber-reinforced foam concrete containing silica fume: An experimental study. Construction and Building Materials, 326, 126861.

[69] Kaplan, G., Gulcan, A., Cagdas, B., & Bayraktar, O. Y. (2021). The impact of recycled coarse aggregates obtained from waste concretes on lightweight pervious concrete properties. Environmental Science and Pollution Research, 28(14), 17369-17394.

[70] Bayraktar, O. Y., Kaplan, G., Gencel, O., Benli, A., & Sutcu, M. (2021). Physico-mechanical, durability and thermal properties of basalt fiber reinforced foamed concrete containing waste marble powder and slag. Construction and Building Materials, 288, 123128.

[71] Gencel, O., Kazmi, S. M. S., Munir, M. J., Kaplan, G., Bayraktar, O. Y., Yarar, D. O., ... & Ahmad, M. R. (2021). Influence of bottom ash and polypropylene fibers on the physico-mechanical, durability and thermal performance of foam concrete: An experimental investigation. Construction and Building Materials, 306, 124887.

doi:10.55385/kastamonujes.1193007 KUJES 8(2):135-144, 2022

Kastamonu University
Journal of Engineering and Sciences
e-ISSN 2667-8209
http://dergipark.gov.tr/kastamonujes

# ANFIS-based Parameter Estimation of a Single Phase Inverter Circuit with Isolation Transformer

**Busra Aslan [a]*, Selami Balci [b], Ahmet Kayabasi [b]**

[a] Department of Mechatronics Engineering, Karamanoglu Mehmetbey University, Karaman, Türkiye
[b] Department of Electrical and Electronics Engineering, Karamanoglu Mehmetbey University, Karaman, Türkiye
***Corresponding Author:** busraaslan@kmu.edu.tr

Received: **October 21, 2022** ◆ Accepted: **December 15, 2022** ◆ Published Online: **December 26, 2022**

**Abstract:** This study aims to isolate the output interface of single-phase inverter circuits and the grid from each other. For this purpose, the electromagnetic modeling of the isolation transformer was carried out in three dimensions (3D) with the Ferrite N87 core material. In order to determine the leakage inductance behavior of the transformer, a data set was obtained as a specific parametric scenario by changing the geometric dimensions of the primary-secondary windings with parametric linear steps. Thus, the estimation process of the electromagnetic modelling of the transformer has been successfully carried out thanks to the training and testing processes of Adaptive Network Based Fuzzy Inference Systems (ANFIS) with the numerical information obtained from the finite element analysis (FEA) parametric data set. After the estimation processes, the percentage error is calculated as 0.3470% and 0.4448% for training and testing. Thus, the determination of the isolation transformer with the optimum values designed for the inverter circuit has become easier. Also, experimental analysis is performed on inverters to prove the robustness of the proposed method. In this context, first of all, RMS values that vary according to the different operating parameters of the inverters are created. The proposed ANFIS-based system estimates RMS values with 7,057 % error.

**Keywords:** Isolation transformer, Leakage inductance, Inverter, FEA, ANFIS

**Öz:** Bu çalışmada, tek fazlı evirici devrelerinin çıkış arayüzü ile şebekenin birbirinden izole edilmesi amaçlanmıştır. Bu amaçla, izolasyon transformatörünün elektromanyetik modellemesi Ferrite N87 çekirdek malzemesi ile üç boyutlu (3D) olarak gerçekleştirilmiştir. Transformatörün kaçak endüktans davranışını belirlemek için birincil-ikincil sargılarının geometrik ölçüleri parametrik lineer adımlar ile değiştirilerek spesifik bir parametrik senaryo halinde bir veri seti elde edilmiştir. Böylece sonlu elemanlar analizi (SEA) parametrik veri setinden elde edilen sayısal bilgilerle Bulanık Mantık Sistemine Dayalı Uyarlanır Ağlar (BMSDUA) eğitim ve test süreçleri sayesinde transformatörün elektromanyetik modellemesinin tahmin süreci başarıyla gerçekleştirilmiştir. Tahmin işlemlerinden sonra eğitim ve test için hata yüzdesi %0,3470 ve %0,4448 olarak hesaplanmıştır. Böylece evirici devresi için tasarlanan optimum değerlere sahip izolasyon trafosunun belirlenmesi kolaylaşmıştır. Ayrıca önerilen yöntemin sağlamlığını kanıtlamak için eviriciler üzerinde deneysel analizler yapılmıştır. Bu kapsamda öncelikle eviricilerin farklı çalışma parametrelerine göre değişen RMS değerleri oluşturulur. Önerilen BMSDUA tabanlı sistem, RMS değerlerini %7.057 hata ile tahmin etmektedir.

**Anahtar Kelimeler:** İzolasyon transformatörü, Kaçak endüktans, Evirici, SEA, BMSDUA

## 1. Introduction

The use of renewable energy sources has increased in recent years. There has been a need to isolate the inverter circuits, which are among the power electronic converters, and the grid interface from each other. For this reason, it is essential to design an isolation transformer that keeps costs and losses to a minimum. In recent years, it has become necessary to isolate the circuits used in power electronics grid integration with the increase in the installed power of renewable energy sources. In this context, it is extremely important to design an isolation transformer, which is included in DC-AC converter circuits, as large as possible with the lowest cost and the highest efficiency. In addition, the electromagnetic performance of an isolation transformer between the load and the inverter greatly changes the power electronics circuit performance in order to obtain a voltage close to a pure sinusoidal waveform. In this way, more efficient operation of the systems connected to the inverter output can be achieved.

The use of transformers in our daily life and in the industry is quite common. Although their use is usually to step-up or step-down of the voltage level to make it suitable at the desired level, it is also often used to isolate two or more electrical power systems from each other [1]. One of the reasons why transformers work efficiently is that they have no moving parts. As a general need, transformers have an important component in the transmission of electrical energy over long distances and distribution in the grid structure. For this reason, transformers are one of the most important power electronic components used in electrical energy transmission/distribution lines [2].

It has been determined that many analyzes have been made on the leakage inductance parameters of transformers. In fact, although leakage fluxes are undesirable because they affect the regulation in power distribution transformers, in medium/high-frequency transformers used in power electronics circuits, leakage flux inductance emerges as an important parameter in the resonance circuit as a circuit element.

Isolating transformers isolate the output voltage and the input voltage from each other, isolating the source and the load from each other. Especially based on this advantage, it ensures the safe operation of highly affected electrical devices such as computer-based information systems and grid integration circuits. On the other hand, electrical accidents that may occur due to wetness and humidity can be prevented in terms of the safety of living things [3]. Not much has been changed in the structure of transformers since they were invented. However, studies to reduce the size of the core materials and transformer used are still continuing [4]. In the design of the transformer, attention is paid to keeping the power losses as low as possible in terms of higher efficiency. In order to design low-power loss transformers, studies on the power losses of ideal wound transformers are frequently carried out [5]. Aghaei, et al. [6 ] discussed in detail the leakage inductance behavior of transformers whose primary and secondary windings are not regular, and thanks to FEA simulation studies, it is possible to have an idea about power losses and voltage regulation before the prototype production phase, and to prevent critical situations that may be encountered. The use of medium-frequency transformers is common in power converter circuits and power distribution grids. The correct adaptation to the increasing switching frequency depends on some parameters of the transformers. Therefore, many parameters of the electromagnetic behavior of transformers must be estimated before they are integrated into the power electronics circuit. In this context, Tian, et al. [7] developed an operating frequency-dependent method to estimate the leakage inductance value of an isolation transformer in the mid-frequency range. Thus, the relationship between the leakage inductance value and the magnetic field intensity distribution and electromagnetic behavior was investigated. In this way, the leakage inductance has been calculated successfully. In order to minimize the leakage inductance value, the advantages of interspersed winding structures and different winding structures and their effects on leakage inductance were compared with test the presented new method, such as 10kW, 500 / 5000V, and 5kHz specifications. Also, it was determined and reported that the results obtained at the end of the test phase were compatible with the results obtained using FEA. Similarly, Mogorovic and Dujic [8] designed a high-frequency transformer in power electronics grid integration circuits and made detailed analytical modeling of the leakage inductance behavior of this transformer providing galvanic isolation. Analyzes were made with the Finite Element Method (SEM). Prieto, et al. [9] aimed to estimate the leakage inductance and AC resistance of the transformer. Thus, Finite Element Analysis (FEA) based modeling techniques can be used to calculate different frequency and geometry effects. With the proposed method, it is ensured that the designer uses interleaving techniques effectively. Thus, a simple calculation is sufficient to determine the best winding shape of the designed transformer. It is presented that the leakage inductance value can be reduced up to nine times using the interleaving technique. Ramachandran and Deverajan [10] designed a fuzzy-based three-phase inverter circuit with a single DC source for a grid-connected photovoltaic (PV) system using a three-phase transformer. The aim of using fuzzy logic in this study is to meet high-quality output, minimum total harmonic distortion (THD) value and fast response. Rossmanith, et al. [11] used 3D finite element method (FEM) simulation to model common mode chokes leakage inductance. Artificial Neutral Network (ANN) was applied for the estimation of the obtained leakage inductance data. At the end of the study aimed at the relationship between leakage inductance and winding parameters, ANN successfully predicted leakage inductance values.

Spacecraft contain an inverter to obtain high voltage from a low-power source provided by solar panels. The power drawn from the low-voltage DC source is rectified and filtered using a pair of power transformers with an oscillator. Due to the natural inductive behavior of transformers, if the core is saturated and the voltage value exceeds the voltage value of the transistors connected to the inverters, the probability of the system tripping increases. In this context, a report detailing the results of a research program conducted to examine the magnetic properties of some materials for use in spacecraft transformers, static power converters and transformer rectifier power supplies is presented [12].

In this study, an electromagnetic FEA-based modeling method is presented for the inverter circuits to operate more efficiently. Ferrite N87 soft magnetic material, which is suitable for high frequency designs, was chosen as the core material of the isolation transformer modeled for the inverter circuit. This core material is defined in the designed E core form in the FEA software in terms of core geometry, specific core loss and saturation flux density values. First, parametric simulation studies were carried out with FEA software in order to obtain leakage inductance values according to variables such as the geometric properties of the primary-secondary windings of the isolation transformer, which can be found at the outputs of the inverter circuits, and the number of turns and a data set was obtained as leakage inductance values. This data set is assigned for the training and testing of Adaptive Networks Based on Fuzzy Logic System (ANFIS). In this way, the leakage inductance of the isolation transformers with different winding sizes that have not yet entered the production phase has been accurately estimated and the isolation transformer with the most efficient operating parameters has been determined. In the second step, the RMS values of the output voltage were obtained depending on the different leakage inductance values of the transformer integrated into the inverter and the PWM switching variables were determined.

## 2. Inverters

Today, with the rapidly developing technology, the increasing need for energy has increased the importance of environmentally friendly clean energy sources and their use has become widespread. However, in such application areas, the need to isolate the power electronic circuits of the grid and the renewable energy source from each other efficiently has arisen. In line with this need, performing the design of an isolation transformer is of great importance for the safe and efficient operation of the system.

Since almost all electrical devices work with alternating current electrical energy, it is necessary to have an AC power supply. Inverter circuits are also known as adjustable frequency AC voltage source, that is, inverters that convert the output from a DC voltage level to AC voltage at the desired voltage and desired frequency [13]. That is, the working principle of an inverter is to convert a certain level of DC input voltage to AC output voltage with a desired frequency and amplitude [14]. The input of the inverters can be fed from various sources such as batteries, solar cells or through the rectifier circuit. Depending on the type of source used in its input, inverters are divided into two parts voltage source inverter and current source inverter [15]. The frequency and amplitude of the AC output voltage can be changed or kept constant by keeping the DC input voltage and the inverter gain constant. In addition, if the DC input voltage has a fixed value and a variable output AC voltage is requested, a variable output voltage can be obtained with the changes made on the inverter gain. This is done with Pulse Width Modulation (PWM) control for the inverters. The gain of the inverters can be found by the ratio of DC input voltage to AC output voltage [16].

The waveform of the output voltage of ideal inverters is sinusoidal. However, the inverter output voltages obtained in practical applications do not have a sinusoidal form and have some harmonics. In high-power applications, waveforms with the sinusoidal form with little distortion are required. In low and medium power applications, square wave or partial square wave output voltages are requested. In response to this demand, the effect of harmonics on the output voltage can be greatly reduced by using semiconductor technology and switching techniques that have developed in recent years [16].

Mostly, any DC source (battery, fuel cell, solar cell, wind cell) can be at the input of inverters used in industrial applications such as variable speed AC motor drives, renewable energy sources, transportation services, induction heating, off-the-shelf power supplies and uninterruptible power supplies [16]. The desired number of output phases can be obtained with inverters. Although single-phase and three-phase inverters are preferred more frequently in industrial applications, the development of more than three-phase AC motors has recently gained importance in order to increase the reliability of some critical applications. Therefore, the production and design of inverters with the same phase number have been accelerated [15].

In the past, Silicon Controlled Rectifiers (SCRs) were used in high and medium-power inverters. SCR-based inverters needed commutation circuits to turn off the SCRs. While these commutation circuits increase the size and cost of the inverter, it also reduces their reliability and switching frequency. Due to these disadvantages, with the development of fully controlled semiconductor power switches, Insulated Gate Bipolar Transistors (IGBT) and Gate Turn Of (GTO) are used in medium power inverters, and Integrated Gate-Commutated Thyristors (IGCT) are used in high power inverters [15]. There is a reverse parallel connected diode next to each semiconductor power element (such as SCR, Bipolar Junction Transistor (BJT), MOSFET, IGBT) used in inverter circuits. The purpose of the use of this diode is to protect the circuit elements against the reverse current that may pass through it [17].

### 2.1. Single-Phase Two-Level Inverter

Regarding two-level inverters, the single-phase full-bridge inverter circuit given in Figure 1 has four active and four passive circuit elements. Square wave, partial square wave and PWM techniques can be used to control this type of inverter [17]

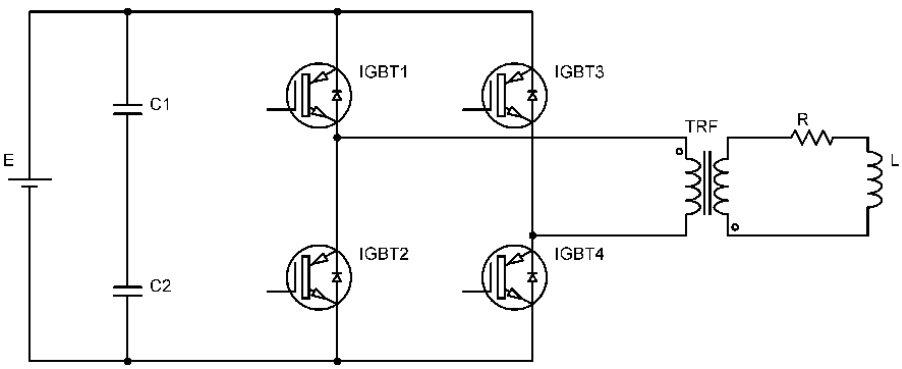


**Figure 1.** Single-Phase Two-Level inverter circuit

In a single-phase two-level inverter circuit consisting of four choppers, E input voltage is seen on the load when $I_1$ and $I_2$ IGBTs turn on at the same time. When $I_3$ and $I_4$ IGBTs turn on, the negative value of input voltage -E occurs on the load. In this circuit topology, Equation 1 can be given for the effective value of the AC voltage obtained at the inverter output [16].

$$V_o = \sqrt{\frac{2}{T_0}\int_0^{\frac{T_0}{2}} E^2 dt} = E \tag{1}$$

AC voltage induced at the output is obtained by the difference of the phase voltages a and b given in Equation 2, which has 180° phase difference [17].

$$V_{ab} = V_o = V_{ao} - V_{bo} \tag{2}$$

### 3. Isolation Transformers

Generally, isolation transformers are electrically separating the source and the load from each other by isolating the secondary output voltage from the primary voltage by means of magnetic coupling for the purpose of use. In this way, isolation transformers play an active role in the protection of sensitive electrical devices, especially from current and DC components with harmonic components [3, 18].

#### 3.1. Leakage Inductance

In a transformer with two windings, not all of the magnetic flux induced by the windings connects the other winding. That is, there is magnetic flux induced by a winding in the gap between the core and the windings, in the gap between layers, inside the conductors, and inside the insulation between the windings. Since these flux components have no connection with the other winding, the coupling coefficient is less than one (k< 1). This leakage flux between the windings can be characterized as an inductance as it stores magnetic energy. These inductances, called leakage inductances, are modelled as $L_{l1}$ and $L_{l2}$ connected in series with the windings, as shown in Figure 2 [19].

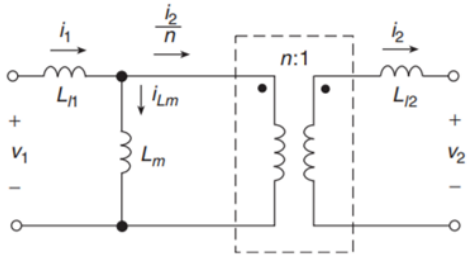


**Figure 2.** Transformer equivalent circuit.

The leakage inductance value varies depending on the winding arrangement of the transformer, the core geometry, and the core relative permittivity. Many studies have been done in the literature to reduce the leakage inductance value of the transformer. For this purpose, in some of these, the windings of the transformers are designed with wide and low thickness, the insulation between the windings is reduced, and the windings are placed in such a way that they overlap each other, double-strand windings are used and the number of turns is reduced. It has been determined that the leakage inductance is low in transformers with wide and flat windings with minimum insulation. In addition, making transformer windings from Litz wire or a twisted bundle of insulated wire also reduces leakage inductance. The use of wide and thin foil is required for the lowest leakage inductance value [19].

The equivalent circuit of a two-winding transformer includes a magnetizing inductor (Lm), leakage inductors $L_{l1}$ and $L_{l2}$, as well as an ideal transformer with a conversion ratio n. Thus, the coupling coefficient (k) and conversion ratio (n) of the ideal transformer can be defined by Equations 3-5. In these equations, $N_1$ and $N_2$ are the turns of primary and secondary windings; $L_{pr}$ and $L_{sc}$ represent self inductance values of primary and secondary windings, respectively [20].

$$n = \frac{N_2}{N_1} = 1 \ (for\ isolation\ transformer) \tag{3}$$

$$k = \frac{L_m}{L_m + L_{lk}} \tag{4}$$

$$L_{l1} = L_{pr}(1 - k^2) \tag{5}$$

$$L_{l2} = L_{sc} - L_m(n)^2 \tag{6}$$

## 4. Parametric Simulation Studies

### 4.1. Design of the Isolation Transformer

The application developed in this article belongs to the thesis study in reference [21, 22]. The isolation transformer designed for inverters is given in Figure 3. The ferrite N87 is defined as the core material of the three-dimensionally modeled isolation transformer in order to verify of the leakage inductance data set.

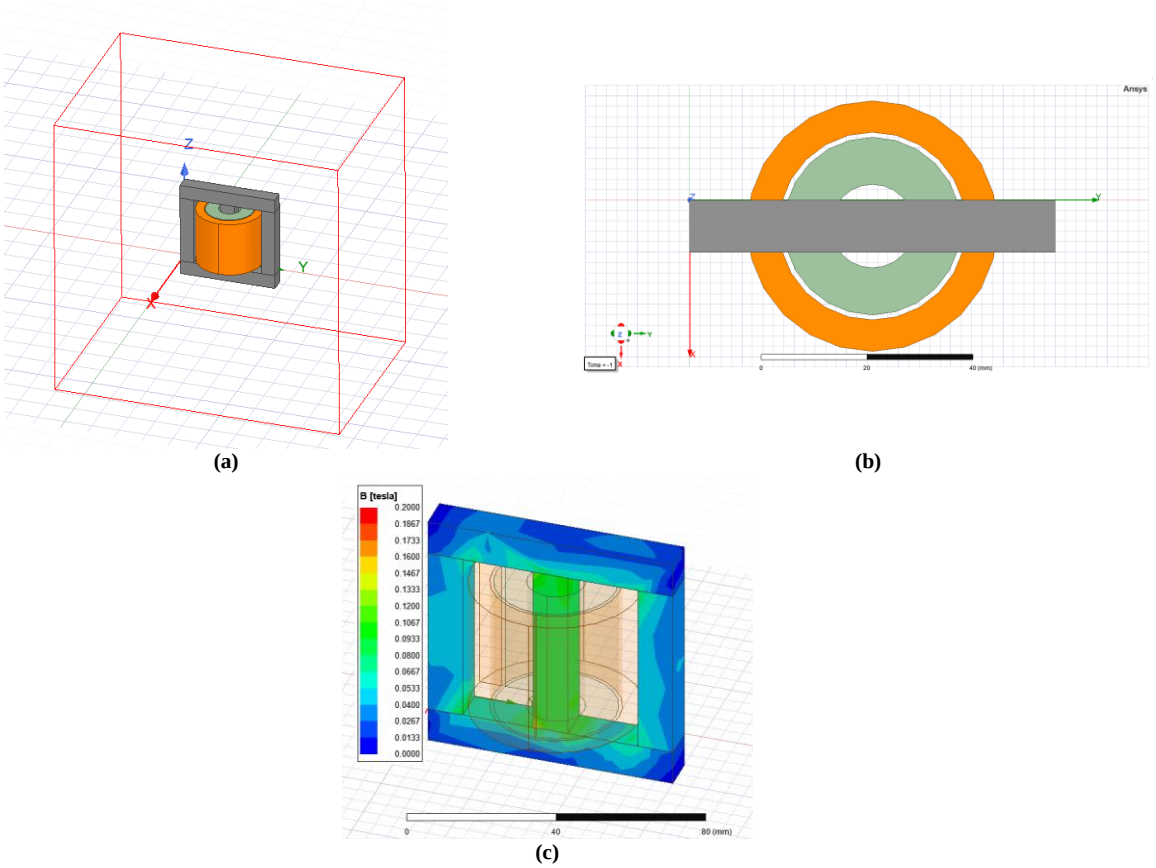


**Figure 3.** Isolation transformer design with FEA software, (a) 3D image of the electromagnetic modeling, (b) the top view of the primary and secondary windings, (c) 3D flux density of the transformer core.

For parametric FEA simulation studies, the number of turns (N), primary winding radius (Lpr) and secondary winding radius (Lsc) variables of the windings of the isolation transformer are calculated according to different variations by defining the linear steps given in Table 1. Thus, in the transformer design parameters, the leakage inductance behavior of the three input variables is extracted and a parametric data set is obtained [22].

**Table 1.** The parameters of the FEA simulation issue.

| Parameters | Value | Step |
|---|---|---|
| $L_{pr}$ | 10-17 mm | 0.5 |
| $L_{sc}$ | 18.5-24 mm | 0.5 |
| N | 20-50 | 5 |

### 4.2. Design of the Two-Level Inverter

The values of the circuit elements to be used for the design of the single-phase two-level inverter were determined and designed as given in Figure 4.

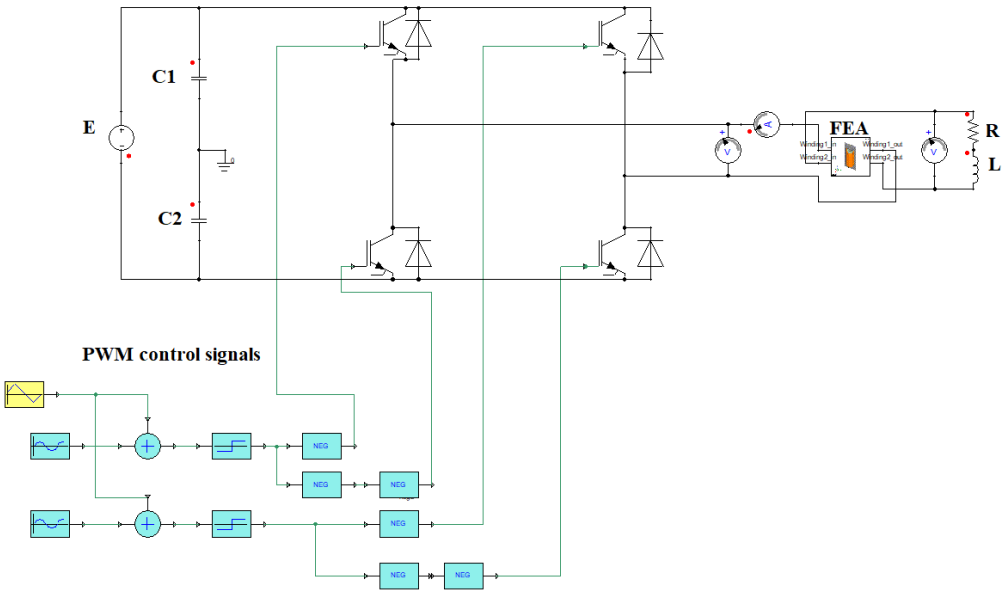


**Figure 4**. Single-phase two-level inverter circuit

Values of active and passive circuit elements used in circuit design are as given in Table 2. Parametric simulation studies are carried out with certain variational steps according to these data.

**Table 2**. Values of used circuit elements

| Circuit Element | Value |
|---|---|
| E | 400 V (DA) |
| C1, C2 | 6600 uF |
| R | 10 ohm (load) |
| L | 10 mH (load) |

The parametric simulation method was used to determine the RMS value occurring at the output voltage of the inverter given in Figure 4. For parametric analysis, a data set was obtained by changing the leakage inductance (L_lk) of the transformer at the inverter output, the frequency of the PWM signal used in the control circuit of the inverter, and the frequency of the sine waves with linear steps given in Table 3.

**Table 3.** Parametric values of a single-phase two-level inverter circuit

| Parameters | Value | Step |
|---|---|---|
| $L_{lk}$ | 0-10 $\mu$H | 2 $\mu$H |
| PWM | 15-30 kHz | 5 kHz |
| $f$ | 1-10 kHz | 1 kHz |

### 5. The Estimation Studies with ANFIS

The unpredictability of possible future uncertainties and risks is a serious problem for many projects in general. The reason why risks and uncertainties cannot be determined is the adverse effects of inaccessible parameters on the systems. In other words, it is possible to predict future uncertainties and risks. However, it is not possible to accurately predict future events without an accurate analysis of past events. In this context, past events, whose data were previously recorded, should be recorded accurately and effectively, should be easily accessible when necessary, and the desired data should be easily produced [10]. Thus, ANFIS is one of the artificial intelligence techniques developed in recent years and Artificial Neural Networks are used to determine fuzzy logic parameters. Thus, it was established by taking advantage of the learning ability of artificial neural networks, considering the reasons such as the fuzzy logics inability to adapt easily to environmental conditions and its lack of learning ability. The uses of ANFIS can be listed as modeling nonlinear functions, linearly defining nonlinear components and estimating a chaotic time series [23, 24].

The leakage inductance values of the isolation transformer, which can be integrated into the outputs of the inverter circuits, were obtained using a parametric simulation technique. As input variables data to the ANFIS modeling, $L_{pr}$, $L_{sc}$ and N parameters are defined for the parametric simulation setup. Leakage inductance values obtained by parametric simulations are presented as output parameters. With a total of 1260 data, the training and testing phase of the ANFIS system has been completed. 1008 of these data are used in the training phase of ANFIS and 252 in the testing phase. In order to divide the data into train and test, first the order of the data is randomly mixed. Then, random selection is made from these data.

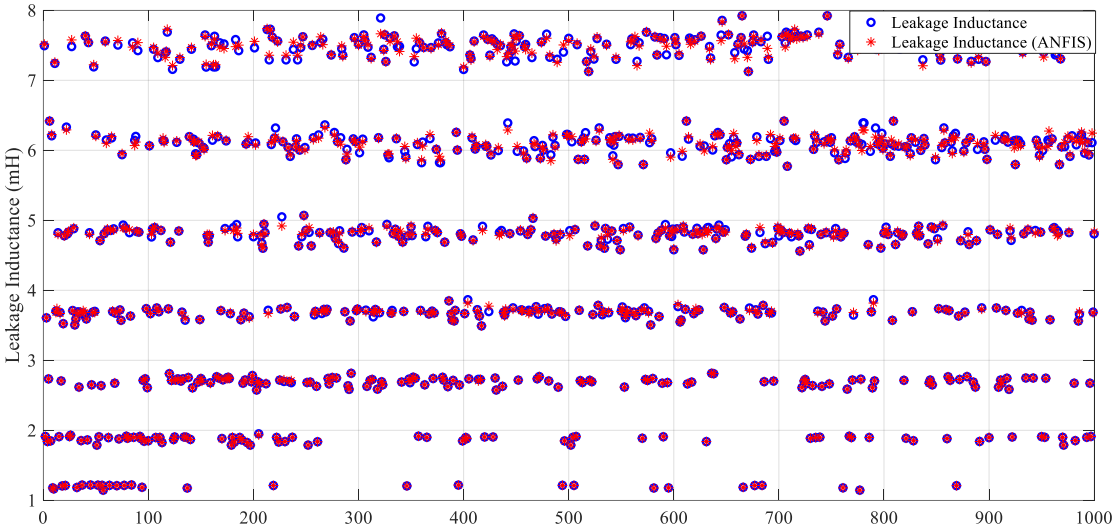


**Figure 5**. The training graph

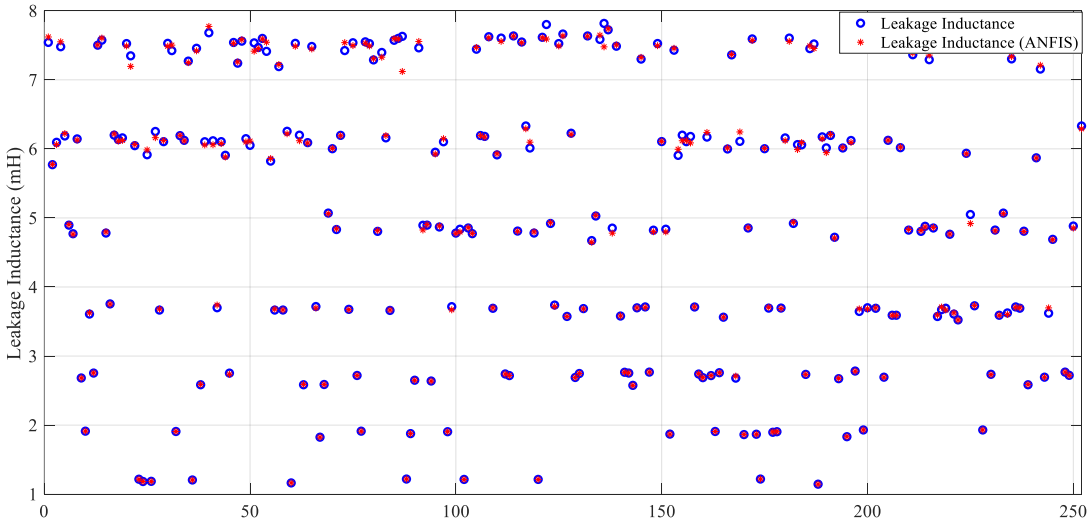


**Figure 6**. The testing graph

$$\boldsymbol{Error} = \frac{\sum\left(\frac{|\boldsymbol{Actual\ Value(i)} - \boldsymbol{Predicted\ Value(i)}|}{\boldsymbol{Actual\ Value(i)}}\right)}{\boldsymbol{i}} \boldsymbol{x100} \tag{3}$$

The most efficient membership function has been determined by making many preliminary studies in the ANFIS interface. The training and test graphics obtained as a result of the studies are given in Figure 5 and Figure 6. The differences between the actual and ANFIS-estimated values were analyzed with the formula given in Equation 3 and error values were calculated. According to the results obtained with the rule-based viewer given in Figure 7, the average percentage error is obtained as 0.3470% and 0.4448%, respectively, because of the training and testing phases.

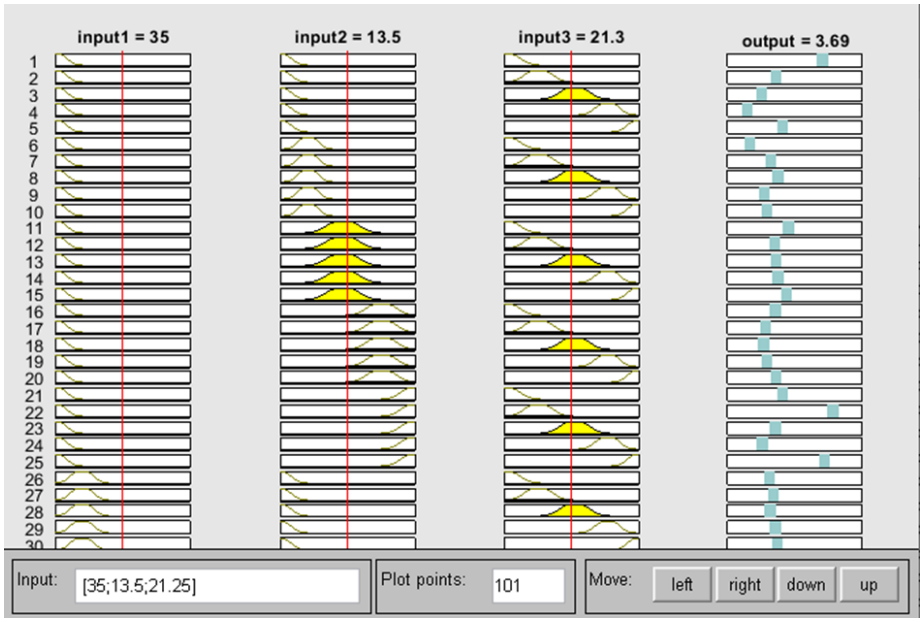


**Figure 7**. Testing ANFIS Model

As a result of the studies, the most efficient isolation transformer was easily determined. Then this transformer was used at the output of a single-phase two-level inverter. Simulation studies have been carried out to estimate the RMS value that changes depending on the various parameters of the designed inverter. The data set obtained as a result of the simulations was processed with ANFIS, one of the artificial intelligence methods, and a successful estimation was made.

The graph where the system's training estimated values and actual values are together is given in Figure 8.

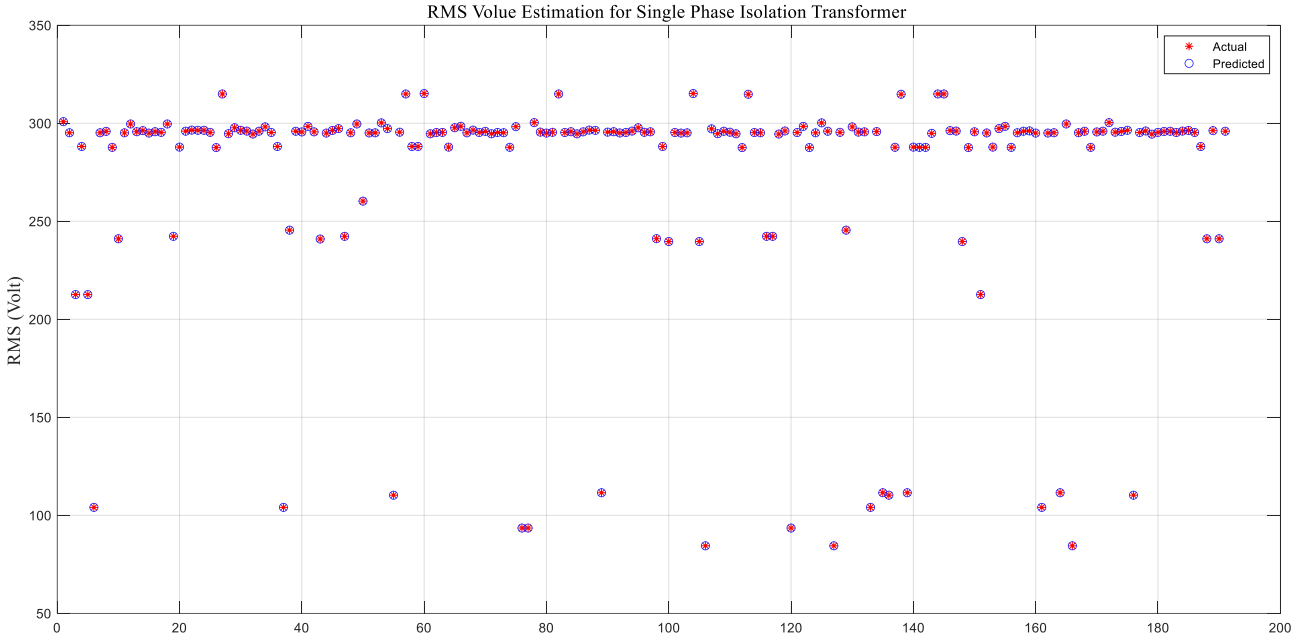


**Figure 8**. Trainig ANFIS Model

After the training process is completed and the test phase is started, the test prediction values and actual values obtained as a result of the system study are given in Fig. 9

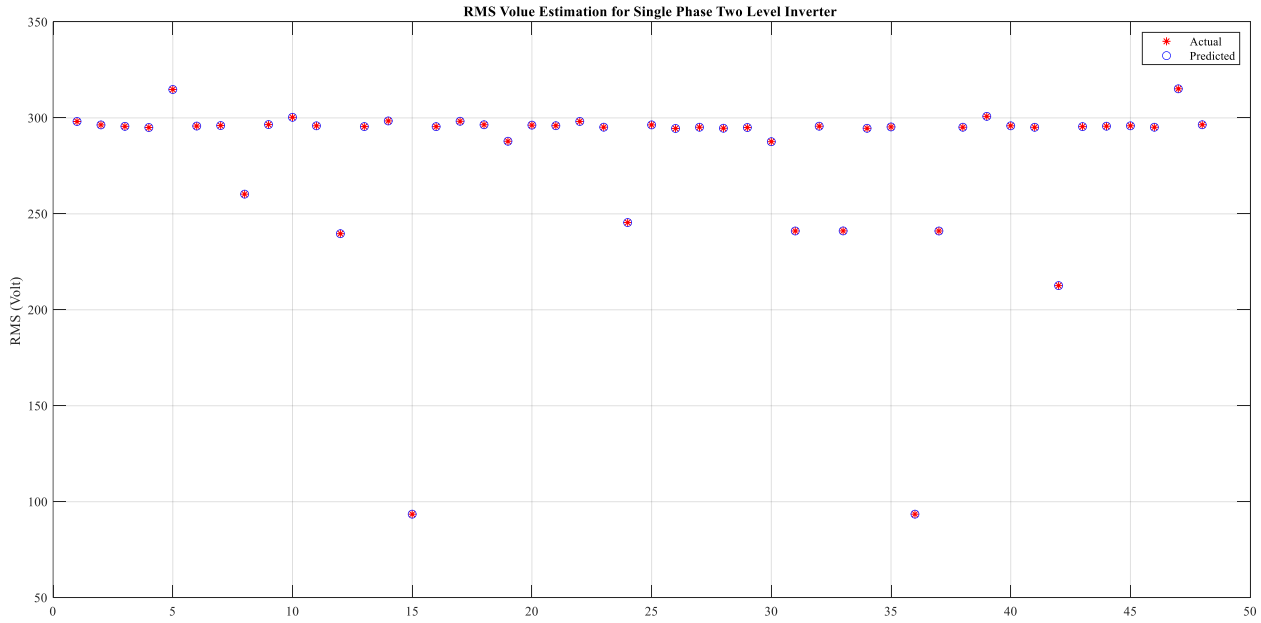


**Figure 9.** Testing ANFIS Model

The average percent error for the test was calculated as 6.7522%. Thus, by examining the given graphs and calculated error values, it was determined that the estimation phase was very successful.

## 6. Conclusion and Discussion

In this study, two different methods are presented for the analysis of the leakage flux effects of isolation transformers for the waveform of output voltages of two level inverter circuits to have a smooth sinusoidal form. In the first method, it is aimed that the output wave of single-phase two-level DC-AC inverter circuits, which can be adjusted at the desired level and frequency, is close to a smooth sinusoidal. In this direction, parametric simulation studies of an isolation transformer are carried out by using ANSYS-Maxwell software, which can be analyzed with SEM in an efficient and realistic way. Leakage inductance changes are observed by changing the radius and number of turns of the primary and secondary windings of the isolation transformer. Thus, because of parametric simulations, a data set is created for the estimation of the leakage inductance value of the isolation transformer, which varies depending on the radius of the primary and secondary windings and the number of turns. This data set is analyzed with ANFIS, one of the widely used artificial intelligence algorithms, and as a result, leakage inductance values were successfully estimated. In this context, the determination of the much more effective operating isolation transformer, which can be determined because of actually quite long-term and process-requiring studies, has been facilitated. In addition, the efficient isolation transformer designed according to the leakage inductance behavior is integrated into the output of two single-phase DC-AC inverter circuits and the output voltages of the inverters are observed. As a result of the study, the RMS value of single-phase two-level inverters with different operating parameters has been successfully estimated. As future studies, different high-frequency transformer designs can be made and their behavior in power electronics circuits can be deduced. In addition, designs can be made with nanocrystalline core material, which has been very popular in recent years, instead of ferrite core material for a certain power and frequency value. Thus, comparative performance studies can be made with ferrite core materials. The regression results obtained showed that the use of artificial intelligence in estimation of leakage inductance provided effective results. In this way, faster analysis can be done. However, more data are needed for more reliable results.

## Competing Interest / Conflict of Interest

The authors declare that they no conflict of interest. The none of the authors have any competing interests in the manuscript.

## Funding

There is no financial support and commercial support.

## Acknowledgements

We cordially acknowledge to the Ninth European Conference on Renewable Energy Systems (ECRES 2021) in Madrid, and thanks to Prof. Dr. Erol KURT.

**7. References**

[1] Karsai, K., Kerenyi, D. and Kiss, L., (1987) Large Power Transformers. Elsevier, New York.

[2] Winders, J., (2002). Power transformers: principles and applications. CRC Press, 1st edition, England.

[3] Li, X., Huang, W., Cui, B., and Jiang, X., (2019). Inductance Characteristics of the High-Frequency Transformer in Dual Active Bridge Converters, IEEE 22nd International Conference on Electrical Machines and Systems (ICEMS), pp. 1-5.

[4] Balci, S., Sefa, I., and Altin, N., (2016). An investigation of ferrite and nanocrystalline core materials for medium-frequency power transformers, Journal of Electronic Materials, vol. 45, no. 8, pp. 3811-3821.

[5] Mannam, R., Gorantla, S. R., and Vangala, N., (2019). A practical technique to measure transformer losses in high frequency SMPS," SN Applied Sciences, vol. 1, no. 3, p. 227, doi: 10.1007/s42452-019-0239-4.

[6] Aghaei, M., Mohsenzade, S., and Kaboli, S., (2019). On the Calculation of the Leakage Inductance in Transformers With Nonideal Windings," IEEE Transactions on Power Electronics, vol. 35, no. 8, pp. 8460-8471.

[7] Tian, H., Wei, Z., Vaisambhayana, S., Thevar, M. P., Tripathi, A., and Kjær, P. C., (2018). Calculation and Experimental Validation on Leakage Inductance of a Medium Frequency Transformer, IEEE 4th Southern Power Electronics Conference (SPEC), pp. 1-6.

[8] Mogorovic, M., and Dujic, D., (2017). Medium frequency transformer leakage inductance modeling and experimental verification, IEEE Energy Conversion Congress and Exposition (ECCE), pp. 419-424.

[9] Prieto, R., Cobos, J., Garcia, O., Alou, P., and Uceda, J., (1998). Taking into account all the parasitic effects in the design of magnetic components," in APEC'98 Thirteenth Annual Applied Power Electronics Conference and Exposition, vol. 1: IEEE, pp. 400-406.

[10] Ramachandran, R., and Deverajan, N., (2015). A fuzzy logic based three phase inverter with single DC source for grid connected PV system employing three phase transformer," International Journal of Renewable Energy Research (IJRER), vol. 5, no. 3, pp. 739-745.

[11] Rossmanith, H., and Stenglein, E., (2016). Prediction of the leakage inductance in high frequency transformers, 2016 18th European Conference on Power Electronics and Applications (EPE'16 ECCE Europe), pp. 1-10, doi: 10.1109/EPE.2016.7695281.

[12] Mclyman, W. T., (1973). Design and material selection for inverter transformer cores, NASA Tech Brief, NPO-11726.

[13] Sharma, C. P., Sapkota, K., Newpaney, S., and Bhutia, J. N., (2019). Harmonic analysis and comparison between single phase three-level pulse width modulation (PWM) inverter and sinusoidal pulse width modulation (SPWM) inverter implementing analog circuits, IEEE Second International Conference on Advanced Computational and Communication Paradigms (ICACCP), pp. 1-5.

[14] Bedford, B. D., (1967). Inverter circuit," ed: Google Patents.

[15] Trzynadlowski, A. M., (2015). Introduction to modern power electronics. John Wiley & Sons.

[16] Rashid, M. H., (2004). Power Electronics circuits, devices, and applications, Published by Dorling Kindersley (India) Pvt. Ltd.

[17] Bodur H., (2012). Güç elektroniği. Birsen Yayınevi, Turkiye.

[18] Guo, S., Liu, P., Zhang, L., and Huang, A. Q., (2017). Design and optimization of the high frequency transformer for a 800V/1.2 MHz SiC LLC resonant converter, IEEE Energy Conversion Congress and Exposition (ECCE), pp. 5317-5323.

[19] Kazimierczuk, M. K., (2009). High-frequency magnetic components. John Wiley & Sons

[20] Bryce H., (2007). Analysis and Modeling of Magnetic Coupling. IEEE Power Electronics Society, Denver Chapter of IEEE PELS Discovery Learning Center, University of Colorado.

[21] Aslan, B., (2021). Estimation and analysis of electrical parameters of single phase isolation transformer with adaptable networks based on fuzzy logic for inverters, MsC Thesis, Karamanoğlu Mehmetbey University, Karaman, Turkiye.

[22] Aslan, B., Balci, S., Kayabasi, A., (2021). Estimation of Leak Inductance of A Phase Isolation Transformer via ANFIS. 9th Eur. Conf. Ren. Energy Sys. 21-23 April 2021, Istanbul, Turkey

[23] Jang, J.S., (1993). ANFIS: adaptive-network-based fuzzy inference system, IEEE transactions on systems, man, and cybernetics, vol. 23, no. 3, pp. 665-685.

[24] Atar T., Balcı S., Kayabaşı A., (2022). The analysis of three level inverter circuit with regard to current harmonic distortion by using ANFIS. Journal of Energy Systems. 143-152.